View metadata, citation and similar papers at core.ac.uk
brought to you by CORE
provided by ScholarBank@NUS

ADVANCED CONTROL OF ACTIVE MAGNETIC BEARINGS WITH LEANRING CONTROL SCHEMES

WU DEZHENG

(*B.Eng., Shanghai Jiao Tong University*)

A THESIS SUBMITTED
FOR THE DEGREE OF MASTER OF ENGINEERING
DEPARTMENT OF ELECTRICAL AND COMPUTER ENGINEERING
NATIONAL UNIVERSITY OF SINGAPORE
2004

Acknowledgements

Firstly I would like to express sincere gratitude and appreciation to my supervisor, Dr. Bi Chao, for giving me challenging tasks to grow up, for his guidance and support, for what I learned from him about knowledge and life. He provides me with sound advice on my research works, nice suggestions on research methods, and valuable information that broaden my vision on hard disk. I would like to regard him as my role model in my future career.

I also wish to thank Dr. Liu Zhejie and Dr. Jiang Quan, my supervisors, for their encouragement, support and directions during my graduate study in DSI.

Special thanks also go to: the lab officer Mr. Lim Choon Pio for helping me a lot in laboratory despite his busy schedule in projects; my fellows Mr. Lin Song, Mr. Wei Taile, and Mr. Huang Ruoyu for their help and remarks to my work as well as their effort to make the laboratory an enjoyable place to work in.

I would also like to thank my parents, Mr. Wu Minglun and Ms. Su Zhongliang, not only for bringing me up, but also for their endless support and care in the past 26 years.

Most sincerely, I wish to thank my wife, Ms. Jin Leilei. Her love, encouragement and company over the years energize me to accomplish my Master study in a foreign country.

Last but not least, I would like to thank Data Storage Institute for offering me financial assistance and research facilities to finish this thesis.

Wu Dezheng

Content

Summary

Unbalance effect is a common problem in rotating machinery. When the rotor's geometric axis, inertial axis and magnetic axis are not coincident, the unbalance happens and it can cause undesirable vibrations, acoustic noise and rotor position runout. Runout is a term that describes the motion of a rotating shaft in radial directions. Existence of such motion, repetitive or non-repetitive, in precision spindles (such as disk drive motors) is generally detrimental to their applications. Active magnetic bearing (AMB), which levitates a rotating object (typically, a rotor in electric machine) with a magnetic field, is proven to be a good solution to this unbalance problem. With effective control methods, the unbalance effect can be greatly attenuated in the machines using AMB.

In this thesis, a time-domain iterative learning control (ILC) scheme is firstly applied in AMB to realize unbalance compensation. Then a new control scheme, automatic learning control (ALC), is proposed to achieve better performance in unbalance control, and it works in a wide range of rotational speeds in AMB. ALC is based on the combination of time-domain ILC and gain-scheduled control, and is able to adjust itself to different rotational speeds. Since ALC can work at different rotational speeds, the negative effect of speed fluctuations on the ILC scheme doesn't appear in ALC scheme. The unbalance compensation is carried out in two modes. One is to achieve rotation about rotor's geometric axis with the benefit of precise positioning. The other is to achieve rotation about rotor's inertial axis, resulting in reduced transmitted force

to the bearing housing and vibrations. In this thesis, both compensation modes are realized with ILC and ALC.

Simulations and experiments are carried out to verify the effectiveness of ILC and ALC schemes. Simulations and experimental results prove that both ILC and ALC can effectively compensate the unbalance force in AMB, and ALC has better performance in presence of fluctuations in speed. Rotor position runouts and fluctuations of coil currents in all radial degree-of-freedom are substantially attenuated.

List of Tables

List of Figures

Nomenclature

AMB	Active magnetic bearing
ILC	Iterative learning control
ALC	Automatic learning control
DOF	Degree-of-freedom
HDD	Hard disk drive
NRRO	Non-repeatable runout
FDB	Fluid dynamic bearing
TPI	Track per inch
EM	Electromagnetic
PWM	Pulse width modulation
PM	Permanent magnet
AFB	Adaptive forced balancing
CPU	Central processing unit
FILC	frequency-domain iterative learning control
AVC	Adaptive vibration control
DSP	Digital signal processor
PID	Proportional-integral-differential
A/D	Analog-to-digital
D/A	Digital-to-analog
PC	Personal computer
I/O	Input/output

MCM Multi-chip module

1. Introduction

This chapter discusses the motivation of the research on Active Magnetic Bearing (AMB) and provides background knowledge on AMB and unbalance effect. The reasons to cause unbalance effect are analyzed. Various existing unbalance control methods for AMB are reviewed. In addition, their advantages and limitations are also discussed.

1.1 Research Motivation

1.1.1 AMB for HDD Spindle Motors

Following the rapid developments of magnetic hard disk drives (HDD) in recent years, all the components used in hard disk drive are facing challenges for realizing high-density data recording. One of the bottlenecks in limiting the data recording density is spindle motor. The vibrations and non-repeatable runout (NRRO) of the motor limit the track density in data recording. They also cause acoustic noise in HDD operation. So far, all the solutions for reducing vibrations and NRRO are based on mechanical methods, for example, using precision ball bearings and fluid dynamic bearings (FDB). Success of these mechanical solutions relies heavily on the development of precision machining technology. The track density, i.e., the tracks-per-inch or TPI of HDDs has increased rapidly in past years, and will be increased further in the coming

years. This will make it difficult to meet more strict requirements of HDDs in future using mechanical solutions. Many potential bearing solutions are considered by HDD researchers, and the contact free suspension by AMB is one of them. Comparing with the ball bearing and FDB spindle motors, spindle motors using AMB have the following advantages

(1) Absence of mechanical friction and wear. Therefore, the motor lifetime can be increased, and the vibration and acoustic noise of the motor can be reduced.

(2) No lubricant leakage problem, which is a very big concern in HDD.

(3) AMB's performance is not very sensitive to the precision in dimension of components. As the rotor movement is controlled by an electric system, for the same precision, AMB is able to show better performance in the runout and vibration.

(4) AMB is an electronics solution to the high performance rotational system. Its performance can be improved significantly following the fast developments of electronics technology and advanced control methods.

1.1.2 Unbalance Effect

Research on AMB includes Electromagnetic (EM) design, sensing technology, and control techniques. The aim of this research project is to investigate the control techniques of AMB, and to provide the foundation for employing AMB in the next generation of HDD. This thesis focuses on performance improvement of AMB by utilizing control methods without additional manufacturing complexity.

Unbalance is a common problem in rotating machinery. When a rotor's geometrical axis does not align with the axis of inertia and the axis of electromagnetic field, the unbalance force is induced. This unbalance force is transmitted to the stator and housing through the bearing, resulting in serious vibration and acoustic noise, especially at critical speeds of the rotor [1]. Furthermore, the position runout of the rotor makes it difficult to realize precise positioning and high-speed operation. In HDD area this brings difficulties to achieve accurate data reading/writing.

Rotor unbalance results from rotor asymmetry in shape, material non-uniformity, asymmetric EM parameters, misalignment of bearings, asymmetric rotor deformations, etc. As perfect rotor system without unbalance is almost impossible, rotor balancing technique must be used in high standard applications.

The conventional method of balancing is realized by employing mechanical approaches, for example, the addition or removal of small amount of mass from the rotor to reduce the residual imbalance. This is a time consuming and costly procedure. Besides, the imbalance in some machines often changes during operation, and mechanical balancing has limited benefit in such case. Moreover, this mechanical balancing is not practical for mass production, such as in the HDD spindle motor area. Recently active magnetic bearing is proven to be a good solution to the unbalance problem. Through effective control methods, the unbalance effect can be greatly attenuated in machines using AMB. In this thesis the unbalance compensation techniques will be investigated and a suitable control method will be proposed for AMBs used in HDD spindle motors.

1.2 Introduction to AMB

In contrast to conventional bearings, AMB uses EM forces to actively levitate the rotor without any mechanical contact. Due to its attractive features, AMB has been applied in a variety of applications such as turbomachinery [2]-[4], flywheels [5]-[7], artificial blood pumps [8], machine tool spindles [9], vacuum pumps [10], [11], etc. Spindle motor in HDD is also a potential application of AMB and it has attracted wide attentions in recent years [12]-[14].

1.2.1 Working Principle of AMB

AMB uses EM forces to levitate rotors and controls their motions. The rotors are usually made of ferromagnetic materials, and some contain permanent-magnetic (PM) materials. An AMB system consists of EM actuators, position sensors, controller, and amplifiers. Position sensors measure rotor positions and send position signals to the controller. Then the controller uses some control algorithm to generate corresponding control current signals. Power drives, usually using PWM technology, send current to electromagnets to produce resulting control force such that the rotor is stably suspended without any mechanical contact with the stator.

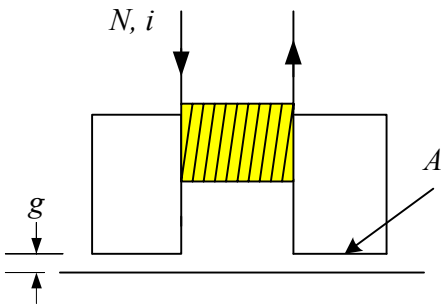

Fig. 1.1. An electromagnet

Suppose an electromagnet has N turns of coil, i is the coil current in this electromagnet. A is its effective cross-area, and g is the air gap. The magnetic field is considered to distribute evenly under the magnetic pole. The EM force in this axis is therefore [10]

$$f = \frac{\mu_0 N^2 A}{4} \cdot \frac{i^2}{g^2} = K_m \cdot \frac{i^2}{g^2} \tag{1.1}$$

where,

$$K_m \triangleq \frac{\mu_0 N^2 A}{4} \tag{1.2}$$

and the permeability of free space is $\mu_0 = 4\pi \times 10^{-7}$ H/m.

Usually two electromagnets are oppositely located in one DOF, so the EM force in this DOF is

$$f_m = K_m \cdot \left(\frac{i_1^2}{(s_0 - s)^2} - \frac{i_2^2}{(s_0 + s)^2} \right), \tag{1.3}$$

where i_1, i_2 are coil current in electromagnets, s_0 is length of the air gap when the rotor is in the center position, s is the rotor displacement with respect to the bearing center in this axis. Thus $(s_0 - s)$ and $(s_0 + s)$ are respectively the lengths of the air gaps for the two opposite electromagnets.

The typical structure of a 2-DOF radial magnetic bearing is shown in Fig. 1.2.

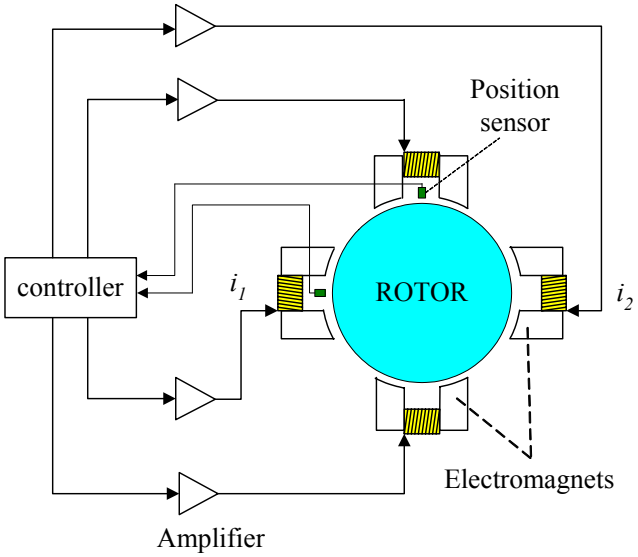

Fig. 1.2. Structure of a 2-DOF magnetic bearing

The two opposite electromagnets are operated in the so-called differential driving mode. In this mode, the coil current in one electromagnet is the sum of bias current i_0 and control current i_c, the coil current in the other electromagnet is the difference of bias current and control current, as shown in (1.4).

$$i_1 = i_0 + i_c, \quad i_2 = i_0 - i_c \tag{1.4}$$

For the reasons explained later, i_0 is normally not zero in many applications. The existence of a non-zero bias current has an obvious advantage that the EM force in (1.3) can be linearized at the equilibrium point ($i_c = i_{c0}$, $s = 0$)

$$f_m = K_i \cdot i_c + K_s \cdot s\,. \tag{1.5}$$

$$K_i \triangleq \frac{\partial}{\partial i_c} f_m \bigg|_{i_c = i_{c0}, s=0} = \frac{4K_m i_0}{s_0^2} \tag{1.6}$$

$$K_s \triangleq \frac{\partial}{\partial s} f_m \bigg|_{i_c = i_{c0}, s=0} = \frac{4K_m (i_0^2 + i_{c0}^2)}{s_0^3} \tag{1.7}$$

In PM-biased AMB (See Fig. 1.3, [15]), bias flux that generated by permanent magnets replaces bias current in conventional AMB to produce the same effect, so its coil currents in the two opposite electromagnets are

$$i_1 = i_c, \quad i_2 = -i_c \tag{1.8}$$

The EM force formula of PM-biased AMB has the same format as (1.5). The difference is that for a PM-biased AMB the force-current factor K_i and force-displacement factor K_s are related to permanent magnet parameters instead of the bias current [15], [16]. Although in these years, nonlinear control techniques have been introduced to eliminate the bias current or flux [17]-[19], there is still a lot of work to do before zero-bias control technique can be applied in industry. As a result, the differential driving mode, including PM-biased flux mode, is still used in our research works.

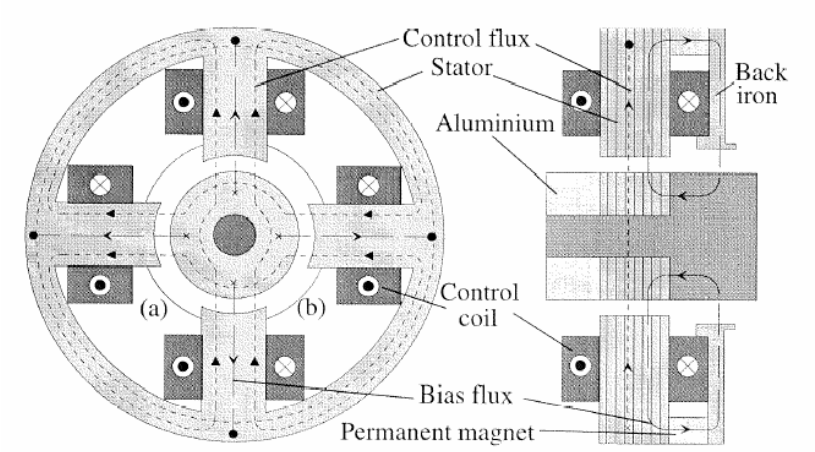

Fig. 1.3. Structure of a PM-biased AMB

From (1.7), $-K_s$ can be regarded as the open-loop stiffness of AMB. From (1.2) and (1.7), it is obvious that

$$K_m > 0, K_s > 0 \tag{1.9}$$

The open-loop AMB system has a negative stiffness, so AMB is open-loop unstable and therefore appropriate control strategies must be employed to stabilize the AMB system.

According to Newton's Law, the motion of the rotor with mass m can be described by

$$\ddot{s} = \frac{f_m + f_u}{m} = \frac{K_i \cdot i_c + K_s \cdot s + f_u}{m} \tag{1.10}$$

where f_u is the disturbance force in this DOF.

The state equation for AMB is

$$\begin{aligned} \begin{pmatrix} \dot{s} \\ \ddot{s} \end{pmatrix} &= \begin{pmatrix} 0 & 1 \\ \frac{K_s}{m} & 0 \end{pmatrix} \begin{pmatrix} s \\ \dot{s} \end{pmatrix} + \begin{pmatrix} 0 \\ \frac{K_i}{m} \end{pmatrix} i_c + \begin{pmatrix} 0 \\ \frac{f_u}{m} \end{pmatrix} \\ y &= \begin{pmatrix} 1 & 0 \end{pmatrix} \begin{pmatrix} s \\ \dot{s} \end{pmatrix} \end{aligned} \tag{1.11}$$

Thus by employing appropriate control algorithm, the AMB system can be stabilized.

1.2.2 4-DOF AMB

A totally suspended magnetic bearing system is composed of 5-DOF suspensions, 4 radial DOF controlled by radial bearings and an axial DOF controlled by a thrust bearing. An AMB system is usually arranged such that the axial subsystem can be separated from the other 4 radial subsystems. So, the axial motion can be individually considered and the motion equation has a simple double integrator format. Because the unbalance effect in radial directions is the major concern in many applications, e.g., HDD, only motions of radial bearings are considered in the thesis.

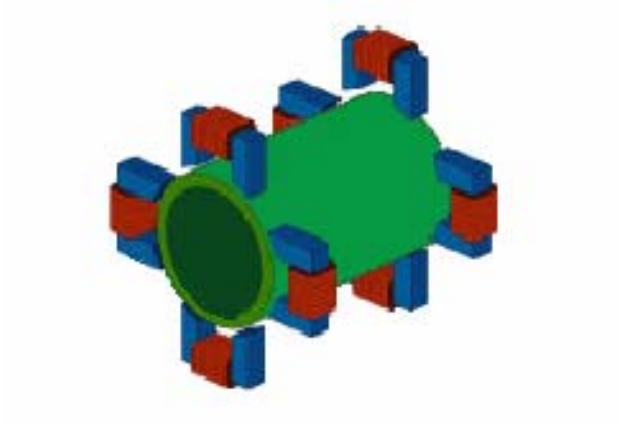

Fig. 1.4. 4-DOF magnetic suspensions

A standard 4-DOF magnetic suspension of the rotor is illustrated in Fig. 1.4. There are two radial bearing planes for an AMB system. Each radial plane includes 2-DOF magnetic suspensions. Therefore the AMB system in our research is a 4-input-4-output system.

1.3 Analysis of Unbalance in AMB

In recent years, some problems on AMB are concerned by researchers such as micro-AMB, self-sensing techniques, unbalance problems, and nonlinear control techniques, etc. The unbalance problem is analyzed in this thesis and a control solution will be proposed to solve this problem.

1.3.1 Analysis of Mass Unbalance

Fig. 1.5 describes the mass unbalance effect in AMB when rotor's geometric axis is not coincident with its inertial axis.

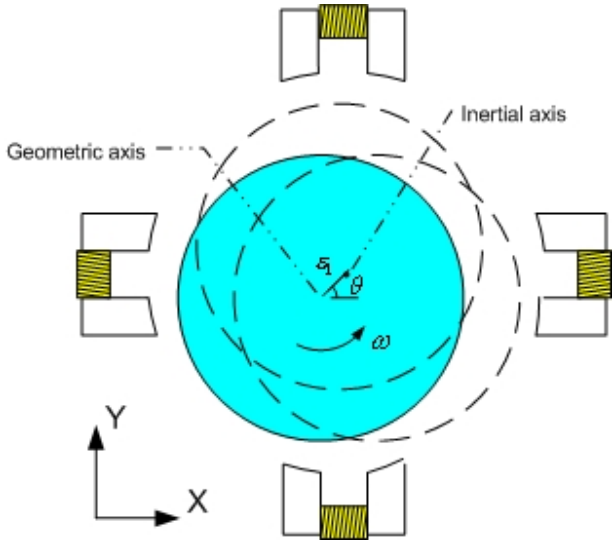

Fig. 1.5. Mass Unbalance

Consider in a 2-D plane, with mass eccentricity ε_1, rotor's angular speed ω, the unbalance force due to mass eccentricity can be modeled as

$$f_{mx} = \varepsilon_1 m\omega^2 \cos(\omega t + \theta) \tag{1.12}$$

$$f_{my} = \varepsilon_1 m\omega^2 \sin(\omega t + \theta) \tag{1.13}$$

where θ is the initial phase of mass unbalance.

1.3.2 Electromagnetic Unbalance

Besides mass unbalance, there also exists EM unbalance in AMB when the geometric axis doesn't coincide with the EM axis, as shown in Fig. 1.6. In Fig. 1.6, O_{mag} is the magnetic center in the cross section of AMB, O_{gm} is the geometric center in this cross section, ε_2 is the EM eccentricity, α is the initial phase angle of the eccentricity, x_1 and x_2 are the air gaps in axis X, y_1 and y_2 are the air gaps in axis Y.

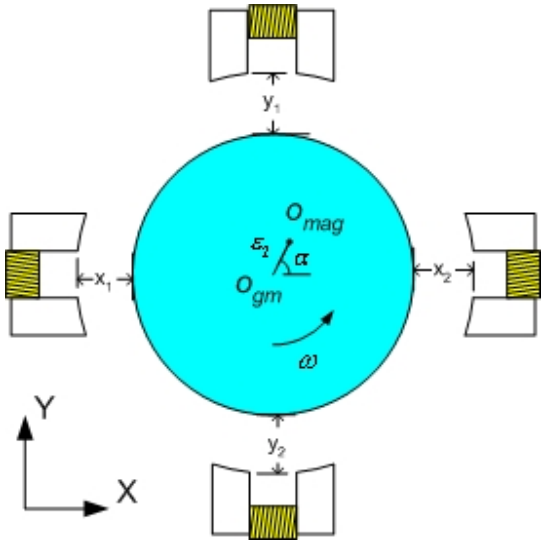

Fig. 1.6. Magnetic Unbalance

If the EM center coincides with the geometric center, air gaps in the axis X should be s_0. Otherwise, the air gaps in axis X are as follows

$$x_1 = s_0 - \varepsilon_2 \cos(\omega t + \alpha) \tag{1.14}$$

$$x_2 = s_0 + \varepsilon_2 \cos(\omega t + \alpha) \tag{1.15}$$

Assuming $s_0 \gg e_2$, the EM unbalance force in axis X is

$$f_{ex} = K_s \varepsilon_2 \cos(\omega t + \alpha). \tag{1.16}$$

Likewise, the air gaps in axis Y are

$$y_1 = s_0 - \varepsilon_2 \sin(\omega t + \alpha) \tag{1.17}$$

$$y_2 = s_0 + \varepsilon_2 \sin(\omega t + \alpha) \tag{1.18}$$

and the EM unbalance force in Y axis is

$$f_{ey} = K_s \varepsilon_2 \sin(\omega t + \alpha). \tag{1.19}$$

(1.14)−(1.19) are based on the assumption that the cross section of the rotor is perfectly round. Otherwise higher-order harmonic components would appear in the

right-hand side of the equations, and they could excite higher-order EM unbalance force in AMB.

1.3.3 Composite Unbalance Effect

From (1.12) and (1.16), the unbalance force in axis X is

$$\begin{aligned} f_{ux} &= f_{mx} + f_{ex} \\ &= \varepsilon_1 m\omega^2 \cos(\omega t + \theta) + K_s \varepsilon_2 \cos(\omega t + \alpha) \\ &= D\cos(\omega t + \delta) \end{aligned} \tag{1.20}$$

where

$$\begin{aligned} D(\omega) &\triangleq \sqrt{\varepsilon_1^2 m^2 \omega^4 + K_s^2 \varepsilon_2^2 + 2\varepsilon_1 \varepsilon_2 m\omega^2 K_s \cos(\theta - \alpha)} \\ \delta &\triangleq \cos^{-1}\left(\frac{\varepsilon_1 m\omega^2 \cos\theta + K_s \varepsilon_2 \cos\alpha}{D(\omega)} \right) \end{aligned} \tag{1.21}$$

The unbalance force in axis Y is

$$\begin{aligned} f_{uy} &= f_{my} + f_{ey} \\ &= \varepsilon_1 m\omega^2 \sin(\omega t + \theta) + K_s \varepsilon_2 \sin(\omega t + \alpha) \\ &= D\sin(\omega t + \delta) \end{aligned} \tag{1.22}$$

Suppose the rotor system is symmetric, and then the motion equation of its geometric center is

$$\begin{bmatrix} \ddot{x}_g \\ \ddot{y}_g \end{bmatrix} + \begin{bmatrix} \omega_n^2 & 0 \\ 0 & \omega_n^2 \end{bmatrix} \begin{bmatrix} x_g \\ y_g \end{bmatrix} = \begin{bmatrix} D\cos(\omega t + \delta)/m \\ D\sin(\omega t + \delta)/m \end{bmatrix} \tag{1.23}$$

where natural frequency $\omega_n = \sqrt{k/m}$, k is the closed-loop bearing stiffness. The damping of the rotor system is so small that it can be neglected.

The rotor's geometric center therefore moves with a circular orbit at the synchronous speed as shown in (1.24).

$$\begin{aligned} x_g(t) &= C\cos(\omega t + \delta) \\ y_g(t) &= C\sin(\omega t + \delta) \end{aligned}, \tag{1.24}$$

The motion amplitude is

$$C(\omega) = \frac{D(\omega)}{m(\omega_n^2 - \omega^2)}. \tag{1.25}$$

The mass center also makes circular motion

$$\begin{cases} x_m = C\cos(\omega t + \delta) + \varepsilon_1 \cos(\omega t + \theta) = C_m \cos(\omega t + \delta_m) \\ y_m = C\sin(\omega t + \delta) + \varepsilon_1 \sin(\omega t + \theta) = C_m \sin(\omega t + \delta_m) \end{cases}, \tag{1.26}$$

where

$$\begin{aligned} C_m &\triangleq \sqrt{C^2 + \varepsilon_1^2 + 2C\varepsilon_1 \cos(\delta - \theta)} \\ \delta_m &\triangleq \cos^{-1}\left(\frac{C\cos\delta + \varepsilon_1 \sin\theta}{C_m}\right) \end{aligned}. \tag{1.27}$$

From (1.20)-(1.27) we know that the composite unbalance force is synchronous with the rotational speed and its amplitude is related to the rotational speed. Both rotor's geometric axis and inertial axis move synchronously in the presence of this composite unbalance force.

1.3.4 Compensation of Unbalance with AMB

Different from conventional bearings, AMB, as an active device, can adopt appropriate control algorithms to obtain required operation performance. Unbalance compensation with AMB is usually implemented in two following modes:

(1) Rotation about geometric axis, such that rotor position runout during operation is reduced. This is quite significant for the applications that require a high level of rotational accuracy. How to effectively reduce the rotational eccentricity in HDD

spindle motors is always concerned in the electric machine area. If the compensation force could counteract the effect of unbalance force in AMB, the rotor could rotate with very high precision and the eccentric movement could be almost reduced to zero. Therefore, it is important to magnetic recording systems, which require high precision for positioning the head.

(2) Rotation about system inertial axis [20]. This is usually realized by reducing fluctuations of AMB coil currents. System inertial axis is defined as the rotor's virtual inertial axis when both mass unbalance and EM unbalance are considered. If the EM unbalance effect is ignored, it coincides with rotor's inertial axis. When rotor rotates about its system inertial axis, no centrifugal force caused by its acceleration is reacted by the bearing and transmitted to the housing. As a result, vibrations of machine housing and noise due to rotor unbalance can be eliminated. This advantage is so attractive that much research works have been done in this mode. Another benefit of this compensation mode is that it could reduce the copper loss in PM-biased AMB (see Fig. 1.3). Because in a vertical PM-biased AMB, synchronous control currents caused by unbalance take to the major portion in AMB coil currents, the copper loss could be reduced substantially when the rotor is forced to rotate about its system inertial axis.

1.4 Literature Review

Unbalance disturbance is common in rotating machinery and it could deteriorate system performance, so AMB researchers pay many attentions on this problem, seeking control

schemes to attenuate unbalance effect with AMB. Various unbalance compensation techniques have been developed since the last decade.

1.4.1 Notch Filters

Early unbalance control techniques are based on the insertion of notch filters in the control loop. By imposing a very low gain to the synchronous frequency while leaving the rest of the spectrum little changed, the notch filter can help to reduce the unbalance effect. The major drawback of this method is that the notch filters affect the stability of the control system so that they can be used in only a limited speed range [21]. A generalized notch filter was then proposed to overcome this problem [22]. This generalized notch filter is actually an internal feedback control block inserted into the control loop, but it has similar characteristic as classical notch filters. The generalized notch filter has an advantage of free pole location, which can enable the filter to process the synchronous unbalance signals at different rotational speeds. The idea of generalized notch filter is also applied in [23]. The difference is that in the latter paper, the convergence is shown with Bode plot instead of the root locus plot in [22], therefore, the robustness against unknown high-frequency dynamics in the plant is clarified.

1.4.2 State Feedback Controllers and Observers

Some designs based on state feedback control approach are also developed to stabilize the AMB system with the ability of unbalance disturbance rejection [24]-[26]. State observers are used in these designs to estimate the state variables which cannot be directly measured by sensors. The differences between these designs are their control algorithms and observer

structures. However, these state feedback controllers need precise plant model which is usually difficult to obtain. The other problem with state feedback controllers is that the required state observers could lead to poor robustness. Furthermore, as pointed out by Shafai et al. [27], both notch filter approach and observer-based state feedback approach have the drawback that they alter the complementary sensitivity function of the system such that the stability margin of the AMB system is eliminated.

1.4.3 Adaptive Controllers

Later more research works were focused on designing an "add-on" controller that could be added to conventional feedback controllers without altering system stability or performance. To cancel the unbalance effect, this kind of additional controller should be able to produce a synchronous control signal according to unbalance signals. To generate this synchronous compensation input, a control method called adaptive forced balancing (AFB) was proposed [28]. In AFB, time-varying Fourier coefficients of unbalance signals are computed on-line and updated at each sampling period. The controller output is the addition of the controller output in the last sampling time and an error correction item. This adaptive forced balancing scheme is based on adaptive control, so the adaptive controller adjusts its control parameters according to feedback variables in each sampling period. Similar approaches with different adaptive laws were also developed for unbalance compensation with AMB [29]-[31]. Taguchi et al. incorporated Kalman filter technique into adaptive control to successively estimate rotor dynamics in real time [32]. The estimation of rotor dynamics is then used in this adaptive control law to generate the desired control signal. All of these control schemes can provide satisfactory unbalance

control performances, but the common problem of this kind of controllers is the heavy computational load. In each sampling period, controllers need to do much computation, which challenges the computational speed of the digital processor used for AMB control, especially when the sampling frequency is high.

In some research works synchronous sensor runout as well as unbalance is also considered to be compensated [33]. It is assumed that not only unbalance but also sensor runout are affecting the movement of rotor in space. The position sensor runout injects periodic disturbances to the measured position signals and thus makes the real rotor position signals unavailable. In this adaptive algorithm, on-line sensor runout and unbalance identification are done by employing multiple angular speed approach or bias current excitation approach. This identification process can finally identify the sensor runout disturbances and unbalance, but the whole control algorithm becomes complicated. Furthermore, according to the authors' comments, there is much work to do before this technique can be used in industrial applications.

1.4.4 FILC and AVC

Application of frequency-domain iterative learning control (FILC) has been applied in AMB [34], [35]. In iterative learning control, the new input to the plant is addition of an error correction item and the old input of the last learning cycle. The new input is generated in such a way that the system output error decreases cycle by cycle. An estimation of the inverse transfer function is employed in the learning law. Knopse et al. proposed an Adaptive Vibration Control (AVC) method which is very similar to the frequency-domain iterative learning control [36], [37]. AVC incorporates a look-up table of learning gain

matrices into the iterative learning law and selects a gain matrix according to operation conditions. This look-up table simplifies the control algorithm by waiving the process of on-line estimation in each learning cycle, but it requires much memory space to store gain matrices, especially for the system operating in a wide range of speed. Therefore, several strategies are then proposed for reducing the memory requirements of AVC [38]-[40]. FILC controllers and AVC are all able to yield good control effects. In addition, FILC controllers and AVC have good transient performances even when there are some sudden changes in unbalance according to experimental results in [37].

1.4.5 Other Advanced Control Methods

Applications of some other advanced control techniques are also found in AMB unbalance control. In [41], the compensation signal is generated with aid of neural networks theory. Controllers based on Q-parameterization theory are also used in AMB to eliminate unbalance effect [42], [43]. Nonlinear control methods such as the back-stepping technique in unbalance control are investigated by some researchers [44].

1.4.6 Discussions

Although various methods have been proposed unbalance compensation with AMB and most of the schemes can provide satisfactory control effect, it is difficult for them to be directly applied in HDD spindle motors. Most of the existing methods require precise knowledge of AMB parameters, which may be not unique for each AMB due to manufacturing errors. Moreover, as analyzed in previous parts, most of the existing unbalance control approaches are so complicated that they require much computation

or memory space in the digital processor. These requirements are not expected in the applications like HDD as the motor speed could be higher than 10k rpm and currently the DSP in HDD already needs to process many issues such as coding, spindle motor drive, servo control, etc. As a result, a practical unbalance control technique, which doesn't require much computation and memory space while provides excellent unbalance compensation effect, is needed for AMB spindle motor in HDD.

1.5 Scope of the Thesis

This thesis deals with the unbalance control method of AMB. The thesis is arranged as follows.

In Chapter 2, a time-domain ILC scheme is proposed for unbalance compensation with AMB. The theory of iterative learning control is briefly introduced. Some considerations about applications of time-domain ILC scheme are also discussed. ILC scheme is applied to realize rotation about geometric axis and rotation about system inertial axis in AMB.

In Chapter 3, a new unbalance compensation method, automatic learning control (ALC), is developed for achieving better performance than ILC. ALC is based on time-domain ILC scheme and it can adjust itself according to the rotational speed. Therefore, it owns some advantages over time-domain ILC scheme against rotational speed variation. The proposed ALC scheme is compared with ILC scheme and its advantages are discussed in that chapter.

In Chapter 4, an analytical model for 4-DOF AMB is built. Simulations of unbalance effect and control effects with unbalance control methods, time-domain ILC and ALC,

are carried out in this model. In addition, Simulations of unbalance compensation with speed disturbance are carried out in order to compare the control effect of these two methods against rotational speed fluctuations.

In Chapter 5, the proposed ILC scheme and ALC scheme are examined in a series of experiments. Comparisons and discussions are provided to analyze the performances of different control strategies.

Chapter 6 summarizes this thesis and presents the outlook for future works. A suitable choice for unbalance compensation in future AMB spindle motors in HDDs is suggested.

2. Time-Domain Iterative Learning Control Scheme for Unbalance Compensation

2.1 Iterative Learning Control

Iterative learning control was initially developed for eliminating periodic tracking errors in robots [45]. Because of its attractive characteristics, ILC has become increasingly popular since its birth in 1984 [46], [47]. Recently ILC has been applied in various industrial applications, such as robotic manipulators [48], [49], process control [50], [51], and motor control [52], [53], etc.

2.1.1 Basic Idea of ILC

ILC improves the control performance in the present cycle by incorporating past control information in current control input [46]. This is the most obvious difference between ILC and most other control methods.

A schematic diagram for typical iterative learning control is illustrated in Fig.2.1. All the signals shown are defined on a fixed interval $t \in [0, T]$. In ILC, firstly the controller calculates the error signal $e_j(t)$, the difference between the system output $y_j(t)$ and the desired output $y_d(t)$. Then the controller computes a new input $u_{j+1}(t)$ for the next cycle (or trial) according to the learning law, and the new input is temporarily stored in the memory. In this process, the new input is the addition of the

old input in previous cycle and an error correction item and it is generated in such a way that the tracking error $e_j(t)$ decreases cycle by cycle. Through this learning process, a desired input signal could be obtained and the tracking error can thus be minimized finally.

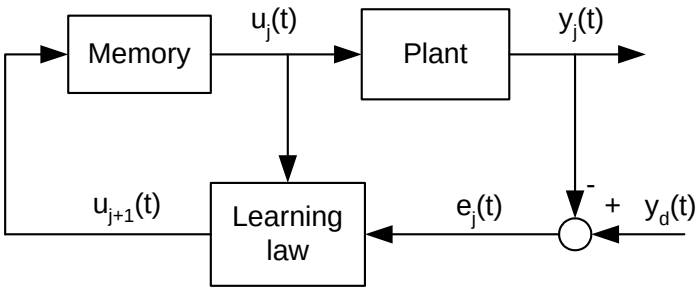

Fig. 2.1. Typical Iterative Learning Control

There are some postulates for iterative learning control as follows [55]:

1. The system performs repeated operation that ends in a finite and fixed duration ($T > 0$).
2. The desired output $y_d(t)$ is given a priori for $t \in [0, T]$.
3. The initial conditions of the system are same at the beginning of each learning cycle (trial).
4. The system dynamics are time-invariant throughout repeated iterations.
5. The system output $y_j(t)$ can be accurately measured or observed.
6. There exists a unique input, $u_\infty(t)$, which produces the desired output.

Among these postulates, some are somewhat strict requirements that can be hardly satisfied in practice. Forgetting factor that will be introduced in the following part could relax these strict requirements.

2.1.2 Time-Domain ILC

Suppose a plant to be controlled has the state-space model like

$$\begin{aligned} \mathbf{X}(k+1) &= \mathbf{A}\mathbf{X}(k) + \mathbf{B}u(k) \\ y(k) &= \mathbf{C}\mathbf{X}(k) \end{aligned} \tag{2.1}$$

A general time-domain iterative learning law can be described by

$$u_{j+1}(t) = u_j(t) + \Phi \cdot e_j(t+1), \quad t \in 0,1,2,...,t_f - 1 \tag{2.2}$$

where t_f is the number of time steps in one learning cycle, $u(t)$ is the controller output, j is cycle number, the scalar Φ is learning gain, and the error in the jth cycle is

$$e_j(t) = y_d(t) - y_j(t) \tag{2.3}$$

According to the convergence condition [54], if the learning gain in (2.2) satisfies

$$\left|1 - \mathbf{C} \cdot \mathbf{B} \cdot \Phi\right| < 1 \tag{2.4}$$

thus for all $t \in [0, t_f - 1]$,

$$\lim_{j \to \infty} e_j(t) = \lim_{j \to \infty} [y_d(t) - y_j(t)] = 0 \tag{2.5}$$

Actually, the model of the system controlled could be ignored in the process of determining the learning gain. The learning gain can be easily obtained by manual tuning until one gets the suitable value. Details about how to choose learning gain for a time-domain ILC controller are discussed in [56]. It can be proven that, when the learning gain Φ is approaching 1/**CB**, the tracking error can be converged with a faster rate [57]. However, in practice, a smaller learning gain is preferred because the big one could lead the learning control to be unstable in the presence of random noise. In addition, since the rotor rotational speed of AMB system is very fast, the time for one learning cycle is very short. Therefore, a number of cycles take only a short while

although the error convergence speed cycle by cycle is not very high. In this case, stability is much more important than the convergence speed of ILC.

For improving the robustness of the controller, a forgetting factor α ($0 \le \alpha < 1$) can be applied in the learning process to increase the robustness of the learning control algorithm against noise, plant changes and other unknown perturbations. The reasons in using such a factor in improving the robustness of learning control have been elaborated in detail by Arimoto et al., [58]. The learning law with forgetting factor is modified as follows

$$u_{j+1}(t) = (1-\alpha)u_j(t) + \Phi \cdot e_j(t+1) \tag{2.6}$$

A negative effect of forgetting factor is that it weakens the control effect of iterative learning control, making the final error not converge to zero. The larger the forgetting factor is, the larger the final error is and the more robust the learning controller is. Therefore, α should be set at a balance point to obtain good control performance as well as satisfactorily adequate robustness for the iterative learning controller.

2.1.3 Low-Pass Filter and its Phase Lag

In the ILC scheme, a low-pass filter is required because high-frequency noises could induce poor learning transients such that the compensation current could go far beyond the normal working region of AMB. In our research, a 2nd order Butterworth low-pass filter is used to filter out high frequency noises. The introduction of the low-pass filter also results in phase lag, which is undesirable in real-time control. To overcome this problem, the learning law is rewritten as

$$u_{j+1}(t) = (1-\alpha)u_j(t) + \Phi \cdot e_j(t+1+n) \tag{2.7}$$

where n is the number of time steps advance used, which produces phase lead to compensate the phase lag effect of the low-pass filter. Another advantage for the phase lead is to keep the learning controller stable in a wide frequency range [56]. Fig. 2.2 shows the phase delay effect of the Butterworth low-pass filter and the phase compensation effect.

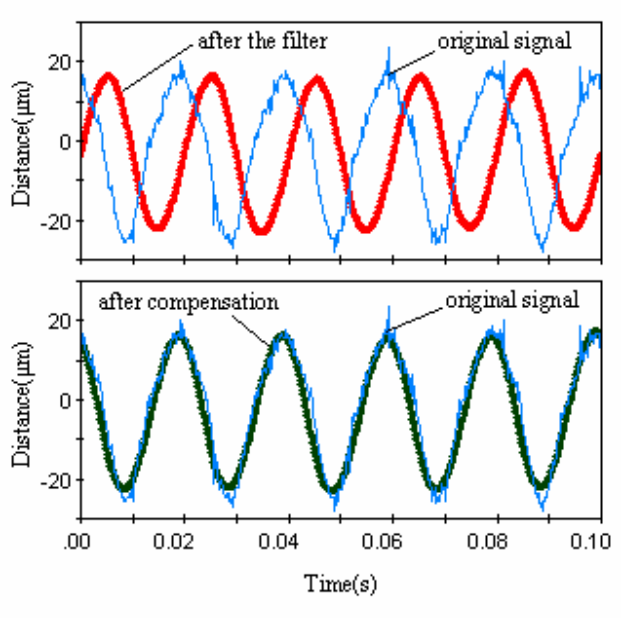

Fig. 2.2. Results of the phase delay and compensation of the filter

The resulting time-domain ILC scheme is shown in Fig.2.3.

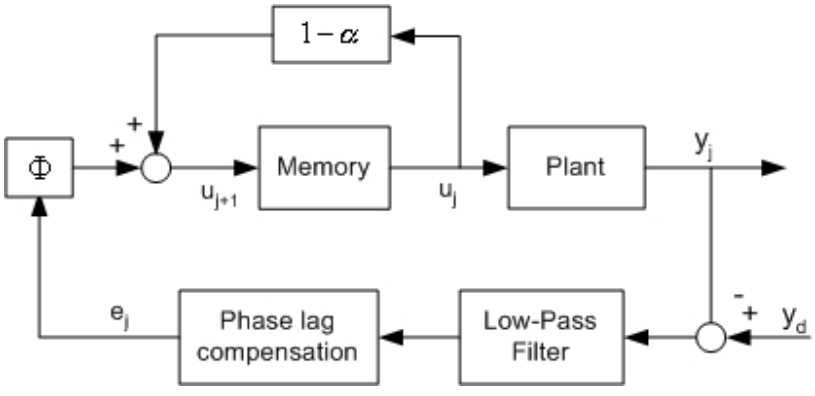

Fig. 2.3. Proposed time-domain ILC scheme

2.2 ILC Scheme for Unbalance Control in AMB

The ILC scheme for unbalance control with AMB includes two modes, rotation about geometric axis and rotation about system inertial axis.

2.2.1 ILC Scheme for Rotation about Geometric Axis

To make the rotor rotate about its geometric axis, the controller needs to produce compensation current (force) to counteract the unbalance disturbance.

$$f_{comp} = -f_u \tag{2.8}$$

Since rotor runout is the target for minimization, the rotor position error signal e_p is the controller input for ILC. The learning controller becomes

$$i_{ILC,j+1}(t) = (1-\alpha) i_{ILC,j}(t) + \Phi_1 \cdot e_{p,j}(t+1+n) \tag{2.9}$$

$$e_p(t) = r_p(t) - y_p(t) \tag{2.10}$$

where i_{ILC} is the controller output, Φ_1 is the learning gain for this control scheme and y_p is the rotor position signal with unbalance disturbance. The rotor position reference for AMB system is

$$r_p(t) = 0 \tag{2.11}$$

The position error will converge to zero in the learning control process (2.9) provided that learning gain Φ_1 satisfies the convergence criterion. Therefore, the compensation scheme can constrain the rotor to the bearing center and make it rotate about its geometric axis. The ILC scheme for rotation about geometric axis is illustrated in Fig.2.4.

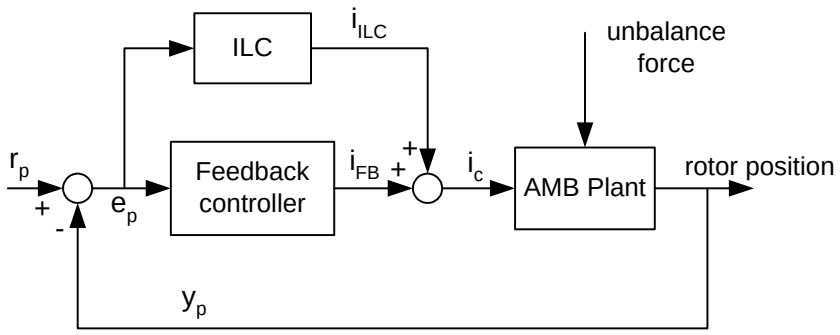

Fig. 2.4. ILC scheme for rotation about geometric axis.

2.2.2 ILC Scheme for Rotation about System Inertial Axis in AMB

The task of the ILC scheme for rotation about system inertial axis is to produce compensation current to reduce the synchronous component of current in AMB coils. Since the rotor position runout caused by unbalance is synchronous with rotational speed, the feedback controller generates corresponding synchronous control current to stabilize the AMB system. Elimination of synchronous current in AMB coils means the unbalance has no influence on AMB actuator, so the rotor is well balanced and spins about its system inertial axis. Much less copper loss in vertical PM-biased AMB is another advantage of this control mode.

In this case the coil current error signal e_i is the controller input for ILC. The learning controller becomes

$$i_{ILC,j+1}(t) = (1-\alpha) i_{ILC,j}(t) + \Phi_2 \cdot e_{i,j}(t+1+n) \tag{2.12}$$

$$e_i(t) = r_i(t) - i_c(t) \tag{2.13}$$

where i_{ILC} is the controller output, Φ_2 is the learning gain for this control scheme and i_c is the control current. The control current reference for AMB system is

$$r_i(t) = 0 \tag{2.14}$$

The control current error will converge to zero in the learning control process (2.12) if that learning gain Φ_2 satisfies the convergence criterion. The ILC scheme for rotation about system inertial axis is illustrated in Fig.2.5.

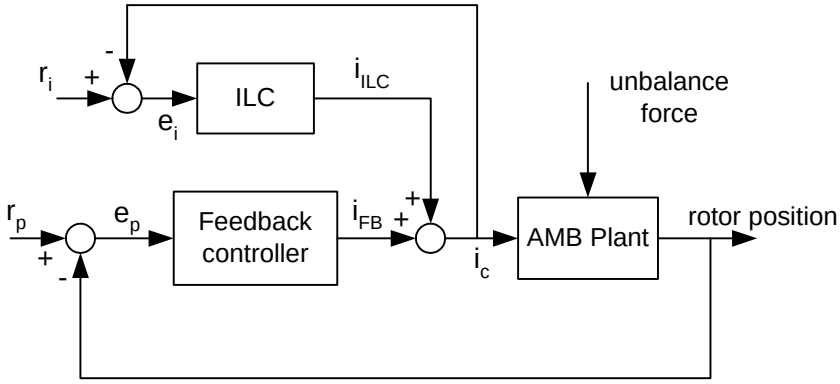

Fig. 2.5. ILC scheme for rotation about system inertial axis.

2.2.3 Decentralized Control

The learning law in (2.9) and (2.12) are designed for 1-DOF AMB control. For the whole system, there are 4 inputs and 4 outputs for the iterative learning controller. To simplify the control algorithm, decentralized control mode is used. That is to say, the 4-DOF system is divided into 4 1-DOF subsystems and the output in one subsystem is only considered in the controller dedicated for that subsystem, as illustrated in Fig. 2.6. The advantage of decentralized control is obvious: the computational load is reduced up to 75% compared to centralized control mode. The system stabilization could be assured and the influence to the system performance can hardly be observed [10].

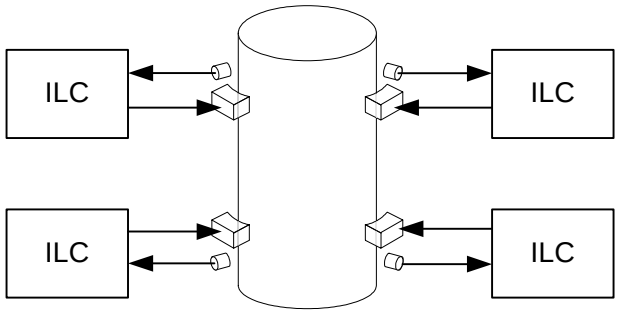

Fig. 2.6. Decentralized control mode for ILC scheme

Let X_1, X_2, Y_1, Y_2 denote the 4 radial axes of an AMB system. With decentralized control mode,

$$u_{j+1,x}(t) = (1-\alpha)u_{j,x}(t) + \Phi_x \cdot e_{j,x}(t+1+n), \quad x \in (X_1, X_2, Y_1, Y_2), \qquad (2.15)$$

where x denotes the name of an axis, $u_{j,x}(t)$ is the ILC output for axis x, $e_{j,x}(t)$ is the error signal for axis x, and Φ_x is the learning gain for axis x.

3. Automatic Learning Control for Unbalance Compensation

3.1 Introduction of Automatic Learning Control

In this chapter a novel concept of automatic learning control (ALC) is introduced for unbalance control with AMB. Based on time-domain ILC, ALC is proposed for better performance against speed fluctuation and flexible operating conditions. Because the ILC unbalance compensation scheme in Chapter 2 is developed for a fixed rotational speed, it is not suitable for the case when motor speed varies. In addition, this ILC scheme is sensitive to the speed disturbance during operation. Although it is still able to maintain stability within a limited range, poor control performance could be observed with the existence of small speed disturbance. Therefore, an improved controller, which can operate in a wide range of speed, is needed in order to obtain better control performance in unbalance compensation.

ALC is based on time-domain ILC. Its basic idea is described as follows.

1. Learning gains for different rotational speeds are stored in a look-up table for use during operation.
2. Obtain the synchronous component from original signal.
3. Use interpolation method to compute the corresponding learning gains for current rotational speed.

4. Change the length of learning cycle with the rotational speed and keep it equal to the synchronous period.

In step 3, the learning gains are automatically determined. In step 4, the length of a learning cycle is automatically determined.

3.1.1 Process Synchronous Signals

Generally in ILC, a low-pass filter is required because the high-frequency noise can make the learning process unstable. In ALC, the controller works in a wide range of rotational speeds, so the filter should be able to obtain the synchronous signals from original signals no matter what the rotational speed is. Fourier analysis technique is used in ALC to process synchronous signal. The synchronous signal can be obtained according to (3.1)-(3.3).

$$a = \frac{2}{T}\int_{t_0}^{T+t_0} y_o(t)\sin\omega t\mathrm{d}t \tag{3.1}$$

$$b = \frac{2}{T}\int_{t_0}^{T+t_0} y_o(t)\cos\omega t\mathrm{d}t \tag{3.2}$$

$$y_\omega(t) = a\cdot\sin\omega t + b\cdot\cos\omega t \tag{3.3}$$

where $y_o(t)$ is the original signal, $y_\omega(t)$ is the synchronous signal, ω is the rotational angular velocity, T is the rotational period, a is the amplitude of synchronous sine component, and b is the amplitude of synchronous cosine component. The process of obtaining synchronous is shown in Fig. 3.1.

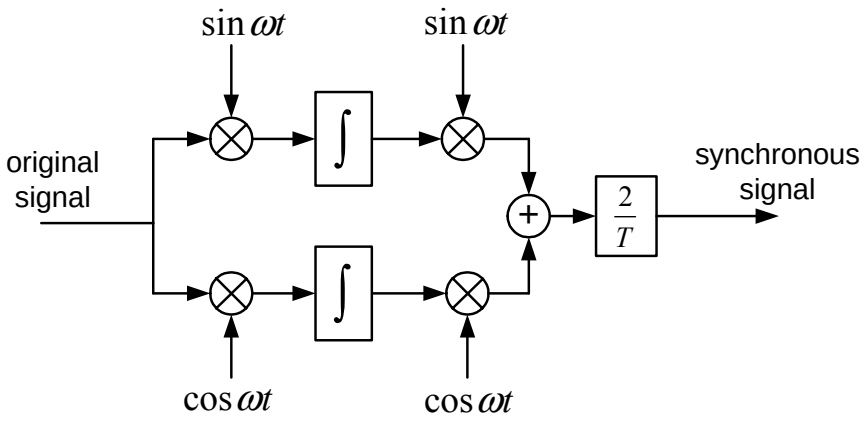

Fig. 3.1. Functional block diagram of processing synchronous signal.

3.1.2 Gain-Scheduled Control

According to [10],[38][37], the changing of rotational speed could lead to the variation of AMB plant parameters, so a learning gain effective in one rotational speed may lead to instability in another rotational speed. To solve this problem, the controller in ALC should be able to adjust its learning gain according to different rotational speeds. Gain-scheduled control is employed to achieve different learning gains according to rotational speeds. The learning law becomes

$$u_{j+1}(t) = (1-\alpha)u_j(t) + \Phi(\omega)\cdot e_j(t+1) \tag{3.4}$$

Suitable learning gains for a set of speeds covering the operating speed range are obtained beforehand. The learning gain for one speed is simply determined by manual tuning, like the tuning process for a feedback controller. As shown in the last chapter, the learning gain should satisfy the convergence criterion, equation (2.4). In practical, although a larger learning gain can give faster convergence rate, a smaller learning gain is more desirable because fluctuations in the error are smaller after steady-state is reached. Once a learning gain for one speed is determined, it is recorded and the

motor is set to the next speed in the look-up table. The tuning process is then repeated for the new speed to get a new learning gain. Once all the learning gains have been determined, they are stored in a look-up table. During operation, the controller can automatically adjust its learning gains according to the rotational speed. For a particular rotational speed, the learning gain can be calculated by linear interpolation [59] between the learning gains for the two nearest speeds in the table. For a rotational speed ω, the learning gain Φ is

$$\Phi(\omega) = \Phi_a + (\omega - \omega_a) \cdot \frac{\Phi_b - \Phi_a}{\omega_b - \omega_a} \tag{3.5}$$

where ω_a and ω_b are the two nearest speeds in the table, Φ_a is the learning gain for speed ω_a, and Φ_b is the learning gain for speed ω_b.

Operating in the decentralized control mode, the ALC controller needs only one learning gain for each DOF at one speed. In comparison with the complicated gain matrices used in AVC [37], these learning gains occupy very little memory space in digital controllers. In addition, the computation complexity is much reduced.

3.1.3 Variable Learning Cycle

In the ILC scheme for AMB unbalance compensation, the length of a learning cycle is fixed. This limits the function of ILC to a specific rotational speed. An ILC controller designed for one rotational speed cannot work at another rotational speed. Furthermore, because the controller cannot adjust itself in presence of speed variation, it is sensitive to the rotational speed disturbance. This speed disturbance could adversely influence the control performance of ILC. If the speed disturbance is large enough, it could even affect the stability of ILC.

In ALC, the length of learning cycle is not fixed. Variable learning cycle is used to adapt the controller to the changing speed. The length of learning cycle varies with the rotational speed during operation and it is kept equal to the rotational period of the motor. The performance comparisons of ALC and ILC against speed disturbance are shown in the simulations and experiments of the following chapters.

The learning law of ALC can thus be described by

$$u_{j+1}(t) = (1-\alpha)u_j(t) + \Phi(\omega)\cdot e_j(t+1), \quad t \in 0,1,2,...,t_f(\omega)-1 \tag{3.6}$$

$$t_f(\omega) = \frac{2\pi f_s}{\omega} \tag{3.7}$$

where f_s is the sampling frequency.

The proposed ALC scheme is illustrated in Fig. 3.2.

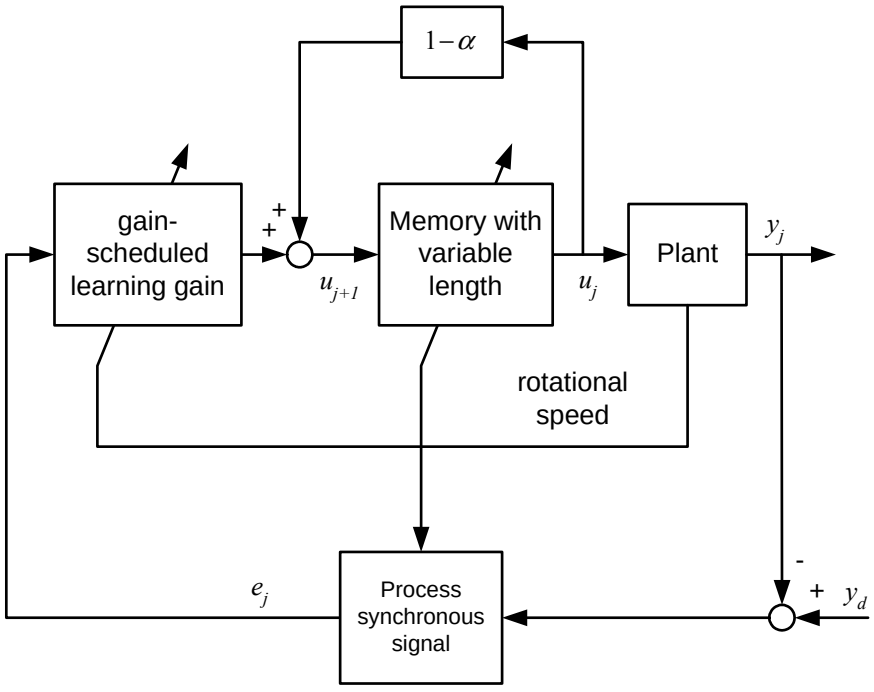

Fig. 3.2. Automatic Learning Control Scheme

3.2 ALC scheme for Unbalance Compensation in AMB

Similarlar to the ILC scheme, ALC aims to provide suitable currents or forces to achieve the task of unbalance compensation with AMB, rotation about geometric axis or system inertial axis.

For rotation about geometric axis, the controller (3.6) becomes

$$i_{ALC,j+1}(t) = (1-\alpha) i_{ALC,j}(t) + \Phi_1(\omega) \cdot e_{p,j}(t+1) \tag{3.8}$$

$$e_p(t) = r_p(t) - y_p(t) \tag{3.9}$$

where i_{ALC} is the controller output. The rotor position reference for AMB system is

$$r_p(t) = 0 \tag{3.10}$$

The ALC scheme for rotation about geometric axis is illustrated in Fig. 3.3.

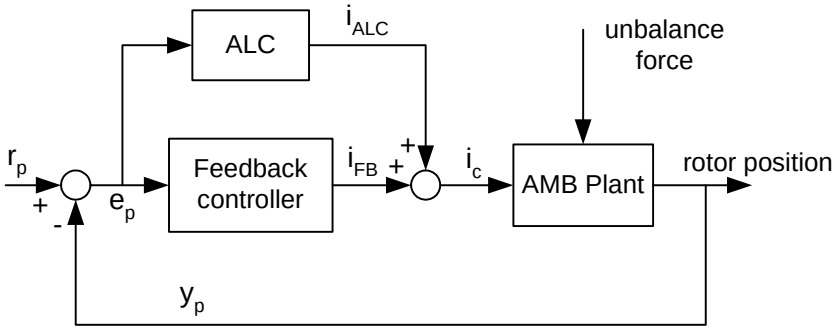

Fig. 3.3. ALC Scheme for Rotation about Geometric Axis

For rotation about system inertial axis, the learning controller in (3.6) becomes

$$i_{ALC,j+1}(t) = (1-\alpha) i_{ALC,j}(t) + \Phi_2(\omega) \cdot e_{i,j}(t+1) \tag{3.11}$$

$$e_i(t) = r_i(t) - i_c(t) \tag{3.12}$$

The control current reference for the controller is

$$r_i(t) = 0 \tag{3.13}$$

The ALC scheme for rotation about system inertial axis is illustrated in Fig. 3.4.

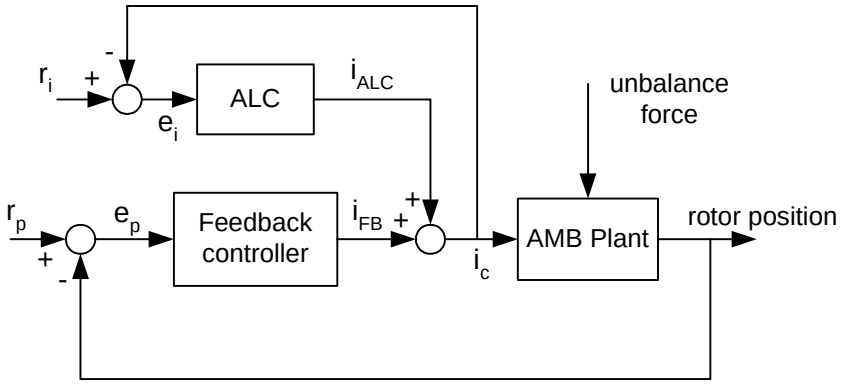

Fig. 3.4. ALC scheme for Rotation about System Inertial Axis

In order to simplify the control algorithm, ALC also employs decentralized control mode, i.e. output of a subsystem is only considered in the controller of that subsystem. If the real-time vibration information can be obtained, ALC can be employed directly for active vibration control. The vibration signal can also be used as the controller input, and the learning law becomes

$$i_{ALC,j+1}(t) = (1-\alpha) i_{ALC,j}(t) + \Phi_v(\omega) \cdot e_{v,j}(t+1), \tag{3.14}$$

$$e_v(t) = r_v(t) - v(t), \tag{3.15}$$

where $v(t)$ is the vibration signal, and $r_v(t)$ is the reference signal.

4. Simulation Results

4.1 A 4-DOF AMB Model

In this section, a 4-DOF AMB model is built for simulating the AMB system used in the experiments. Several assumptions are considered for the dynamic modeling of the shaft shown in Fig.4.1.

1. The shaft is regarded as a rigid body. No flexible deformation exists.
2. The AMB system is electrically and geometrically symmetric, except in the case of unbalance.
3. The position sensors are aligned with corresponding magnetic actuators.
4. All radial axes have an angle of 45^0 with the vertical direction because of the configuration of radial bearings in our experimental setup (see Fig. 5.4).

In Figure 4.1, x_1 and y_1 are the shaft displacements of bearing 1 in axis X and Y, respectively. x_2 and y_2 are the shaft displacements of bearing 2 in axis X and Y, respectively. x and y are the shaft displacements of shaft gravity center s in axis X and Y, respectively. γ and β are the inclination angles of the shaft, and the rotating angular velocity is ω.

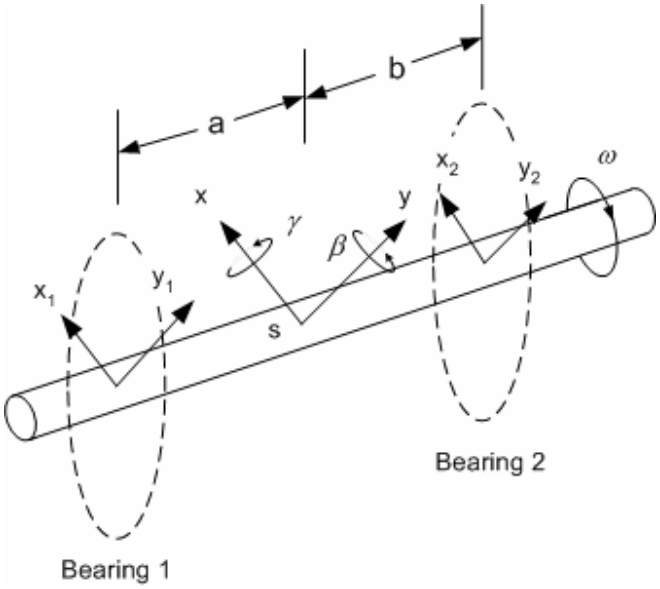

Fig. 4.1. Radial bearing 1 and 2

The motion equation of the mechanical part can be described with (4.1) [10]

$$\begin{bmatrix} m & 0 & 0 & 0 \\ 0 & I & 0 & 0 \\ 0 & 0 & m & 0 \\ 0 & 0 & 0 & I \end{bmatrix} \begin{bmatrix} \ddot{x} \\ \ddot{\beta} \\ \ddot{y} \\ \ddot{\gamma} \end{bmatrix} + \begin{bmatrix} 0 & 0 & 0 & 0 \\ 0 & 0 & 0 & -I_r\omega \\ 0 & 0 & 0 & 0 \\ 0 & I_r\omega & 0 & 0 \end{bmatrix} \begin{bmatrix} \dot{x} \\ \dot{\beta} \\ \dot{y} \\ \dot{\gamma} \end{bmatrix} = \begin{bmatrix} f_x \\ p_y \\ f_y \\ p_x \end{bmatrix} - \begin{bmatrix} 0.707mg \\ 0 \\ 0.707mg \\ 0 \end{bmatrix} \tag{4.1}$$

where f_x and f_y are the forces in axis X and axis Y, p_x and p_y are the torques about axis X and axis Y, m is the mass of shaft, mg is the gravity, and I is the moment of inertia for axis X and axis Y, I_r is the moment of inertia for rotational axis.

It is obvious that

$$\begin{bmatrix} x \\ \beta \\ y \\ \gamma \end{bmatrix} = \frac{1}{a+b} \begin{bmatrix} b & a & 0 & 0 \\ -1 & 1 & 0 & 0 \\ 0 & 0 & b & a \\ 0 & 0 & 1 & -1 \end{bmatrix} \begin{bmatrix} x_1 \\ x_2 \\ y_1 \\ y_2 \end{bmatrix} = T \begin{bmatrix} x_1 \\ x_2 \\ y_1 \\ y_2 \end{bmatrix}, \tag{4.2}$$

where the coordination transfer matrix is

$$T = \frac{1}{a+b}\begin{bmatrix} b & a & 0 & 0 \\ -1 & 1 & 0 & 0 \\ 0 & 0 & b & a \\ 0 & 0 & 1 & -1 \end{bmatrix}, \tag{4.3}$$

and the force vector

$$\begin{bmatrix} f_x \\ p_y \\ f_y \\ -p_x \end{bmatrix} = \begin{bmatrix} 1 & 1 & 0 & 0 \\ -a & b & 0 & 0 \\ 0 & 0 & 1 & 1 \\ 0 & 0 & a & -b \end{bmatrix}\begin{bmatrix} f_{x1} \\ f_{x2} \\ f_{y1} \\ f_{y2} \end{bmatrix}. \tag{4.4}$$

From (4.3)-(4.4),

$$\begin{bmatrix} f_{x1} \\ f_{x2} \\ f_{y1} \\ f_{y2} \end{bmatrix} = \frac{1}{a+b}\begin{bmatrix} b & -1 & 0 & 0 \\ a & 1 & 0 & 0 \\ 0 & 0 & b & 1 \\ 0 & 0 & a & -1 \end{bmatrix}\begin{bmatrix} f_x \\ p_y \\ f_y \\ p_x \end{bmatrix} = T^T f_L, \tag{4.5}$$

where

$$f_L = \begin{bmatrix} f_x & p_y & f_y & p_x \end{bmatrix}^T \tag{4.6}$$

$$M_g = \begin{bmatrix} 0.707mg & 0 & 0.707mg & 0 \end{bmatrix}^T \tag{4.7}$$

In (4.6) f_{x1} and f_{y1} are the control forces of bearing 1 in axis X and axis Y, respectively. f_{x2} and f_{y2} are the control forces of bearing 2 in axis X and axis Y, respectively.

From (4.1)-(4.7), the new motion equation is

$$T^T M T\ddot{z}_L + T^T G T\dot{z}_L = f_L - T^T M_g, \tag{4.8}$$

where

$$M = \begin{bmatrix} m & 0 & 0 & 0 \\ 0 & I & 0 & 0 \\ 0 & 0 & m & 0 \\ 0 & 0 & 0 & I \end{bmatrix}, \tag{4.9}$$

$$G = \begin{bmatrix} 0 & 0 & 0 & 0 \\ 0 & 0 & 0 & -I_r\omega \\ 0 & 0 & 0 & 0 \\ 0 & I_r\omega & 0 & 0 \end{bmatrix}, \tag{4.10}$$

$$z_L = \begin{bmatrix} x_1 & x_2 & y_1 & y_2 \end{bmatrix}^T \tag{4.11}$$

According to the linearized force equation (1.5),

$$f_L = \begin{bmatrix} K_s & 0 & 0 & 0 \\ 0 & K_s & 0 & 0 \\ 0 & 0 & K_s & 0 \\ 0 & 0 & 0 & K_s \end{bmatrix} z_L + \begin{bmatrix} K_i & 0 & 0 & 0 \\ 0 & K_i & 0 & 0 \\ 0 & 0 & K_i & 0 \\ 0 & 0 & 0 & K_i \end{bmatrix} \begin{bmatrix} i_{x1} \\ i_{x2} \\ i_{y1} \\ i_{y2} \end{bmatrix} = K_{sL} z_L + K_{iL} u, \tag{4.12}$$

where

$$K_{sL} \triangleq \begin{bmatrix} K_s & 0 & 0 & 0 \\ 0 & K_s & 0 & 0 \\ 0 & 0 & K_s & 0 \\ 0 & 0 & 0 & K_s \end{bmatrix}, \tag{4.13}$$

$$K_{iL} = \begin{bmatrix} K_i & 0 & 0 & 0 \\ 0 & K_i & 0 & 0 \\ 0 & 0 & K_i & 0 \\ 0 & 0 & 0 & K_i \end{bmatrix}, \tag{4.14}$$

$$u = \begin{bmatrix} i_{x1} & i_{x2} & i_{y1} & i_{y2} \end{bmatrix}^T. \tag{4.15}$$

Therefore,

$$T^T M T \ddot{z}_L + T^T G T \dot{z}_L = K_{sL} z_L + K_{iL} u - T^T M_g \tag{4.16}$$

we set

$$M_L = T^T M T \tag{4.17}$$

$$G_L = T^T G T \tag{4.18}$$

then

$$M_L \ddot{z}_L + G_L \dot{z}_L = K_{sL} z_L + K_{iL} u - T^T M_g \tag{4.19}$$

Define the state vector

$$z_s = \begin{bmatrix} z_L \\ \dot{z}_L \end{bmatrix} = \begin{bmatrix} x_1 & x_2 & y_1 & y_2 & \dot{x}_1 & \dot{x}_2 & \dot{y}_1 & \dot{y}_2 \end{bmatrix}^T \tag{4.20}$$

and matrices

$$A_s = \begin{bmatrix} 0^{4\times4} & I^{4\times4} \\ M_L^{-1} K_{sL} & -M_L^{-1} G_L \end{bmatrix}, \tag{4.21}$$

$$B = \begin{bmatrix} 0^{4\times4} \\ M_L^{-1} K_{iL} \end{bmatrix}, \tag{4.22}$$

$$M_{gL} = \begin{bmatrix} 0^{1\times4} \\ M_L^{-1} T^T M_g \end{bmatrix} \tag{4.23}$$

$$C_s = \begin{bmatrix} 1 & 1 & 1 & 1 & 0 & 0 & 0 & 0 \end{bmatrix} \tag{4.24}$$

The 4-input-4-output AMB plant could be described as

$$\begin{aligned} \dot{z}_s &= A_s z_s + B u - M_{gL} \\ y_s &= C_s z_s \end{aligned}. \tag{4.25}$$

Use a new input u_s to replace u

$$u_s = u - K_{iL}^{-1} T^T M_g, \tag{4.26}$$

then the plant becomes

$$\begin{aligned} \dot{z}_s &= A_s z_s + B u_s \\ y_s &= C_s z_s \end{aligned} \tag{4.27}$$

The simulation parameters for a 4-DOF AMB system are listed in Table 4.1.

Table 4.1. Simulation parameters

Description	Name	Values
Moment of inertia for axis X and axis Y	I	0.0237 kg·m^2
Moment of inertia for rotating axis	I_r	3.989×10^{-4} kg·m^2
Total mass of the rotor	m	1.5410 kg
Distance between mass center and bearing 1	a	0.1753 m
Distance between mass center and bearing 2	b	0.1562 m
Force-displacement factor	K_s	57.97 N/μm
Force-current factor	K_i	30.45 N/A

4.2 Simulation of reducing rotor runout

The simulation of reducing rotor runout with ILC and ALC schemes is carried out with MATLAB/SIMULINK. The 4-DOF AMB model is discretized with a sampling frequency of 10k Hz. The unbalance force is represented by synchronous sine waves with the same amplitude and different initial phases in different axes. Because the bandwidth of position sensors used in AMB experiment system is far beyond rotational frequency, the position sensors are regarded as constant gains in the model. A PID controller is used to stabilize the AMB system.

4.2.1 Simulation Results with a Constant Speed

The effectiveness of the ILC scheme is firstly examined. The rotational speed is set to be 3000rpm (i.e., the 1st order mechanical frequency is 50Hz). The ILC parameters for the 4-DOF are identical as

$$\text{Learning gain: } \Phi = 1.2\times10^{-3}\, A/\mu m\,, \tag{4.28}$$

$$\text{Forgetting Factor: } \alpha = 0.005 . \tag{4.29}$$

The number of time steps t_f in one learning cycle for the ILC controller is set to be 200 in order to compensate synchronous unbalance disturbance. In the first half second, only PID controller works to control the AMB system. When time t = 0.5s, the ILC controller is switched on to work together with the PID controller. The transient response of rotor position is shown in Fig. 4.2. It can be observed that when the ILC is used, the amplitude of rotor runout in this DOF can be reduced to a very small level within a short time.

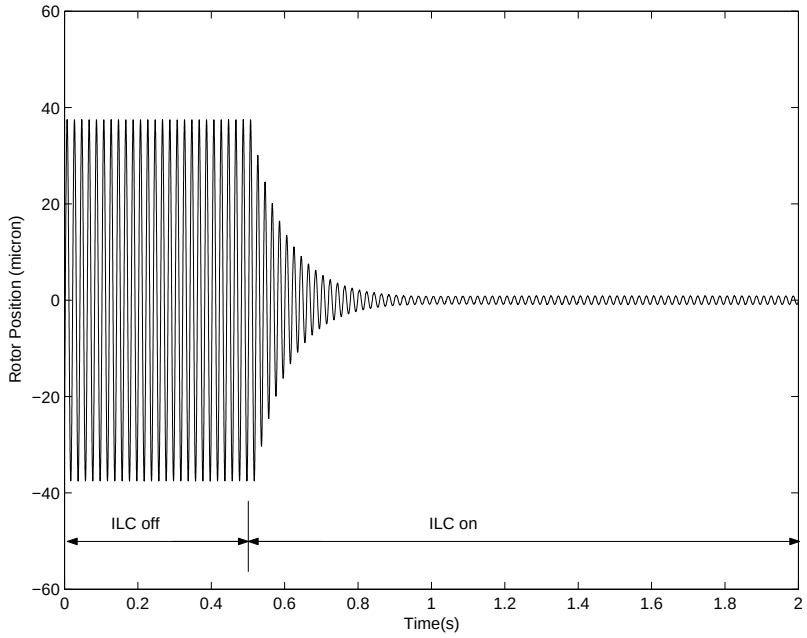

Fig. 4.2. Transient Response of rotor runout with ILC

The steady-state rotor runout is shown in Fig. 4.3 and Fig. 4.4. The amplitude of rotor runout before ILC turning on is 37.5μm. After ILC's turning on, the amplitude of rotor runout is 1.5μm.

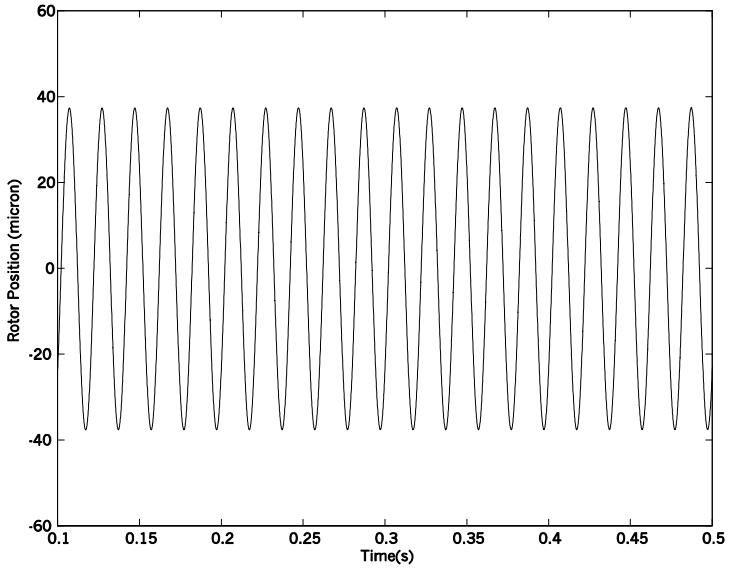

Fig. 4.3. Steady-state rotor runout without unbalance compensation.

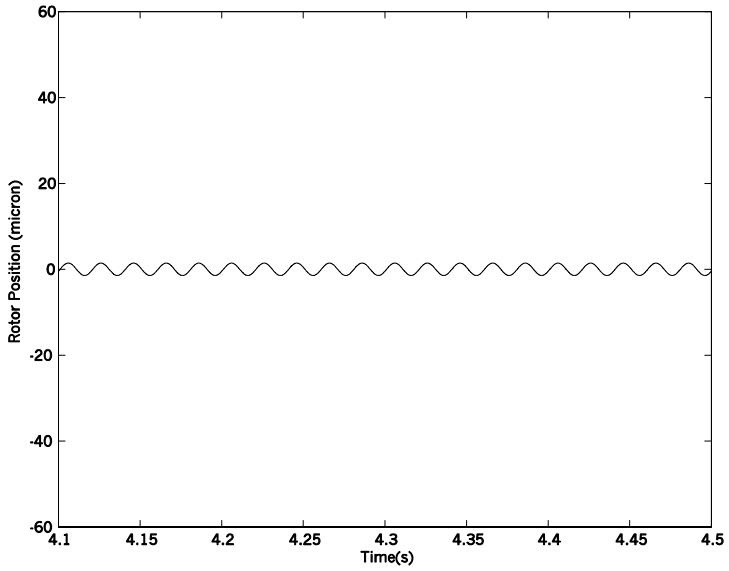

Fig. 4.4. Steady-state rotor runout with ILC

The unbalance compensation with ALC is also simulated. Fig. 4.5 shows the transient response of rotor runout when ALC is used in the AMB system to make the rotor rotate about its geometric axis. In the first half second, only PID controller works to control the AMB system. When time t = 0.5s, the ALC controller is switched on to work together with the PID controller.

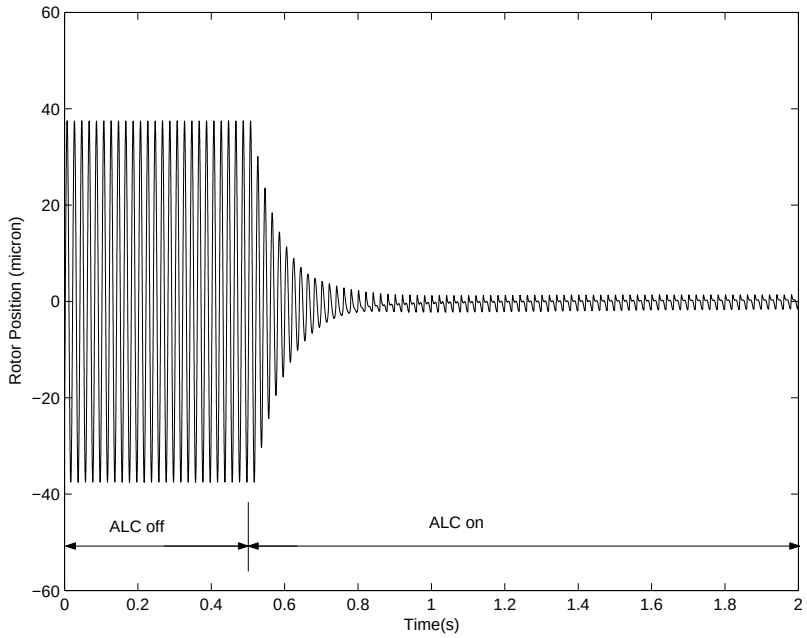

Fig. 4.5. Transient response of rotor runout with ALC.

The steady-state response of rotor runout with ALC is shown in Fig. 4.6. The amplitude of rotor runout with ALC is also 1.5μm.

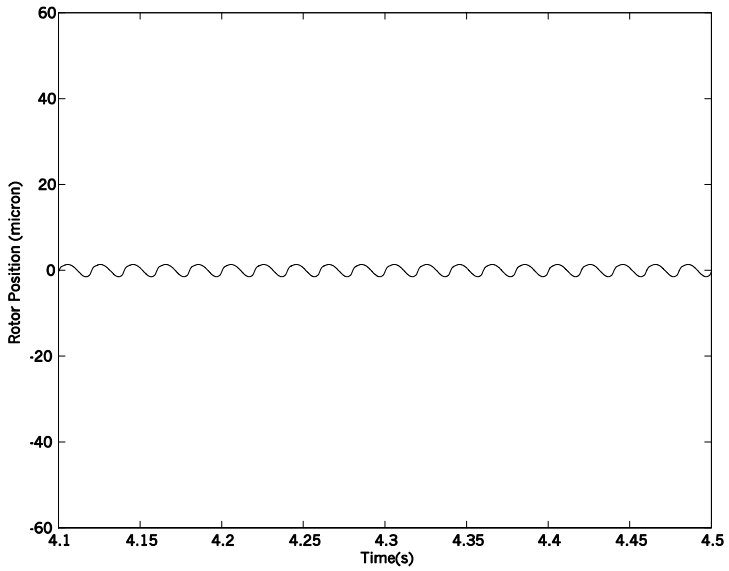

Fig. 4.6. Steady-state rotor runout with ALC.

In simulation results of the constant speed test, both ILC and ALC present good control effect in unbalance compensation. It can be seen from the simulation results

that neither controller can reduce the rotor's repeatable runout to zero. It is due to the existence of the forgetting factor. Theoretically the rotor's repeatable runout can be decreased to zero in the ideal state where the forgetting factor is set to be 0. Fig. 4.7 shows the simulation result when the forgetting factor of ILC controller is set to be 0.

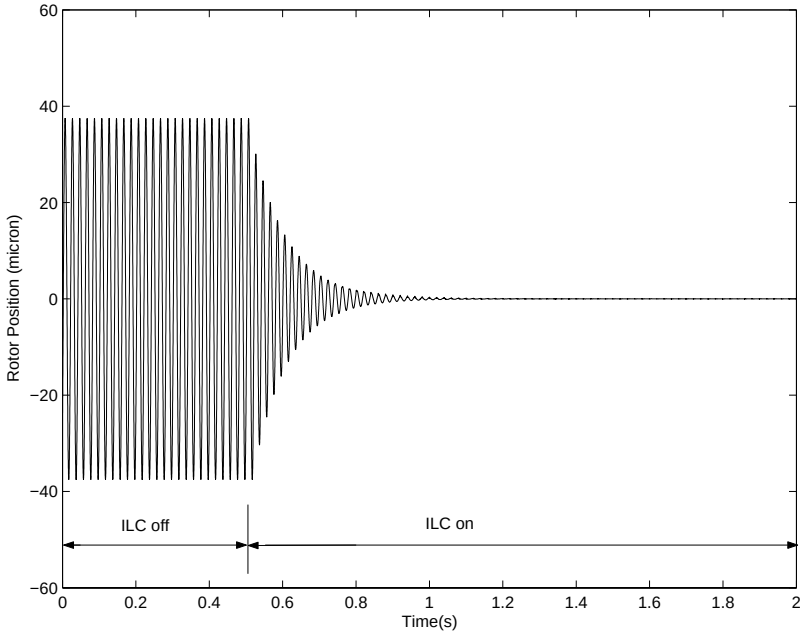

Fig. 4.7. Transient response of rotor runout when $\alpha = 0$.

4.2.2 Simulation with speed fluctuations

Simulation with speed fluctuation is also carried out to show the performance of ALC and ILC under this condition. t_f for ILC controller is still set to be 200 in order to compensate synchronous unbalance disturbance of 50Hz. The simulation condition is set to be:

- From 0 to 2sec., the rotational frequency is 50Hz.
- From 2sec., the rotational frequency is changed to 49Hz.
- Unbalance force and PID controller is same as the previous simulations.

Three simulation tests are carried out, ILC with zero forgetting factor, ILC with a forgetting factor of 0.005, ALC with a forgetting factor of 0.005.

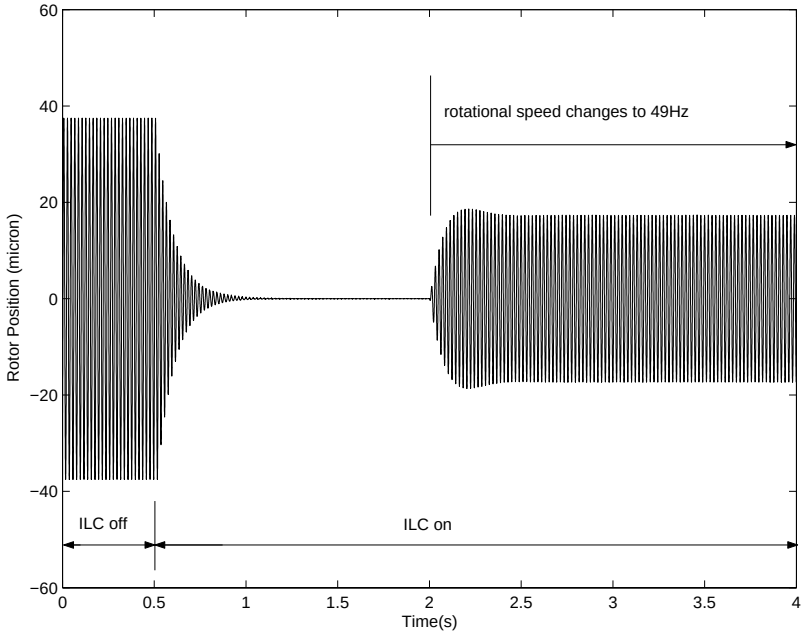

Fig. 4.8. Transient response of ILC with a zero forgetting factor

Fig. 4.8 shows the transient response of ILC with a zero forgetting factor. In the first two seconds, the ILC controller works well at the speed of 3000rpm. Because no disturbances and noises exist in the simulation, the ILC controller can keep stable and rotor runout quickly decreases to zero. However, when the rotor frequency is changed to 49Hz, the ILC controller presents bad performance in this condition. Rotor runout quickly rises and the amplitude of steady-state rotor runout is up to 17.3μm.

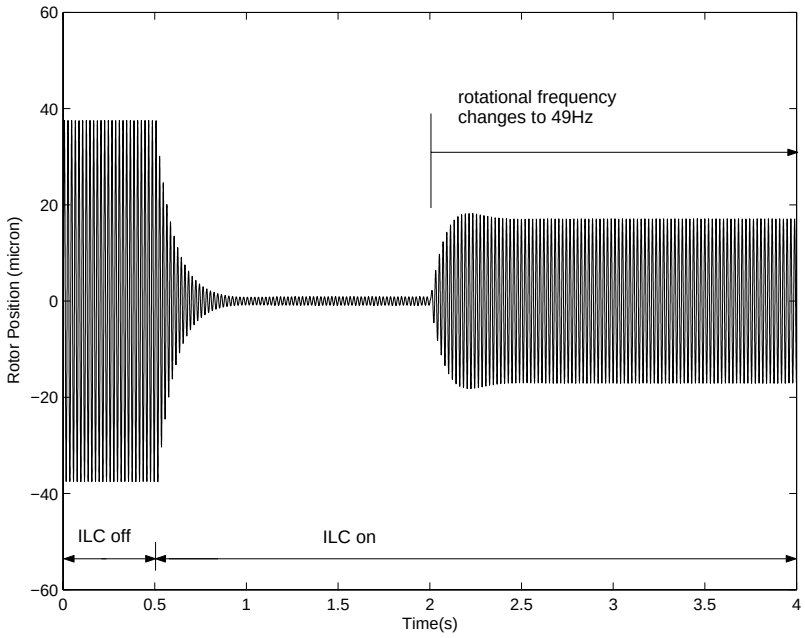

Fig. 4.9. Transient response of ILC with a forgetting factor of 0.005

Fig. 4.9 shows the simulation result of ILC with a forgetting factor of 0.005 when the rotor speed is changing. It can be observed that when the rotational speed changes, rotor runout also quickly rises to a large value. Although the forgetting factor can provide enough robustness during operation, in this case the ILC controller with forgetting factor has very limited advantage over its counterpart without forgetting factor. The amplitude of steady-state rotor runout after 2sec is 17μm. The limited improvement attributes to the small value of forgetting factor. If increase α, the performance during speed fluctuation could be improved, but its performance at constant speed will degrade.

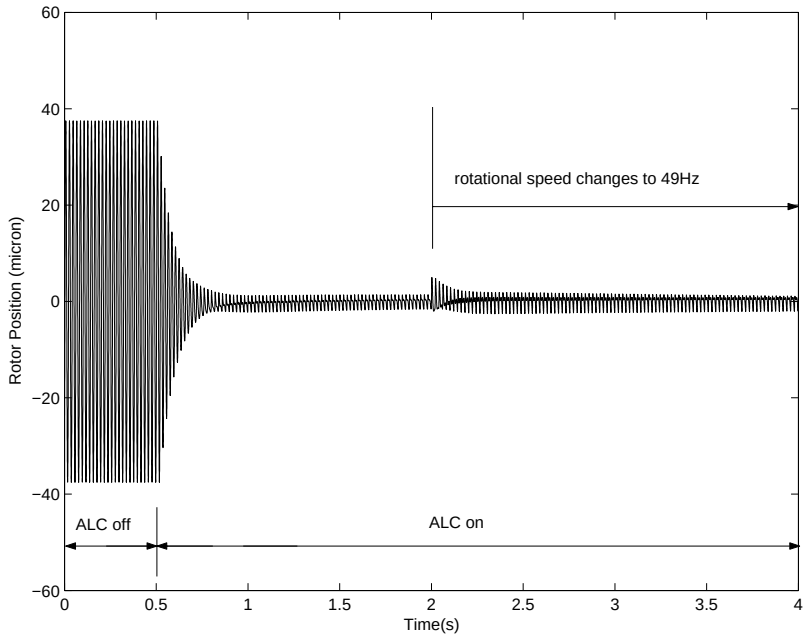

Fig. 4.10. Transient response of ALC with $\alpha = 0.005$

Fig. 4.10 shows the rotor runout with ALC during the period of speed variation. In comparison with the first two controllers, ALC presents much better control performance in this case. When the speed is changing, only a small runout peak appears in the simulation result. Then the rotor quickly resumes to normal condition. The amplitude of steady-state rotor runout is only 2μm. Detailed comparison of the three controllers is shown in Table 4.2.

Table 4.2. Performance comparisons of the three controllers

	ILC ($\alpha = 0$)	ILC ($\alpha = 0.005$)	ALC ($\alpha = 0.005$)
Runout at 50 Hz	0	1.5μm	1.5μm
Peak during speed changing	18.6μm	18.2μm	4μm
Steady-state runout after $t = 2$sec	17.2μm	17.0μm	2μm

The ALC controller has obvious advantage over ILC controllers in the situation of rotational speed fluctuation. The forgetting factor (α = 0.005) can bring limited improvement in this case.

4.3 Simulation Results of Current Fluctuation Reduction

Simulation results of current fluctuation reduction are shown in this section. The simulation condition is same as that in section 4.2. In the first 0.5 second, only PID controller is used, and then the ILC or ALC controller begins to work together with the PID controller. In the first 2 seconds, the rotational frequency is 50Hz, and then it is changed to 49Hz. The number of time steps t_f in each learning cycle for the ILC controller is also set to be 200 in this section.

Controller parameters in the simulation are:

$$\text{forgetting factor } \Phi = 0.07 \tag{4.30}$$

$$\text{forgetting factor } \alpha = 0.005 \tag{4.31}$$

Transient responses of control currents with ILC and ALC schemes are shown in Fig. 4.11 and Fig. 4.12, respectively. The control currents have a constant bias because the integral part of the PID controller produces a constant bias component to counteract gravity. It can be observed that in the first 2 seconds (rotational speed: 50Hz), both the ILC controller and the ALC controller work well and the fluctuations of current are obviously reduced. After the rotational frequency is changed to 49Hz, only the ALC controller can maintain the control performance as before. This is same as the simulation result in section 4.2.

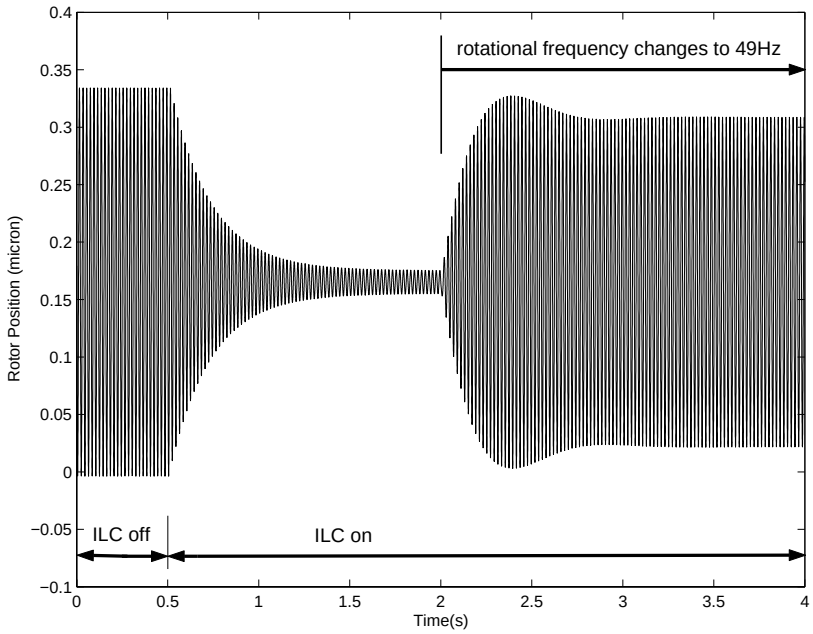

Fig. 4.11. Transient response of control current with ILC scheme

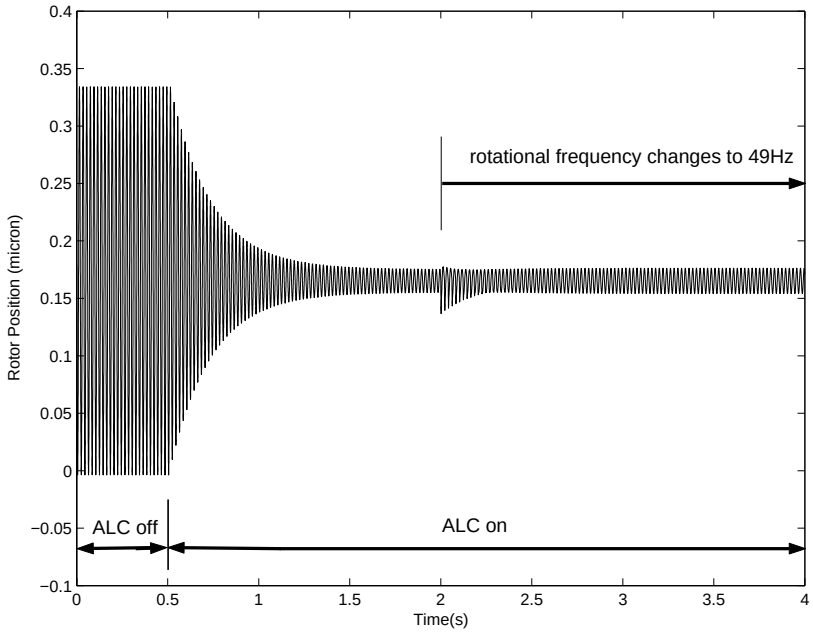

Fig. 4.12. Transient response of control current with ALC scheme

5. Experimental Results

In this chapter effectiveness of proposed ILC scheme and ALC scheme are tested through experiments. Section 5.1 presents the overview of the experimental setup in the research work. Section 5.2 briefly introduces the system hardware for AMB unbalance control experiments. The experimental results of unbalance control are described in the following four sections. Section 5.3 gives the experimental result of the ILC scheme. Section 5.4 describes the rotor runout experiment with ALC scheme, while Section 5.5 describes the experiment of reducing coil current fluctuations with ALC scheme. The control performances of proposed ILC scheme and ALC scheme during rotational speed fluctuation are compared in Section 5.6. Section 5.7 discusses experimental results and some observations in the experiments.

5.1 Experimental Setup

An AMB experimental setup has been built for AMB research works in DSI. The experimental setup consists of

1. A set of AMB system, which includes a magnetic bearing machine, a control box, and an interface box.
2. A dSPACE 1103 system for executing control programs, generating control signals, and performing A/D, D/A conversions.

3. A PC for operating AMB software and Matlab/Simulink software as well as monitoring AMB working conditions.

Fig. 5.1 shows the experimental setup configuration for the unbalance control experiment.

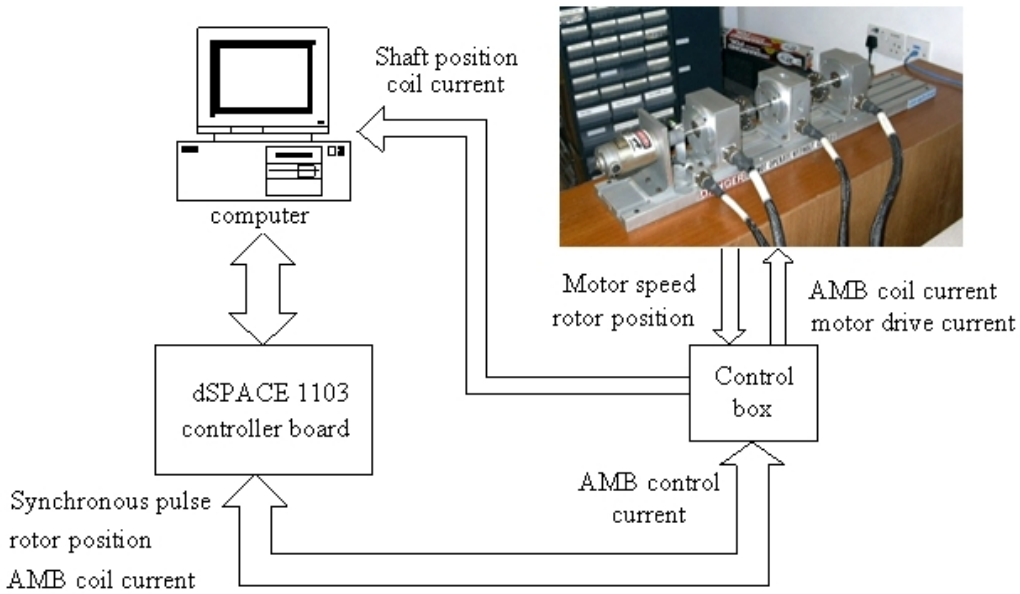

Fig. 5.1. Configuration for the AMB unbalance control experiment

5.2 System Hardware

The experimental system hardware consists of a set of AMB system and dSPACE DS1103 system. In the following subsections, these experimental facilities will be briefly introduced.

5.2.1 AMB Experimental System

The AMB experimental system is composed of a magnetic bearing machine and a control box.

5.2.1.1 The Magnetic Bearing Machine

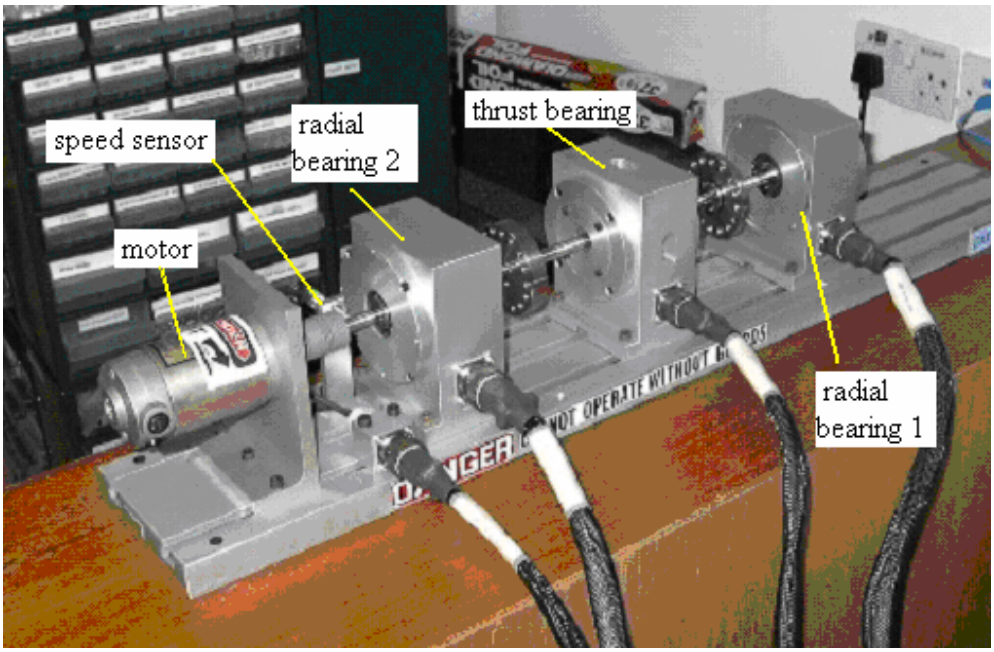

Fig. 5.2. The AMB machine in experiments

The AMB machine is shown in Fig. 5.2. In order to realize magnetic suspension in all DOF, three magnetic bearings were used in the machine. Two radial bearings are used to control shaft motion in radial directions, and one thrust bearing controls the shaft motion in axial axis. The AMB shaft is driven by a DC motor, which makes the shaft rotate at the set speed of the motor. The structure of the AMB machine is illustrated in Fig. 5.3.

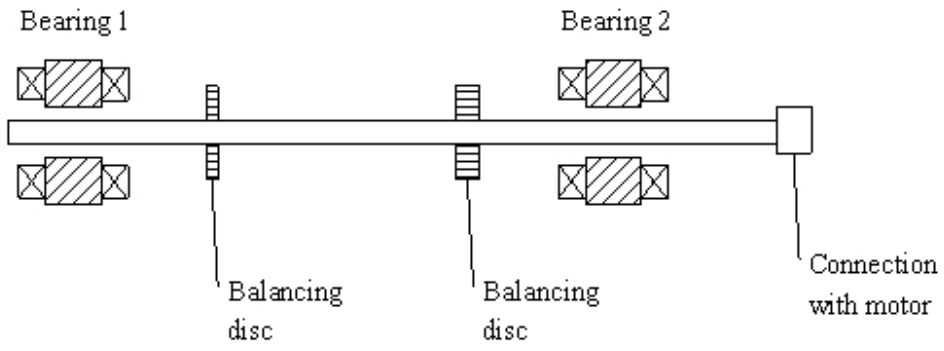

Fig. 5.3. The structure of the AMB machine.

The EM and mechanical parameters are same as the simulation parameters used in the previous chapter. See Table 4.1 for details. The two radial magnetic bearings are magnetically and mechanically identical. Each radial bearing can realize 2-DOF magnetic suspensions, as shown in Fig. 5.4. The two axes are perpendicular to each other and each axis has a 45^0 angle with the vertical direction. Variable reluctance position sensors are used to detect shaft position information in each DOF.

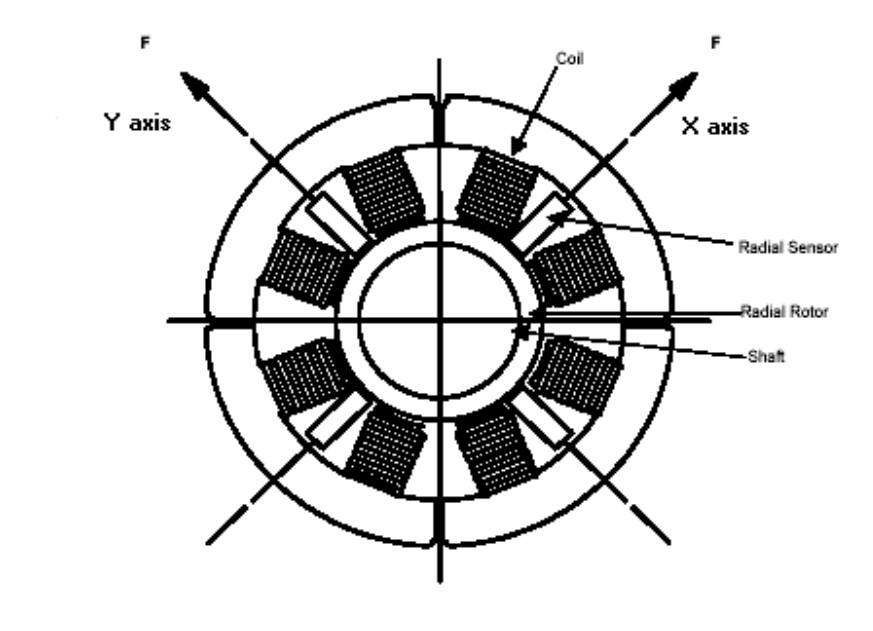

Fig. 5.4. A radial bearing

5.2.1.2 The Control Box

The control box of AMB experimental system is used to

1. Set operation parameters of the AMB system, such as motor speed.
2. Amplify control signals and provide currents to AMB coils.
3. Create communication between AMB machines and computers.
4. Transfer signals to the dSPACE DS1103 controller board. The signals are system output signals from sensors.
5. Get control signals from the dSPACE DS1103 controller board.

5.2.2 dSAPCE DS1103 Controller Board

The dSPACE DS1103 controller board is a real-time digital control development environment for control design, function prototyping, electronic control unit (ECU) testing, etc. To realize rapid control prototyping, the DS1103 controller board is equipped with a PowerPC 604e running at 400 MHz, a Slave DSP TMF320F240, A/D and D/A converters, programmable digital I/O ports, and PWM generation ports. The DS1103 controller board can be directly inserted into the ISA slot of a PC. The voltage range for A/D and D/A converter is from –10V to 10V.

In the experiment, the controllers are built and tuned in Matlab/Simulink. Then the control algorithm can be loaded to the DS1103 controller board to do real-time control works. Hardware working conditions can be monitored through an oscilloscope or the ControlDesk software, which is provided to work together with DS1103. In this process, DS1103 is actually working as a digital controller that can directly employ the control algorithm in Simulink.

5.3 ILC Scheme for Unbalance Compensation

In this section, the proposed ILC scheme for unbalance compensation is evaluated through experiments. The AMB system is stabilized by a decentralized PID controller. When ILC is turned off, only the PID controller works. When ILC is turned on, it works together with the PID controller. In the experiment the sampling frequency for A/D and D/A conversion is 10 kHz. The rotational speed in the experiment is set to be 2800rpm, so the synchronous frequency is 46.67Hz.

5.3.1 ILC Scheme for Rotor Runout Reduction

Time-domain ILC scheme is used to reduce rotor runout as proposed in section 2.2.1. The low-pass filter in ILC scheme is a Butterworth low-pass filter and its cut-off frequency is 75Hz. The learning gain is 0.12 A/μm. Forgetting factor is 0.005. Rotor position orbits without compensation and with ILC compensation are recorded from Fig. 5.5 to Fig. 5.8.

The maximum runout of bearing 1 without ILC is 48μm. With the ILC scheme, the maximum runout of bearing 1 is quickly reduced to 3μm. The maximum runout of bearing 2 without ILC is 25.5μm, while the maximum runout of bearing 2 with ILC scheme is reduced to 1μm. It can be observed that the position obits of both bearings are significantly reduced when the ILC scheme is used. Therefore, the shaft is almost rotating about its geometric axis.

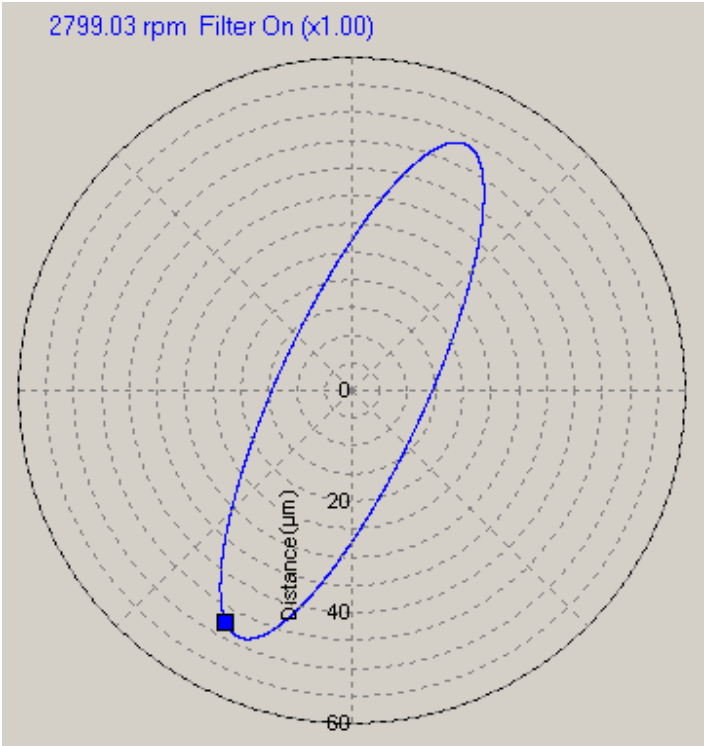

Fig. 5.5. Rotor position orbit of bearing 1 without ILC

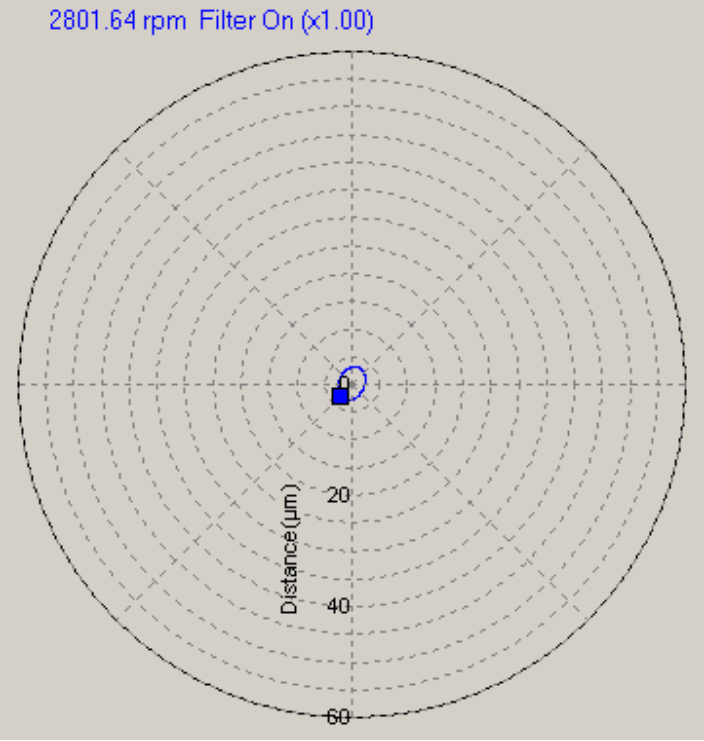

Fig. 5.6. Rotor position orbit of bearing 1 with ILC

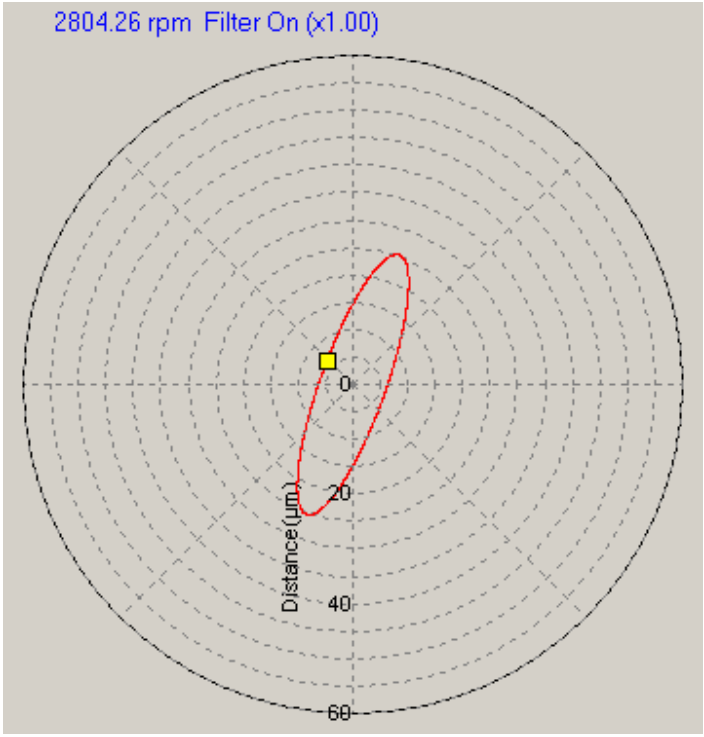

Fig. 5.7. Rotor position orbit of bearing 2 without compensation

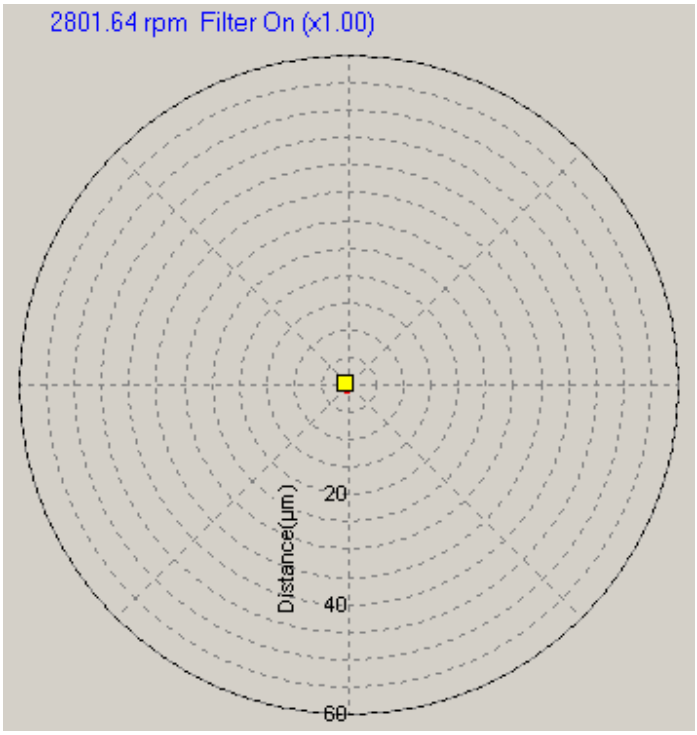

Fig. 5.8. Rotor position orbit of bearing 2 with ILC

During the experiment, the motor speed is controlled at 2800rpm, with ±15 rpm speed variations. According to the previous analysis, this speed disturbance could affect the control performance of the ILC controller. Fig. 5.9 shows the rotor position orbit of bearing 1 with ILC when rotational speed has fluctuations. The rotational speed is 2791.74rpm, but the ILC controller is designed for 2800rpm. Therefore, the speed fluctuation negatively affects its compensation effect and the rotor position orbit becomes large.

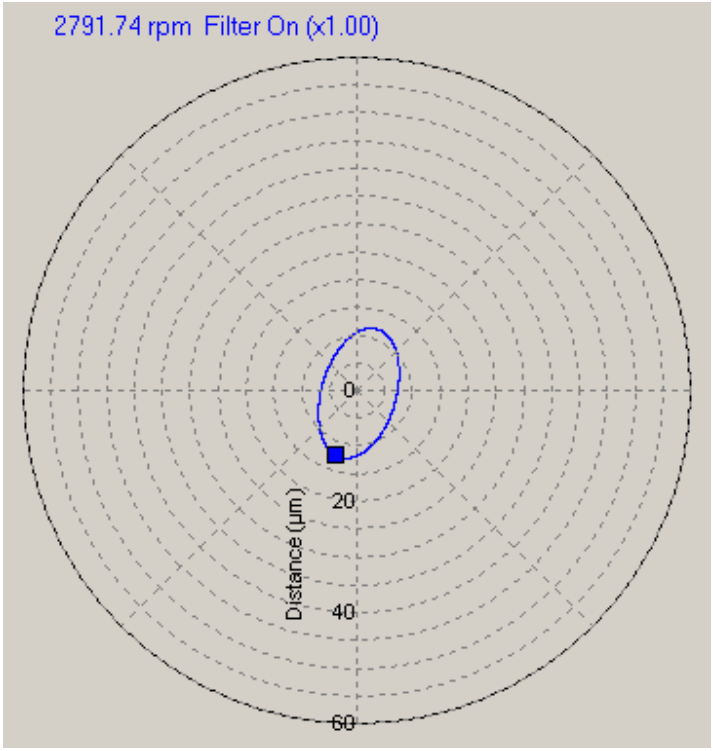

Fig. 5.9. Rotor position orbit with ILC when rotational speed has fluctuations.

The steady-state responses of rotor runouts and their frequency spectrums in 4 radial DOF are shown from Fig. 5.10 to Fig. 5.13.

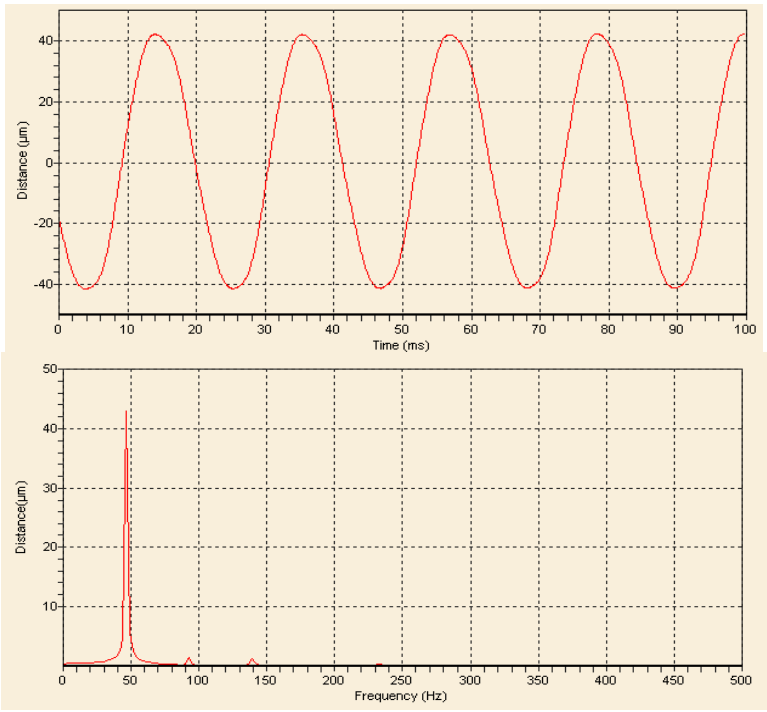

(a) Without compensation

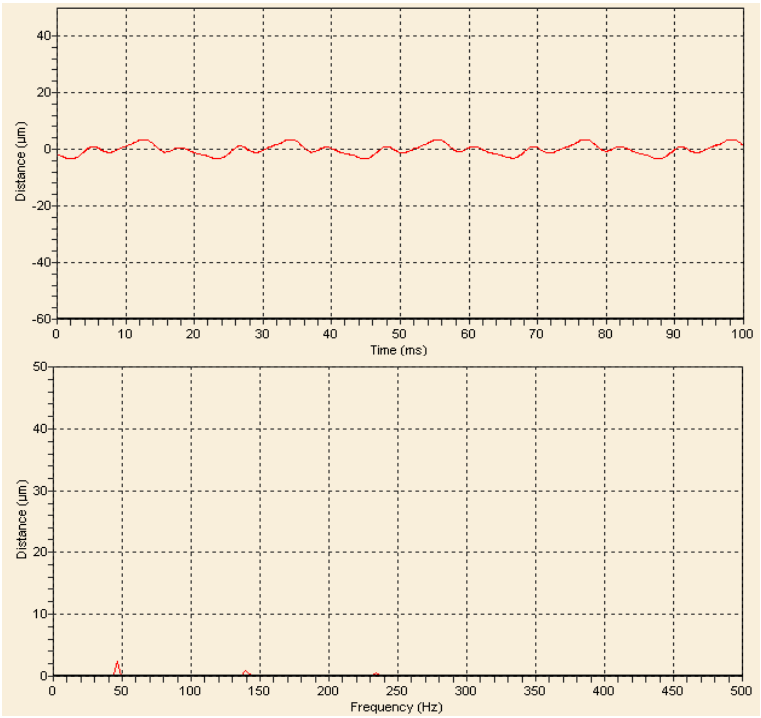

(b) With ILC compensation

Fig. 5.10. Rotor runout in Axis X_1 and its frequency spectrum.

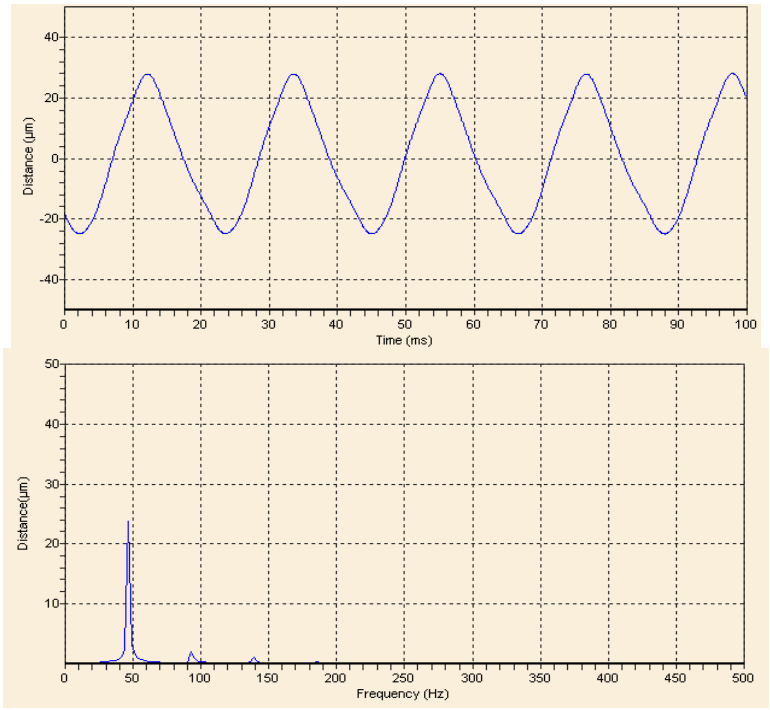

(a) Without ILC compensation

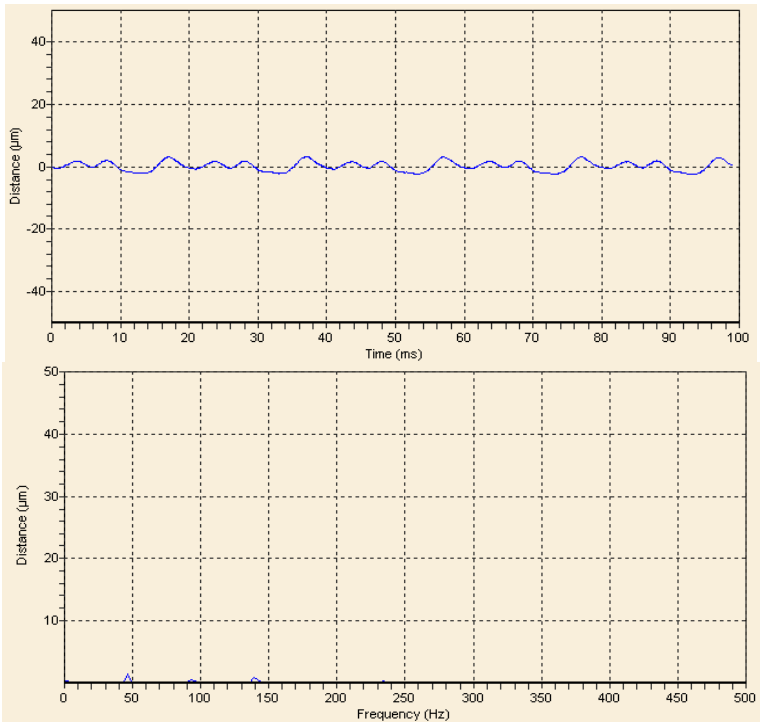

(b) With ILC compensation

Fig. 5.11. Rotor runout in axis Y_1 and its frequency spectrum.

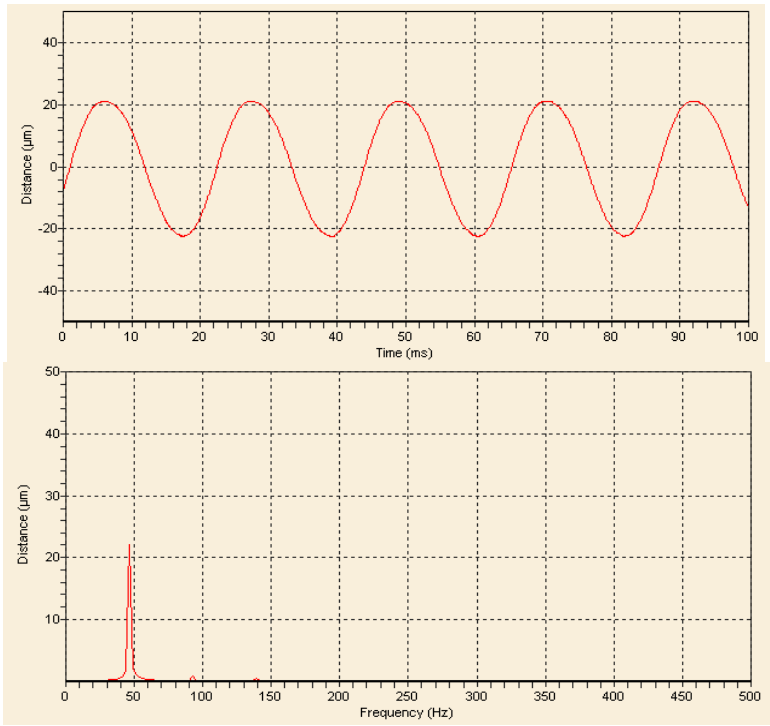

(a) Without ILC

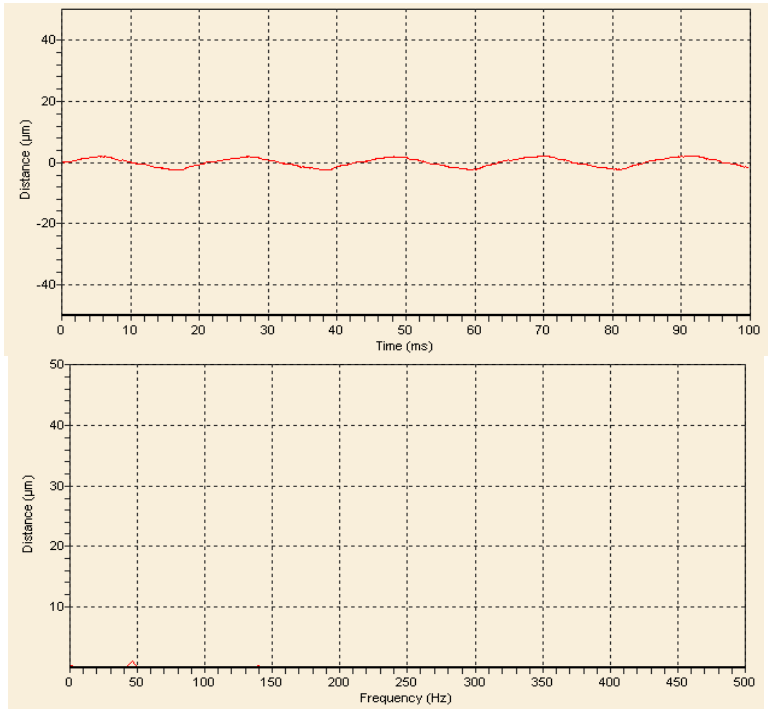

(b) With ILC

Fig. 5.12. Rotor runout in axis X_2 and its frequency spectrum.

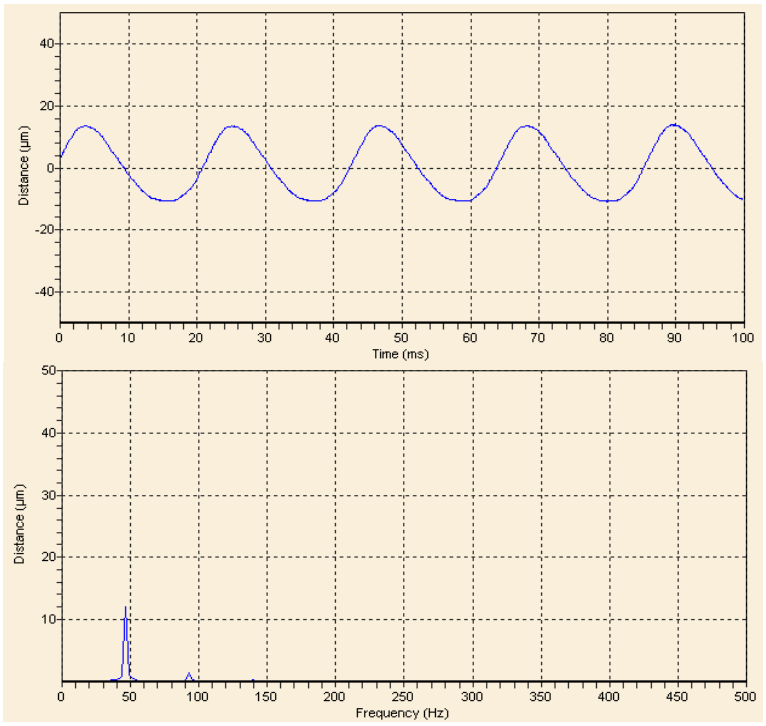

(a) Without ILC

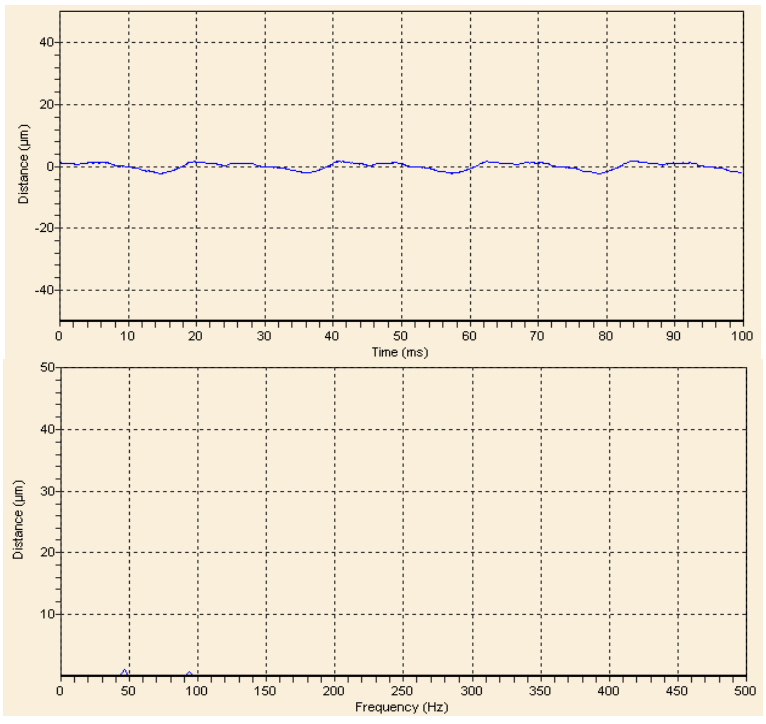

(b) With ILC

Fig. 5.13. Rotor runout in axis Y_2 and its frequency spectrum.

Fig. 5.10(a) shows the steady-state rotor runout in axis X_1 and the corresponding frequency spectrum with only PID control. The magnitude of steady-state runout is 44μm. Fig. 5.10(b) shows the steady-state rotor runout in axis X_1 and its corresponding frequency spectrum with ILC scheme. The magnitude of steady-state runout is 3.3μm.

Fig. 5.11 shows the steady-state rotor runout in axis Y_1 and the corresponding frequency spectrum (a) with only PID control and (b) with ILC scheme. The magnitude of steady-state runout is 26.4μm for PID control. The magnitude of steady-state runout is 2.8μm for ILC control.

Fig. 5.12 shows the steady-state rotor runout in axis X_2 and the corresponding frequency spectrum (a) with only PID control and (b) with ILC scheme. The magnitude of steady-state runout is 22μm for PID control. The magnitude of steady-state runout is 2.4μm for ILC control.

Fig. 5.13 shows the steady-state rotor runout in axis Y_2 and the corresponding frequency spectrum (a) with only PID control and (b) with ILC scheme. The magnitude of steady-state runout is 12.2μm for PID control. The magnitude of steady-state runout is 2.2μm for ILC control.

The reduction of rotor runout in each axis is significant, especially in synchronous frequency. The frequency spectrums suggest that the synchronous runouts are almost eliminated when the ILC scheme is used.

5.3.2 ILC Scheme for Reducing Coil Current Fluctuations

The proposed time-domain ILC scheme is employed to reduce fluctuations of AMB coil currents and the corresponding experimental results are shown from Fig. 5.14 to Fig. 5.17.

According to the analysis in Chapter 2, reducing current fluctuations has the advantage of attenuated machine housing vibrations. The fluctuations of top coil current are recorded and to compare controller performances. Because the two electromagnets are operated in the differential driving mode, where the coil current in one electromagnet is the sum of bias current i_0 and control current i_c, the coil current in the other electromagnet is the difference of bias current and control current, as shown in (1.4), the bottom coil current has the same fluctuation conditions as the top coil current.

The parameters for the ILC controller are:

learning gain $\Phi = 0.07$,

forgetting factor $\alpha = 0.005$.

Fig. 5.14 shows the fluctuation of coil current in axis X_1 and its frequency spectrum (a) without ILC and (b) with ILC. The magnitude of current fluctuation without the ILC scheme is 0.384A. With ILC compensation, the magnitude of current fluctuation becomes 0.038A.

Fig. 5.15 shows the fluctuation of coil current in axis Y_1 and its frequency spectrum (a) without ILC and (b) with ILC. The magnitude of current fluctuation without the ILC scheme is 0.23A. With ILC compensation, the magnitude of current fluctuation becomes 0.034A.

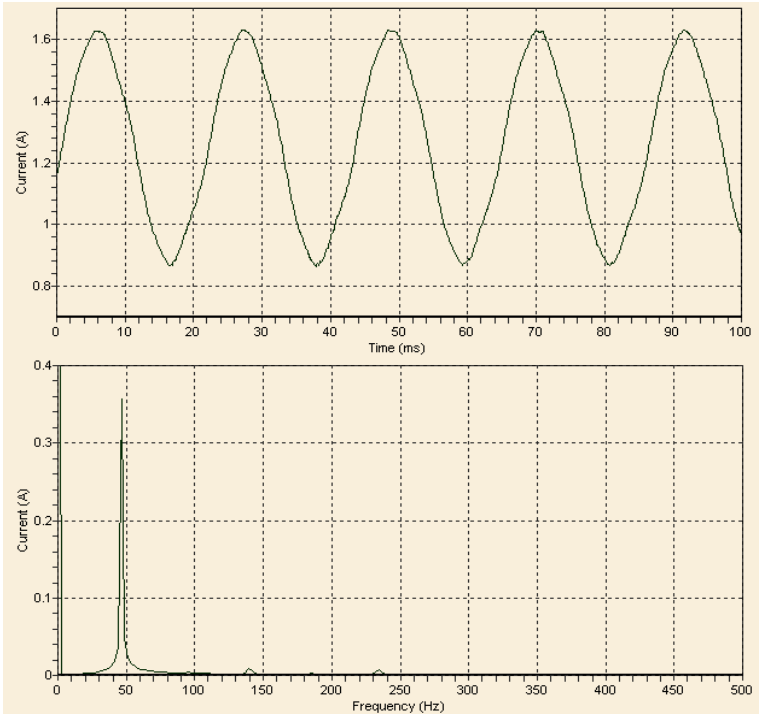

(a) Without ILC

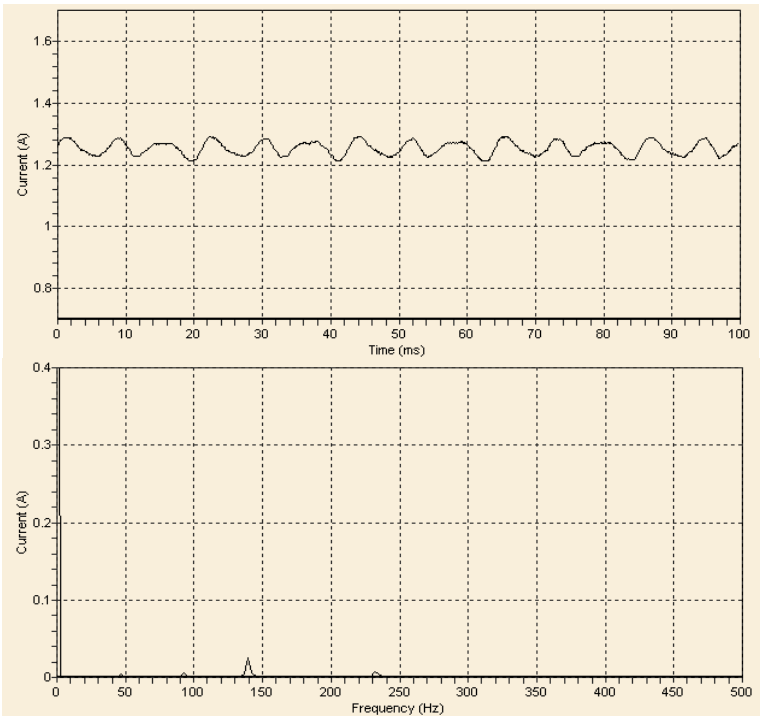

(b) With ILC

Fig. 5.14. Fluctuation of coil current in axis X_1 and its frequency spectrum.

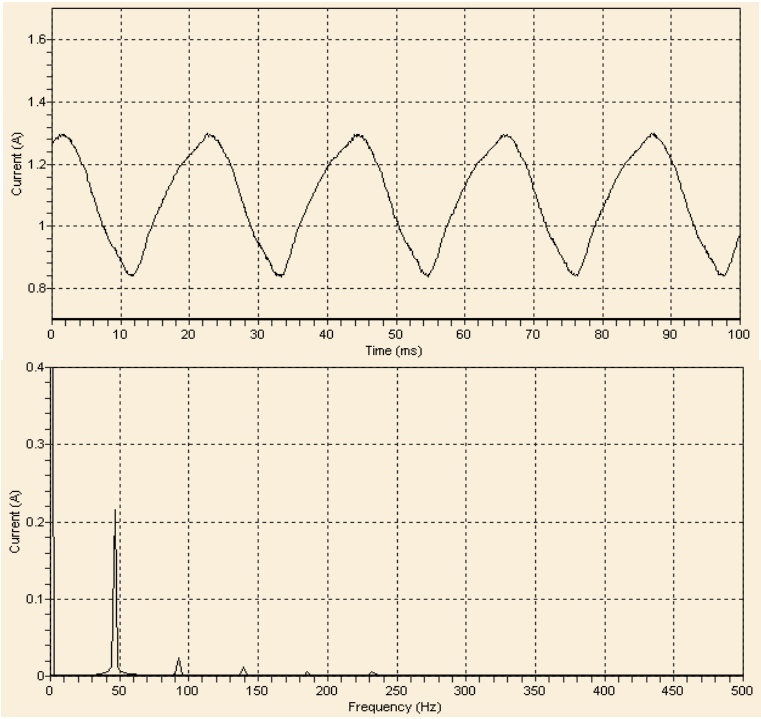

(a) Without ILC

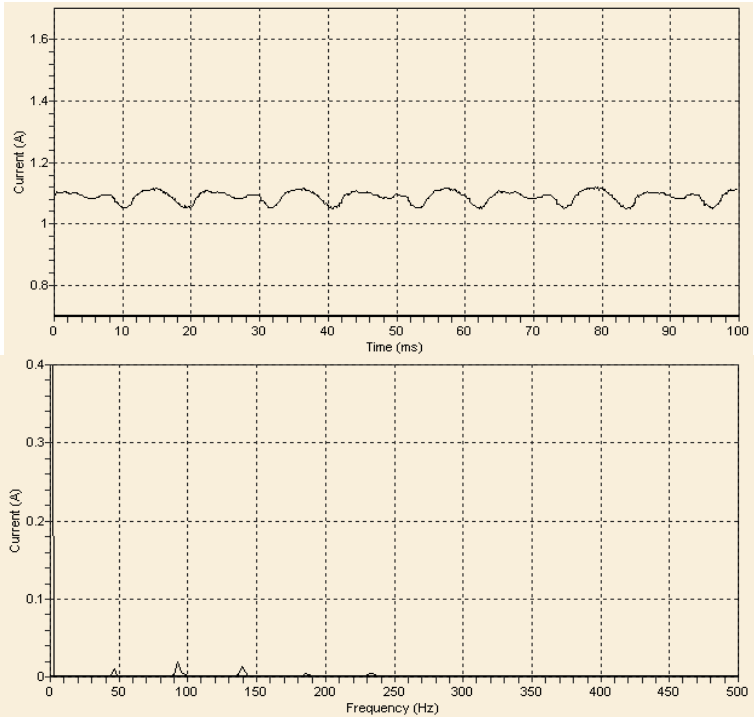

(b) With ILC

Fig. 5.15. Fluctuation of coil current in axis Y_1 and its frequency spectrum.

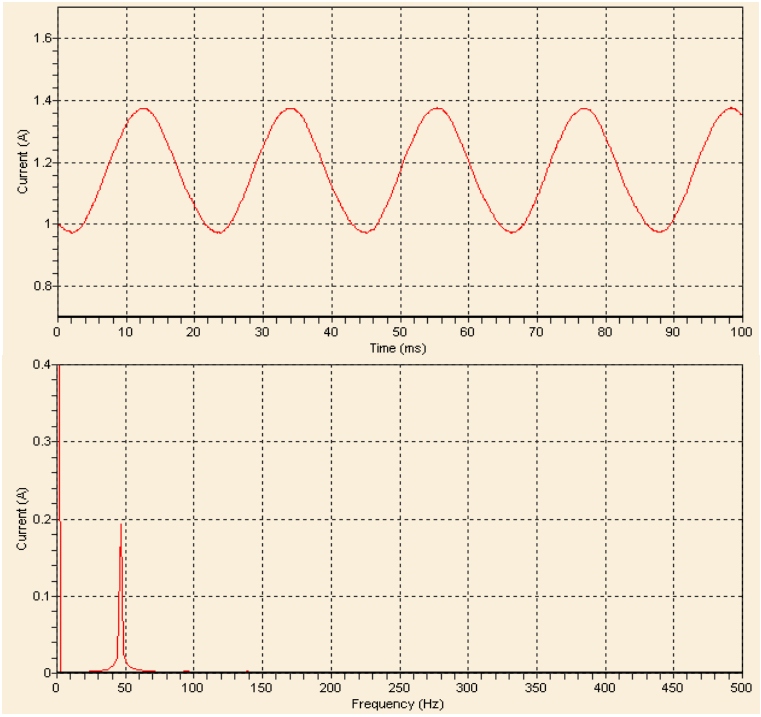

(a) Without ILC

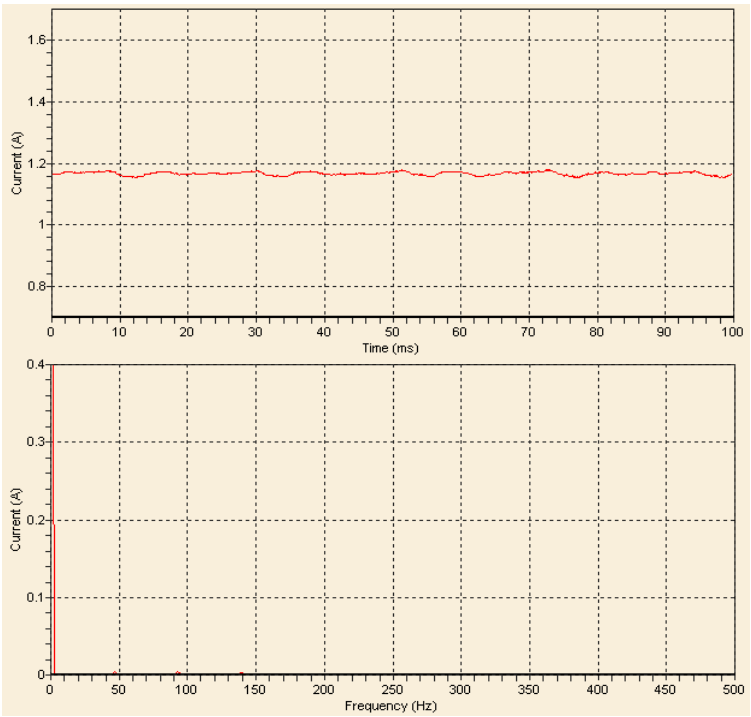

(b) With ILC

Fig. 5.16. Fluctuation of coil current in axis X_2 and its frequency spectrum.

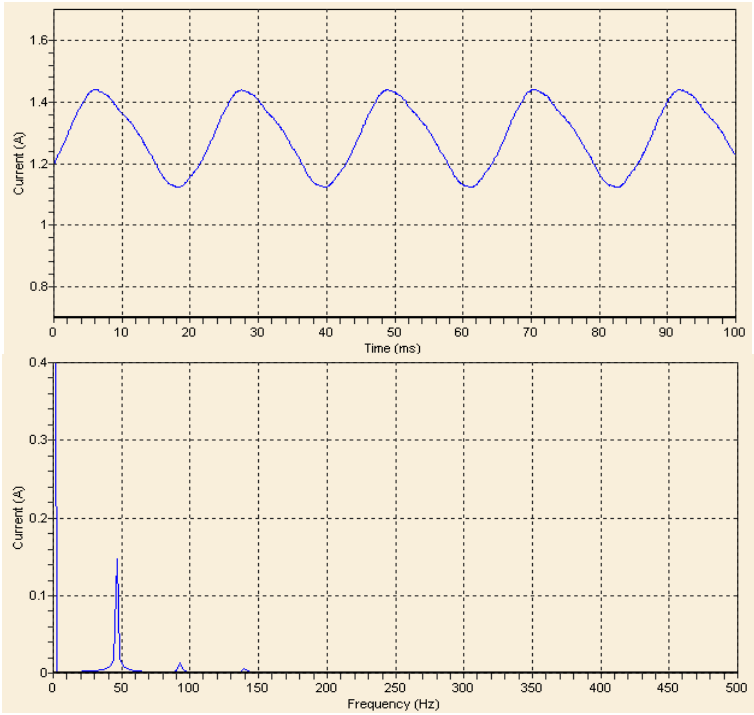

(a) Without ILC

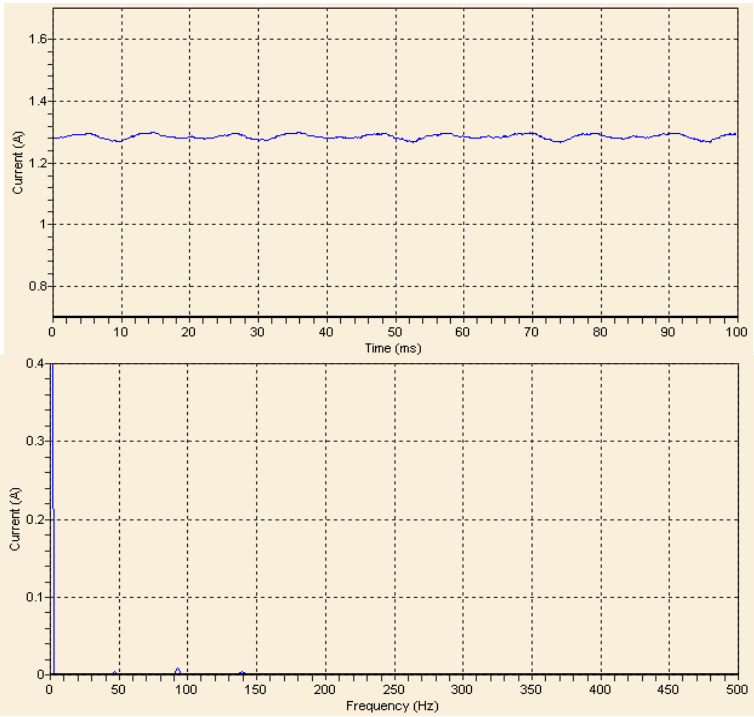

(b) With ILC

Fig. 5.17. Fluctuation of coil current in axis Y_2 and its frequency spectrum.

Fig. 5.16 shows the fluctuation of coil current in axis X_2 and its frequency spectrum (a) without ILC and (b) with ILC. The magnitude of current fluctuation without the ILC scheme is 0.202A. With ILC compensation, the magnitude of current fluctuation becomes 0.014A.

Fig. 5.17 shows the fluctuation of coil current in axis Y_2 and its frequency spectrum (a) without ILC and (b) with ILC. The magnitude of current fluctuation without the ILC scheme is 0.158A. With ILC compensation, the magnitude of current fluctuation becomes 0.016A.

The frequency spectrums indicate that before ILC compensation synchronous components are the dominant component of coil current fluctuations. With the effective control of ILC scheme, the synchronous current fluctuations are almost eliminated, while the higher-order harmonics remain unprocessed. This is because of the Butterworth low-pass filter. The higher-order harmonics are beyond its cut-off frequency, so only synchronous signals are processed in the ILC scheme.

5.4 ALC Scheme for Rotor Runout Reduction

In this section, the proposed ALC scheme for rotor runout reduction is evaluated through experiments. The controller's performances at constant rotational speed and variable rotational speeds are respectively examined in the experiment. The AMB system is also stabilized by a decentralized PID controller. When ALC is turned off, only the PID controller works. When ALC is turned on, it works together with the PID controller. In the experiment the sampling frequency for A/D and D/A conversion is 10 kHz.

5.4.1 Experiment at the Speed of 2800 RPM

Firstly the proposed ALC scheme for realizing rotation about geometric axis is tested in the experiment. The rotational speed is 2800rpm (46.67Hz), so the fundamental frequency of the rotor runout motion is 46.67 Hz.

The key parameters for the ALC controller at 2800rpm are

Learning gain: $\Phi = 0.12$ A/μm

Forgetting factor: $\alpha = 0.005$.

The experimental results at 2800rpm are shown in Fig. 5.18 to Fig. 5.21. Fig. 5.18 shows the position orbit at bearing 1 without unbalance compensation, while Fig. 5.19 shows the position orbit with proposed ALC scheme. Without unbalance compensation, the maximum runout is 48μm. With the effective control of ALC scheme maximum runout is reduced to 3μm.

Fig. 5.20 shows the position orbit at bearing 2 without unbalance compensation, and Fig. 5.21 shows the corresponding position orbit with proposed ALC scheme. The maximum runout before compensation is about 25.5μm, while with ALC compensation the maximum runout is about 1μm. The rotor position orbit is almost reduced to be a point at the origin.

In the previous experiments of the ILC scheme, the rotational speed fluctuation could affect the compensation performance. However, with ALC compensation scheme, this phenomenon doesn't appear when the speed is fluctuating. This is because ALC could automatically adjust the length of learning cycle according to the rotational speed.

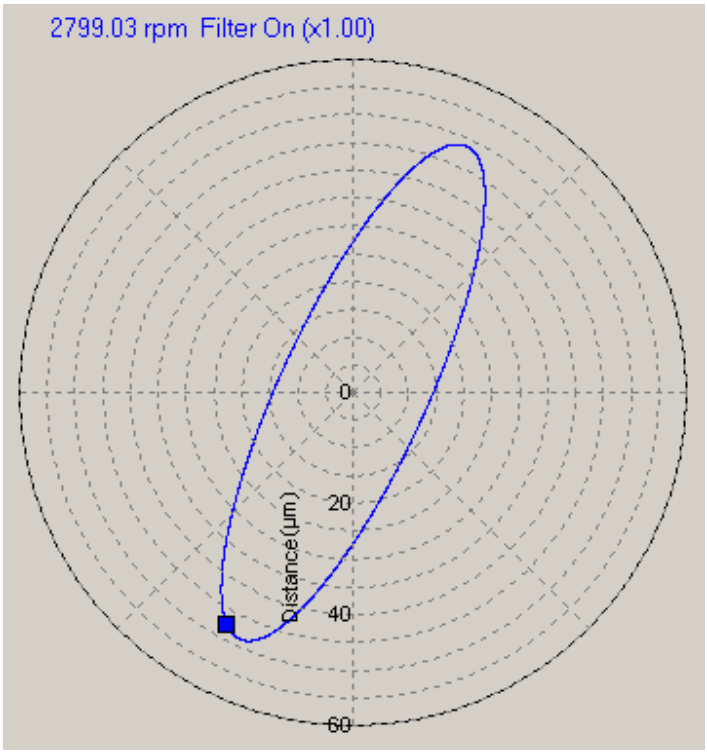

Fig. 5.18. Rotor position orbit of bearing 1 without ALC.

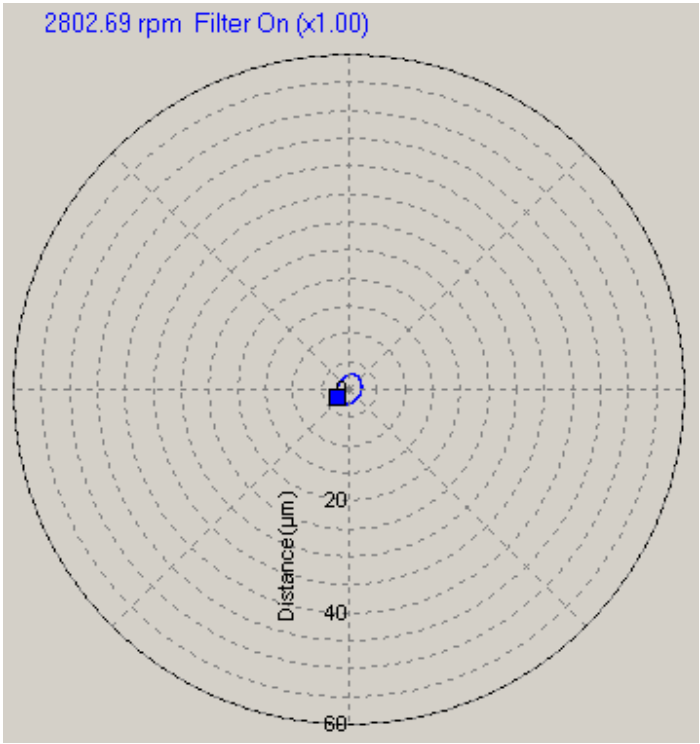

Fig. 5.19. Rotor position orbit of bearing 1 with ALC scheme.

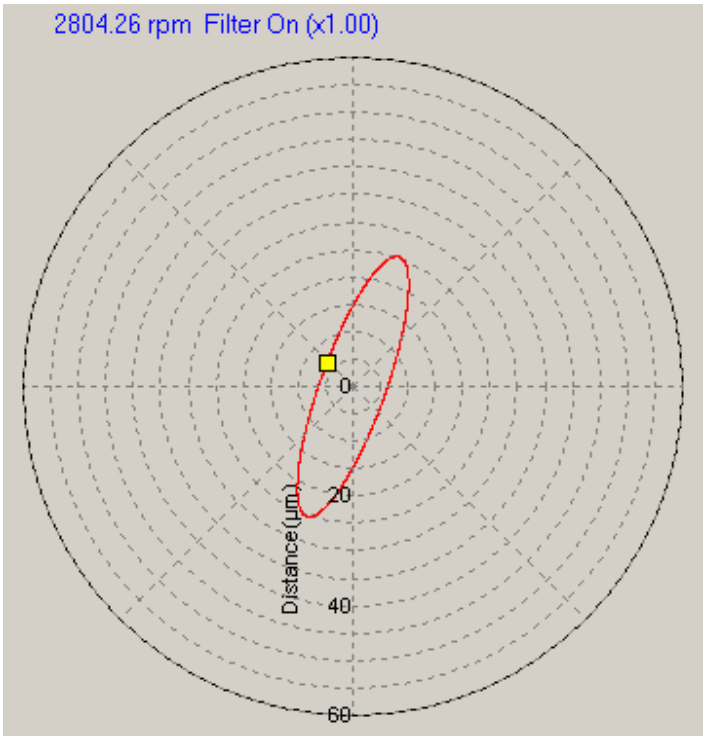

Fig. 5.20. Rotor position orbit of bearing 2 with ALC scheme.

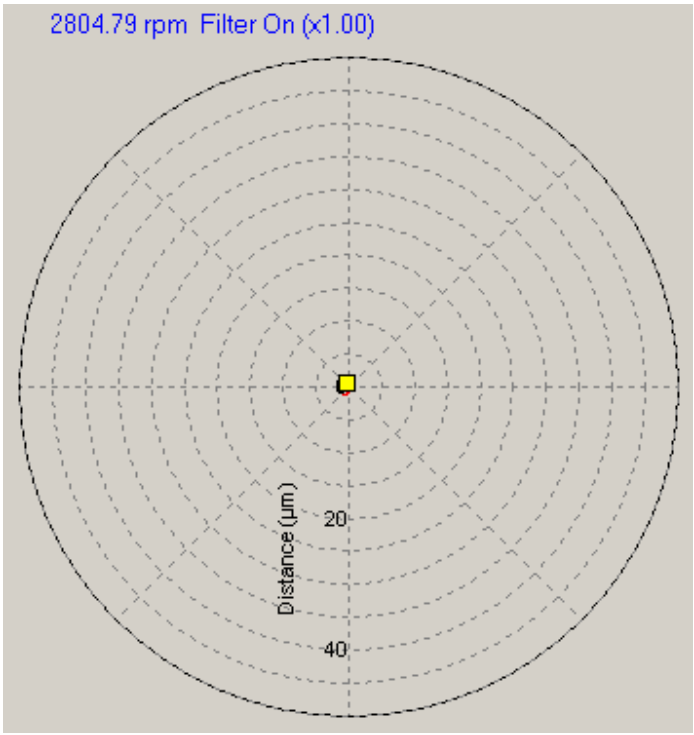

Fig. 5.21. Rotor position orbit of bearing 2 with ALC scheme.

The rotor position waveforms of the 4 radial DOF and their frequency spectrums are shown in Fig. 5.22 to Fig. 5.25.

Fig. 5.22 shows the steady-state rotor runout in axis X_1 and the corresponding frequency spectrum (a) without compensation and (b) with ALC scheme. The magnitude of steady-state runout is 44μm without compensation. The magnitude of steady-state runout is 3.4μm with ALC control.

Fig. 5.23 shows the steady-state rotor runout in axis Y_1 and the corresponding frequency spectrum (a) without compensation and (b) with ALC scheme. The magnitude of steady-state runout is 26.4μm without compensation. The magnitude of steady-state runout is 1.6μm with ALC control.

Fig. 5.24 shows the steady-state rotor runout in axis X_2 and the corresponding frequency spectrum (a) without compensation and (b) with ALC scheme. The magnitude of steady-state runout is 22μm without compensation. The magnitude of steady-state runout is 1.6μm with ALC control.

Fig. 5.25 shows the steady-state rotor runout in axis Y_2 and the corresponding frequency spectrum (a) without compensation and (b) with ALC scheme. The magnitude of steady-state runout is 12.2μm without compensation. The magnitude of steady-state runout is 1.4μm with ALC control.

With the ALC scheme, the synchronous component, the one at 46.67Hz, is significantly reduced to a very small value in each DOF. Therefore the overall runout value decreases substantially in the experiment.

Since ALC is based on time-domain ILC, it should have similar steady-state response as the ILC controller. The experimental results prove this point.

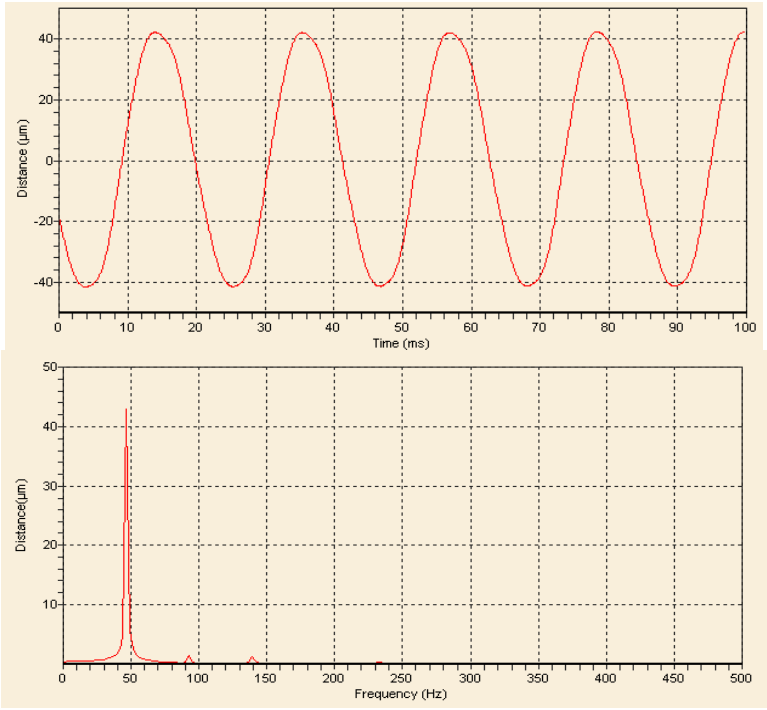

(a) Without ALC

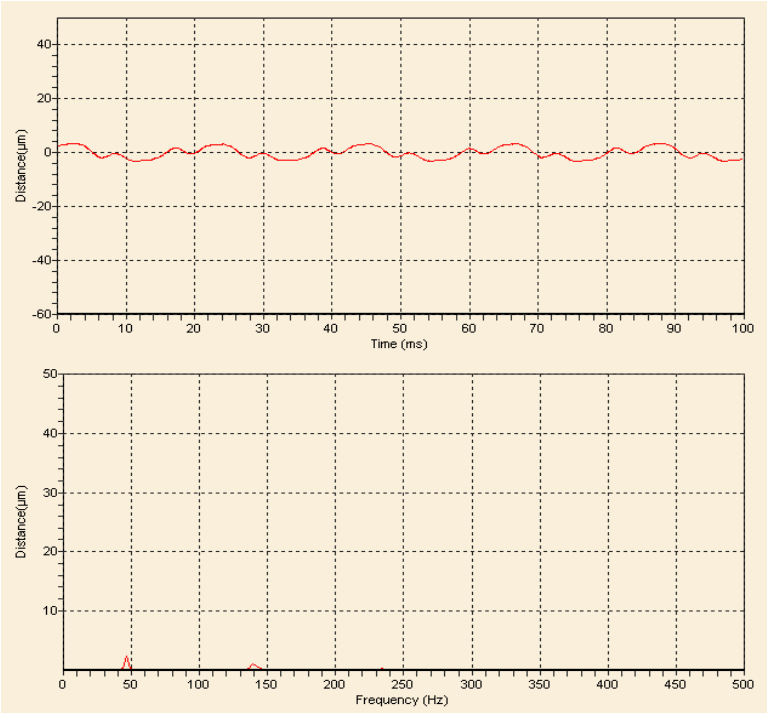

(b) With ALC

Fig. 5.22. Rotor runout in X_1 axis and its frequency spectrum.

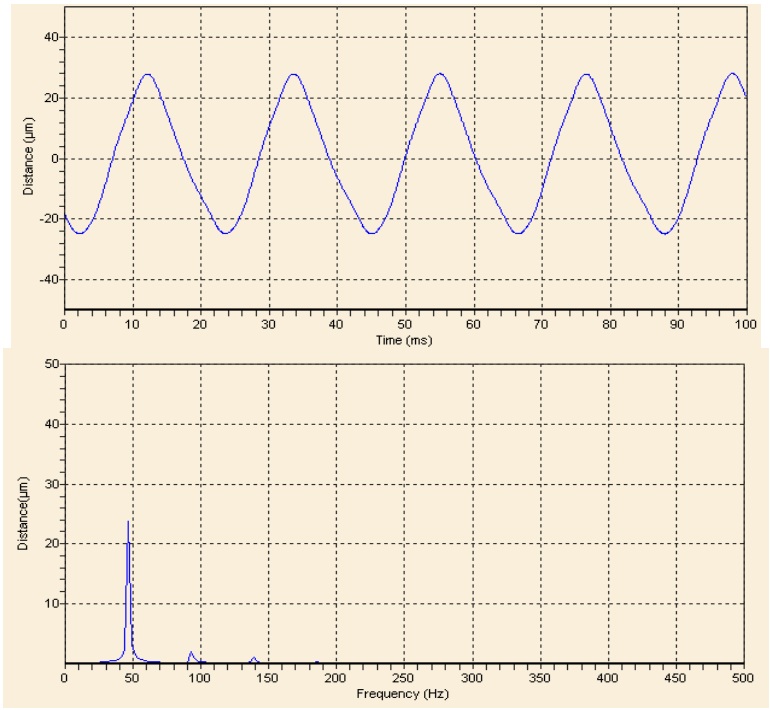

(a) Without ALC

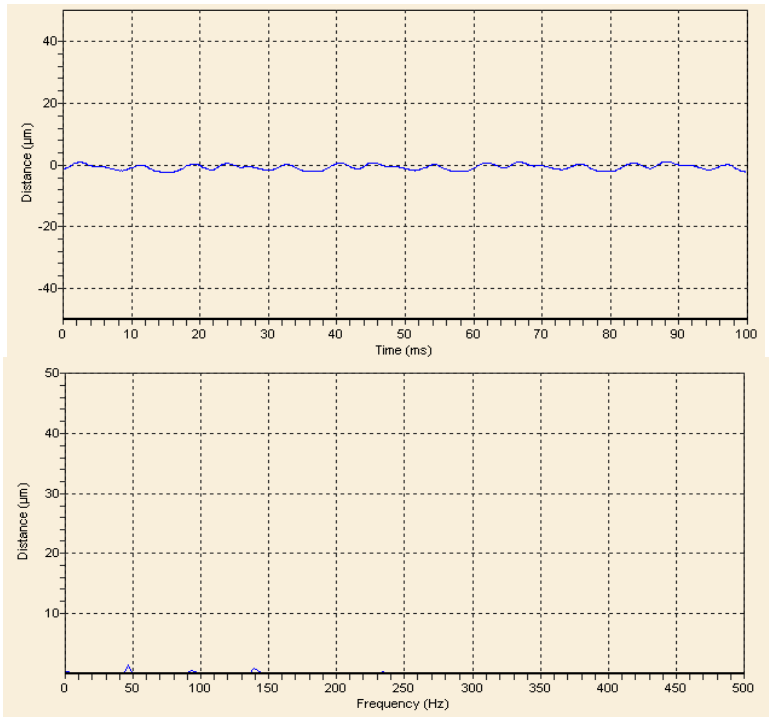

(b) With ALC

Fig. 5.23. Rotor runout in Y_1 axis and its frequency spectrum.

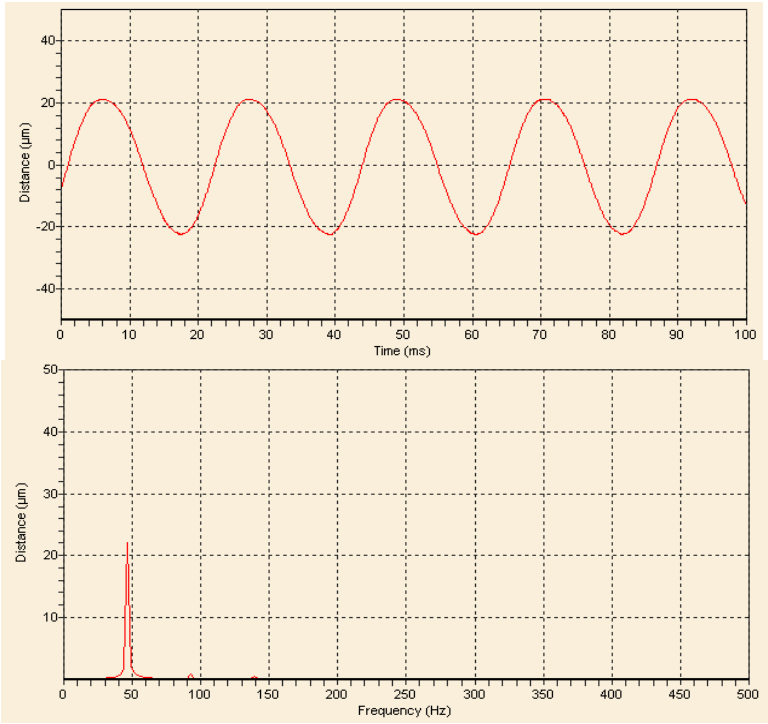

(a) Without ALC

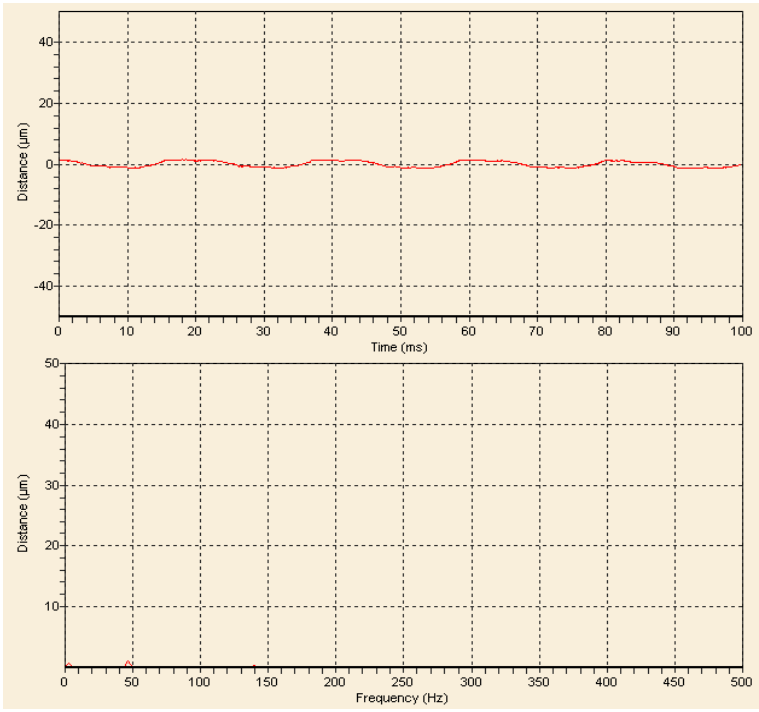

(b) With ALC

Fig. 5.24. Rotor runout in X_2 axis and its frequency spectrum.

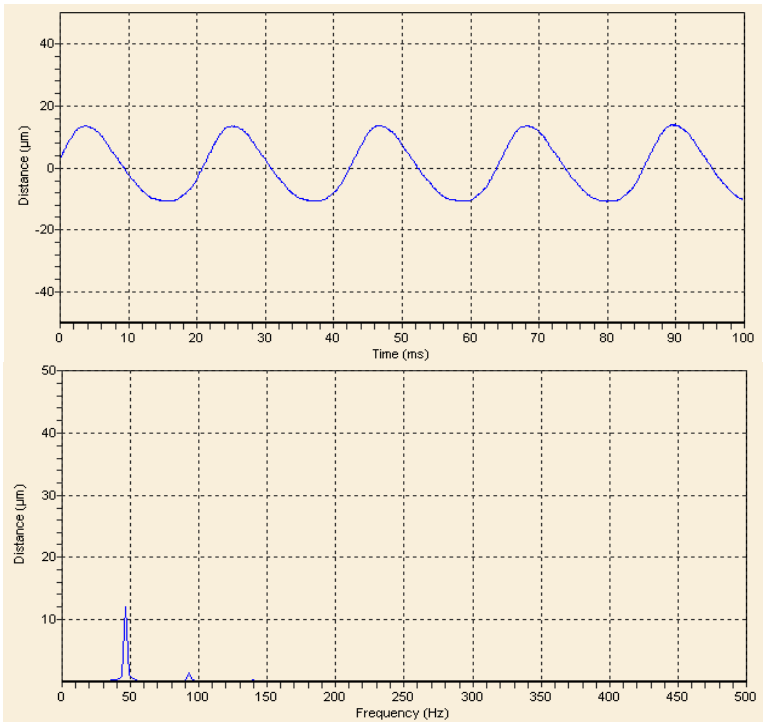

(a) Without ALC

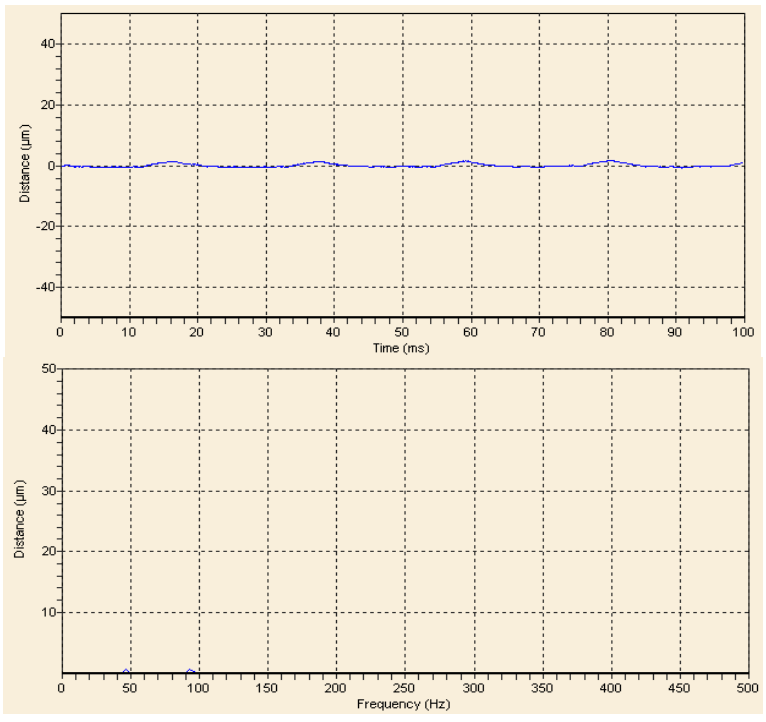

(b) With ALC

Fig. 5.25. Rotor runout in Y_2 axis and its frequency spectrum.

5.4.2 Variable speed Experiment for ALC Scheme

In this speed run-up experiment, the rotational speed is increased from 1200rpm to 3200rpm. The rotational speed, peak-to-peak rotor runout without compensation and peak-peak rotor runout with ALC compensation are respectively recorded for comparison. The 4-DOF run-up test results are shown from Fig. 5.26 to Fig. 5.29. The rotor runouts in all axes are significantly reduced.

Because ALC can automatically adjust its learning cycle and learning gain according to the rotational speed, it exhibits good performance during this experiment. 2800 rpm is around the first critical speed of the rotor, so without ALC the runouts rise dramatically when the rotational speed is approaching 2800rpm. However, with the control of ALC, the runouts are almost flat and have no obvious differences compared to other speeds.

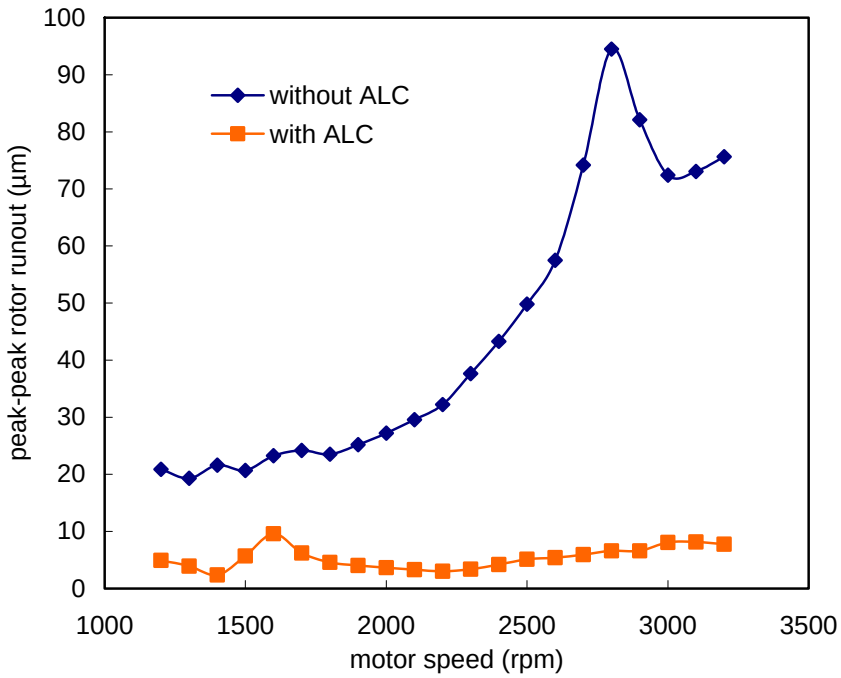

Fig. 5.26. Axis X_1 position runout vs rotational speeds.

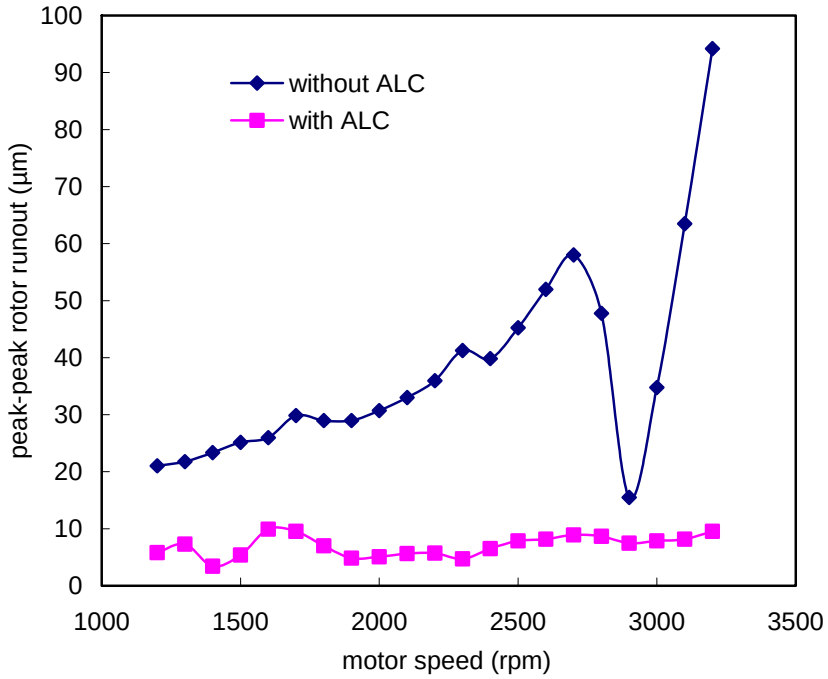

Fig. 5.27. Axis Y_1 position runout vs rotational speeds.

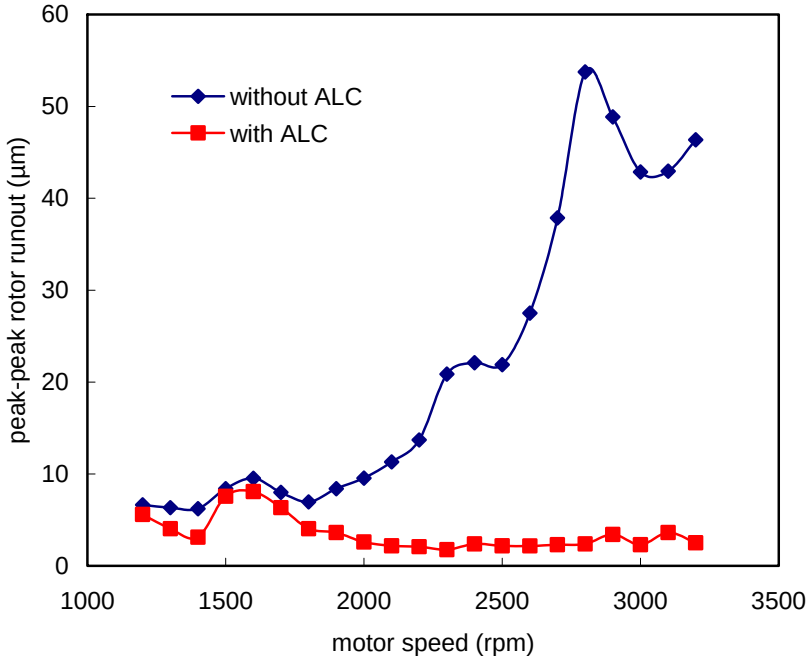

Fig. 5.28. Axis X_2 position runout vs rotational speeds.

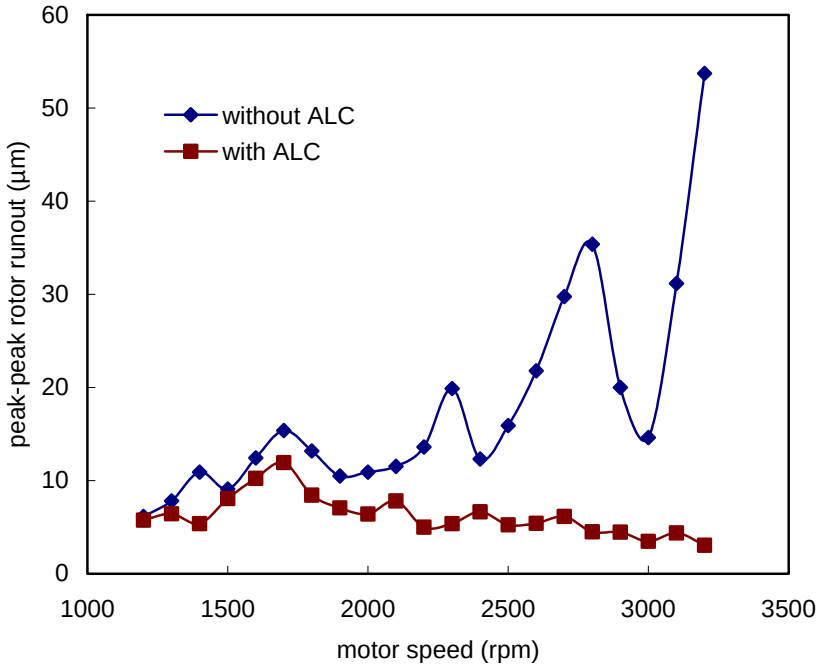

Fig. 5.29. Axis Y_2 position runout vs rotational speeds.

5.5 Reduction of Coil Currents Fluctuations by ALC

The proposed ALC scheme is also applied to reduce fluctuations of AMB coil currents. Likewise, the experiment is composed of two tests, constant speed test and variable speed test. The AMB system is also stabilized by the PID controller used in previous experiments. When ALC is off, only the PID controller works. When ALC is turned on, it works together with the PID controller.

5.5.1 Constant Speed Test

The constant speed test is also carried out at 2800rpm. The parameters for the ALC controller are:

learning gain: $\Phi = 0.06$,

forgetting factor $\alpha = 0.005$.

The fluctuations of top coil current in 4 radial DOF and their frequency spectrums are shown from Fig. 5.30 to Fig. 5.33.

Fig. 5.30 shows the fluctuation of coil current in axis X_1 and its frequency spectrum (a) without ALC and (b) with ALC. The magnitude of current fluctuation without ALC is 0.384A. With ALC compensation the magnitude of current fluctuation becomes 0.036A.

Fig. 5.31 shows the fluctuation of coil current in axis Y_1 and its frequency spectrum (a) without ALC and (b) with ALC. The magnitude of current fluctuation without ALC is 0.23A. With ALC compensation the magnitude of current fluctuation becomes 0.036A.

Fig. 5.32 shows the fluctuation of coil current in axis X_2 and its frequency spectrum (a) without ALC and (b) with ALC. The magnitude of current fluctuation without ALC is 0.202A. With ALC compensation the magnitude of current fluctuation becomes 0.012A.

Fig. 5.33 shows the fluctuation of coil current in axis Y_2 and its frequency spectrum (a) without ALC and (b) with ALC. The magnitude of current fluctuation without ALC is 0.158A. With ALC compensation the magnitude of current fluctuation becomes 0.02A.

It can be observed that the dominant component without ALC compensation, synchronous current in each axis, is substantially reduced with the effective control of ALC.

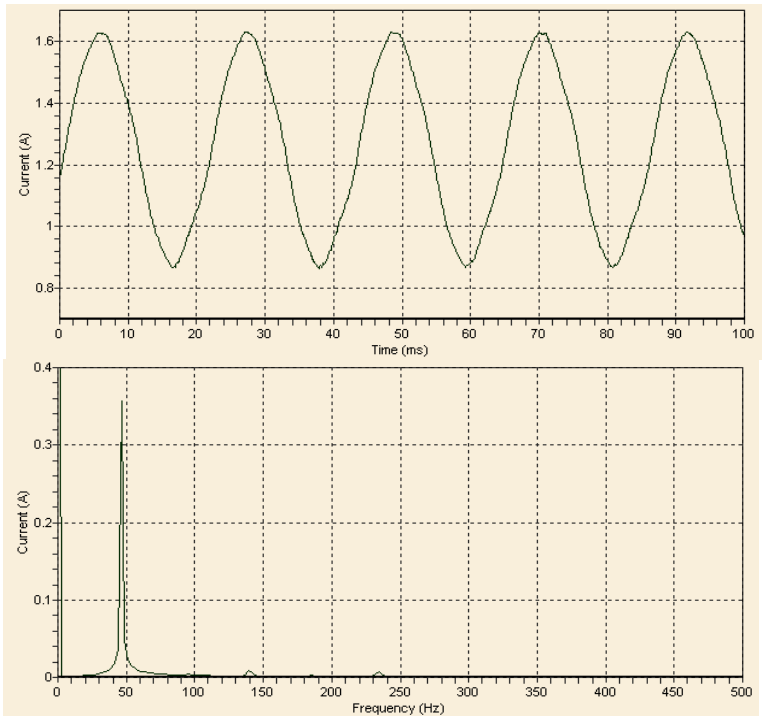

(a) Without ALC

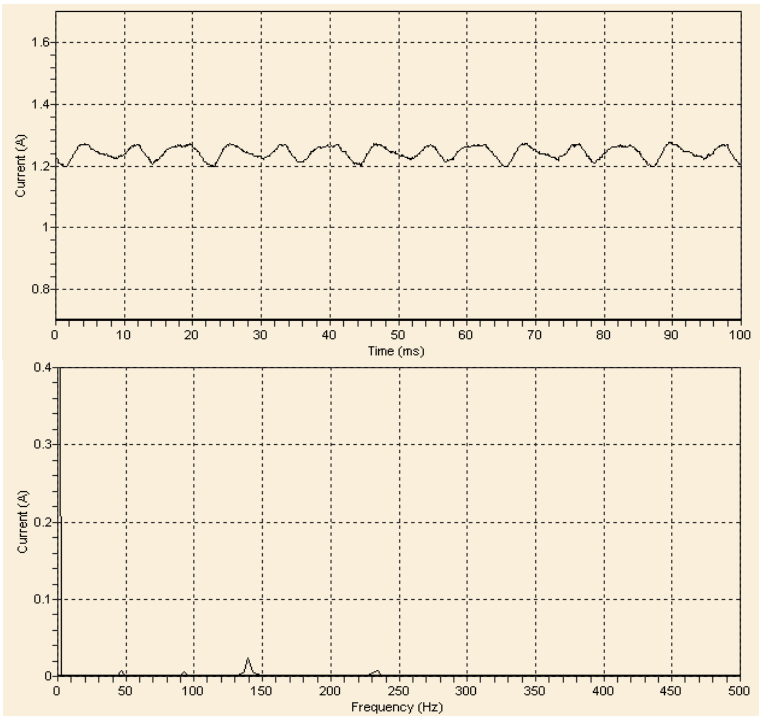

(b) With ALC

Fig. 5.30. Fluctuation of coil current in axis X_1 and its frequency spectrum.

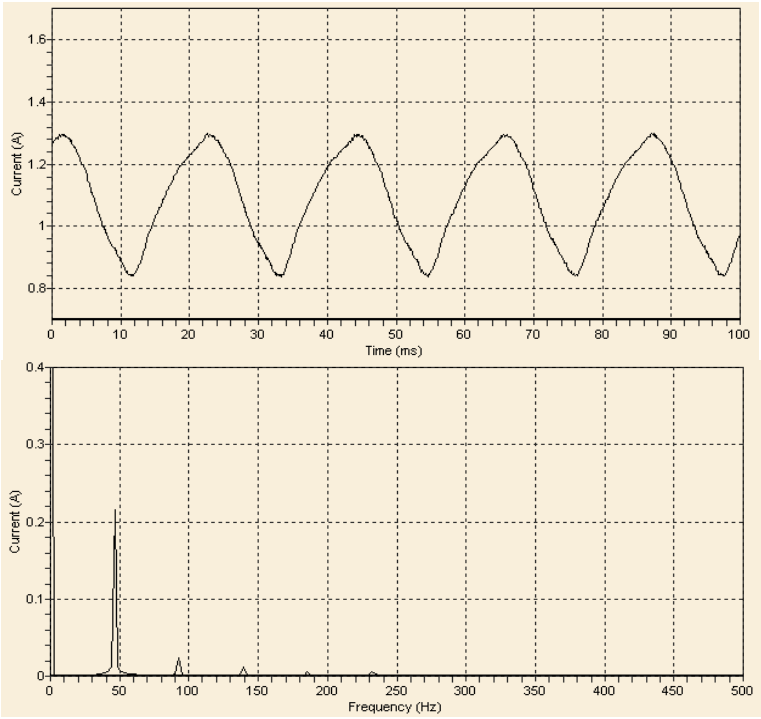

(a) Without ALC

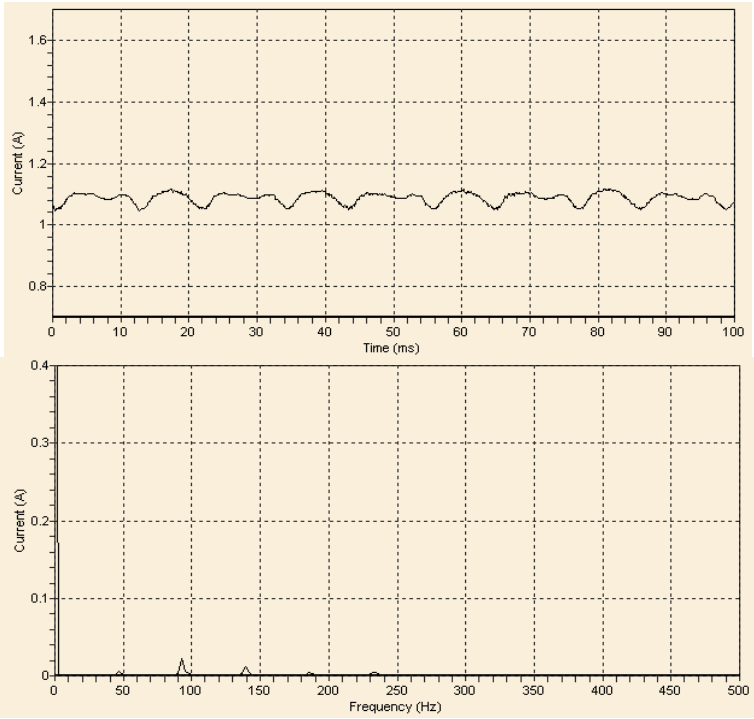

(b) With ALC

Fig. 5.31. Fluctuation of coil current in axis Y_1 and its frequency spectrum.

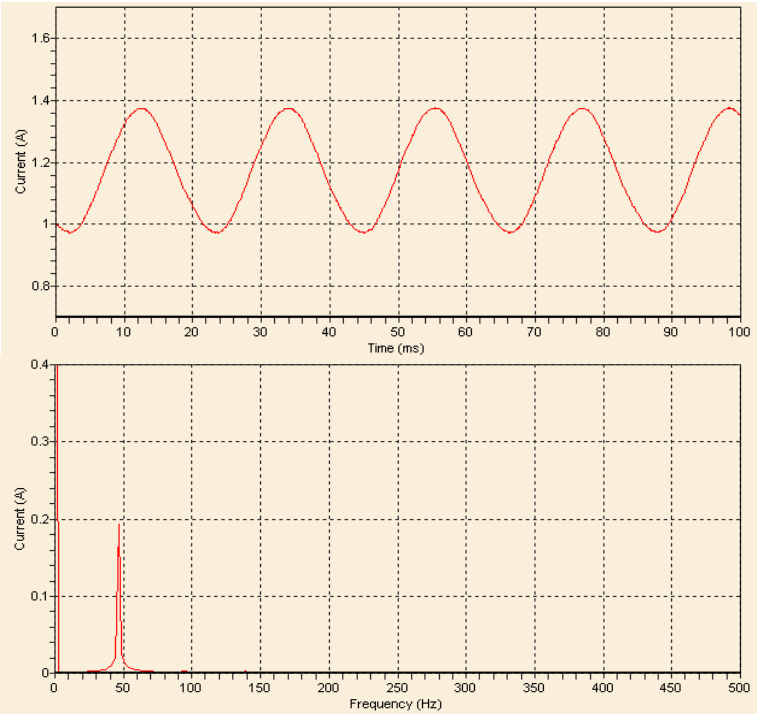

(a) Without ALC

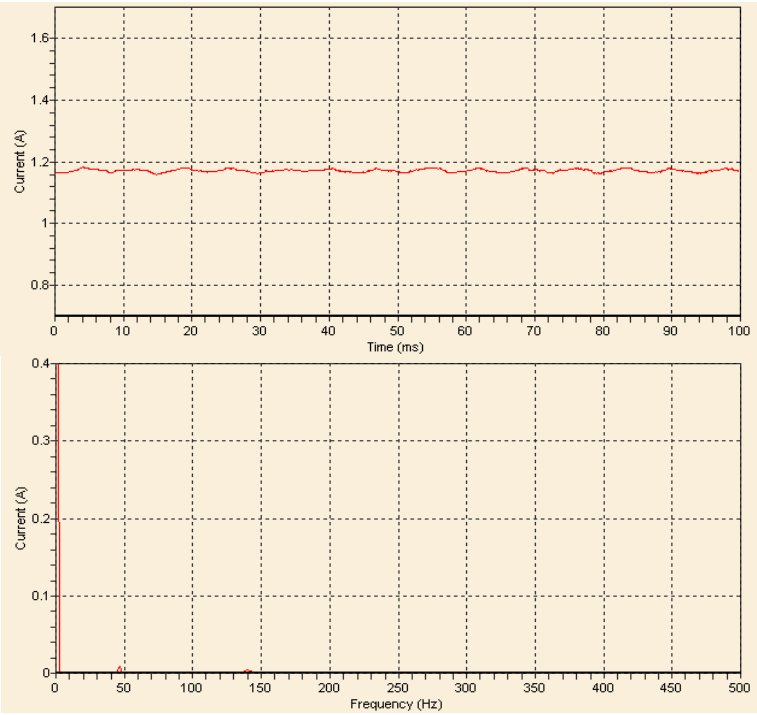

(b) With ALC

Fig. 5.32. Fluctuation of coil current in axis X_2 and its frequency spectrum.

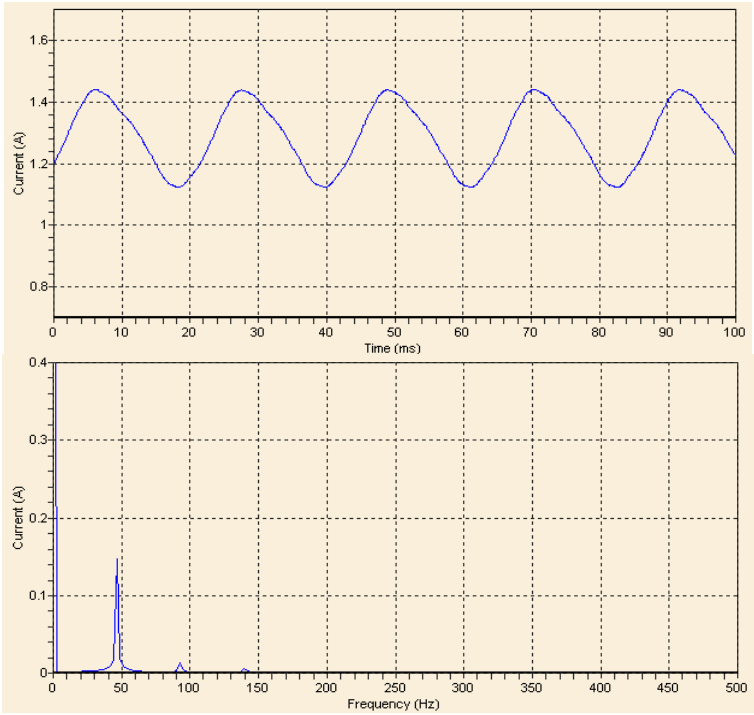

(a) Without ALC

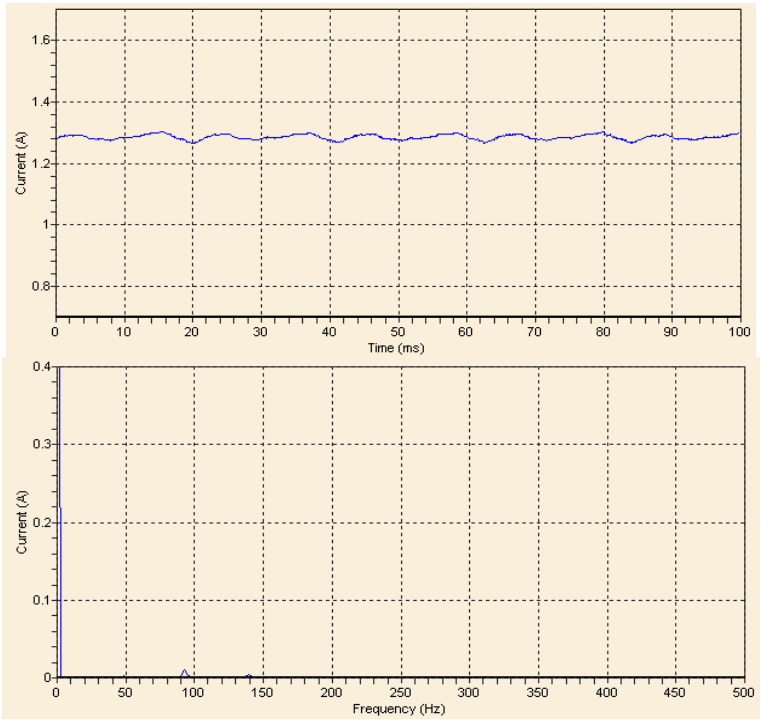

(b) With ALC

Fig. 5.33. Fluctuation of coil current in axis Y_2 and its frequency spectrum.

ALC presents very similar control performance as the ILC scheme in this constant speed test. The steady-state responses of current fluctuations with both schemes are at the same level, with little differences that are within the measurement error range.

5.5.2 Variable Speed Test

ALC scheme is also examined to reduce the coil current fluctuations during rotor speed run-up. ALC also presents satisfactory compensation performance in this experiment. Fig. 5.34 to Fig. 5.37 illustrate peak-to-peak values of coil currents fluctuations in 4 axes. Coil current fluctuations decrease substantially when ALC is turned on. In the experiment, the control current without ALC increases a lot when motor speed is approaching the critical speeds. With ALC, the current fluctuations are always within a small value in the experiment.

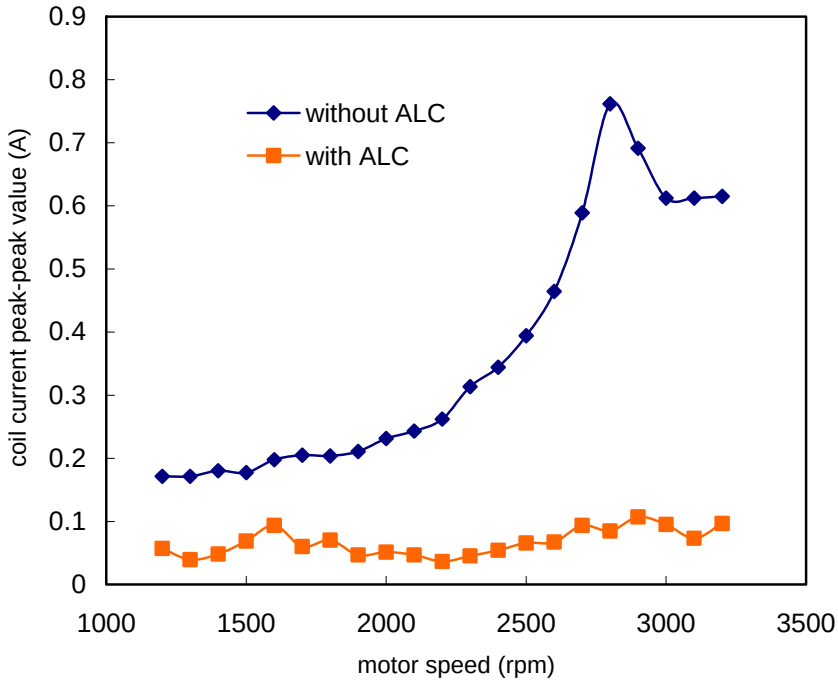

Fig. 5.34. Fluctuation of axis X_1 coil current vs rotational speeds.

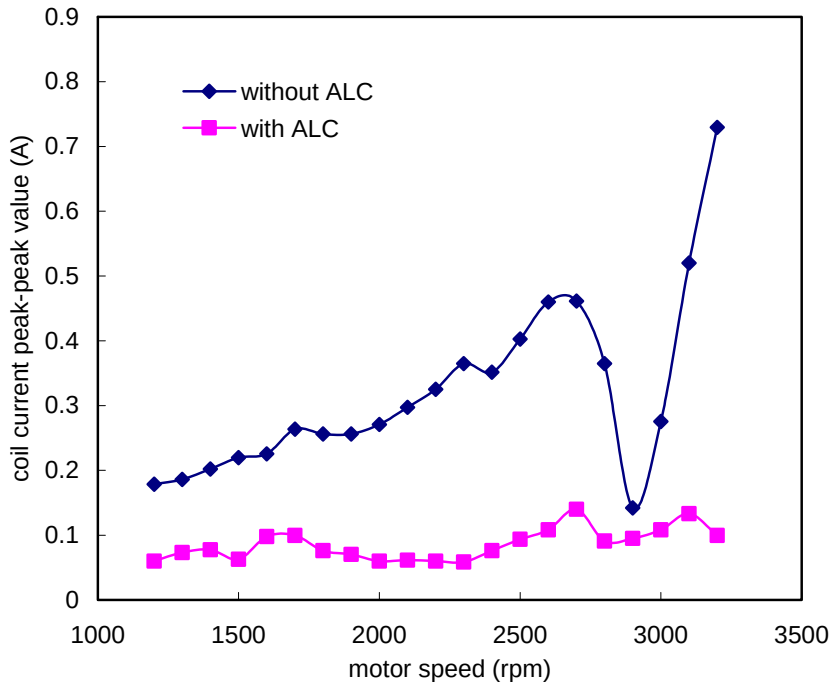

Fig. 5.35. Fluctuation of axis Y_1 coil current vs rotational speeds.

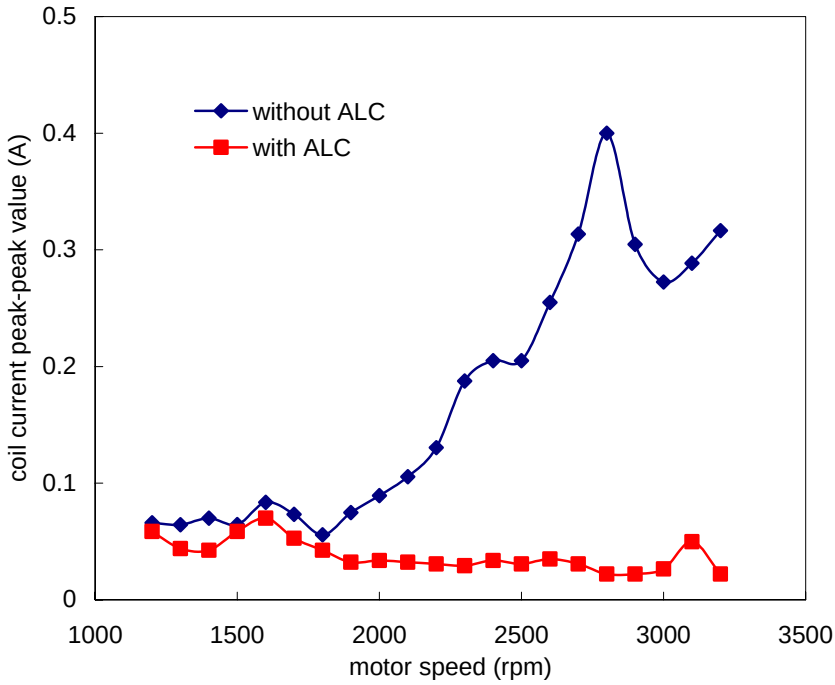

Fig. 5.36. Fluctuation of axis X_2 coil current vs rotational speeds.

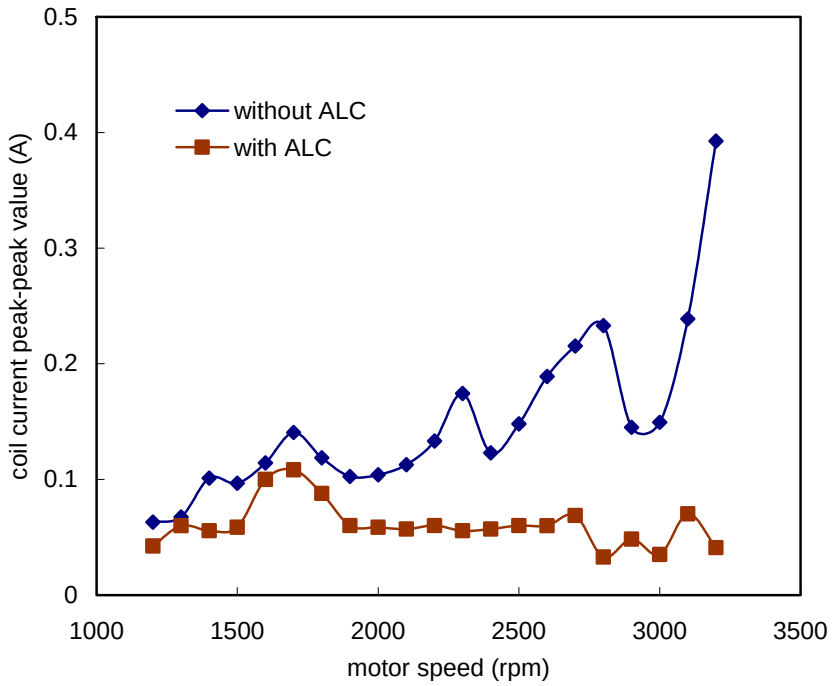

Fig. 5.37. Fluctuation of axis Y_2 coil current vs rotational speeds.

In addition to attenuate vibrations of machine housing, reducing fluctuations of coil current has another advantage, reduction of copper loss in PM-biased AMB [15]. Copper loss is always proportional to the square of the current. Because there is no bias current in PM-biased AMB, control current is the only component in the coil, as shown in (1.8). Copper loss in this kind of AMB is proportional to the square of its effective control current. Thus, its power consumption and generated heat during operation will be reduced significantly by ALC. Smaller control current and less generated heat allow the power electronics to be further integrated, making it possible to put control electronics for small AMB systems in a multi-chip module (MCM).

Fig. 5.38 shows the comparison of effective value of the control current between ALC turned off and ALC turned on. The control current in the latter case can be reduced significantly.

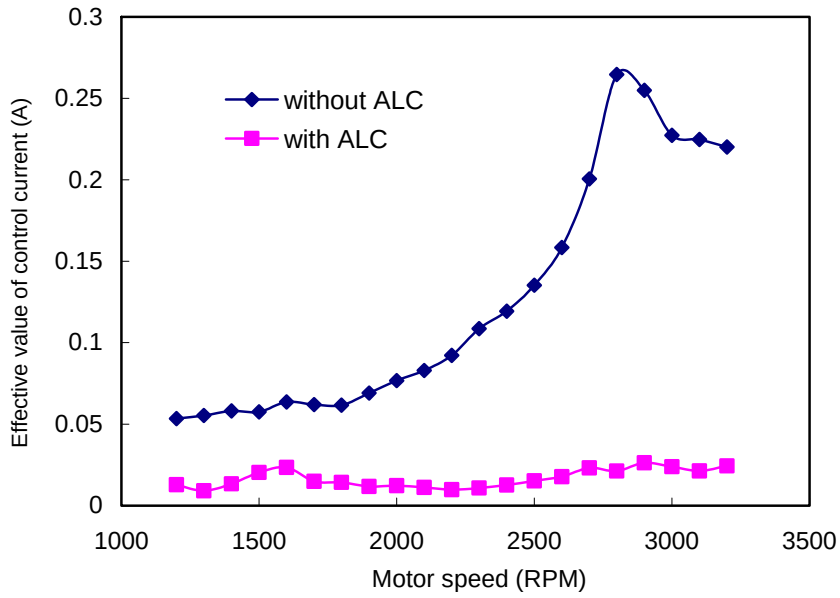

Fig. 5.38. Comparison of effective control current.

5.6 Performance Comparison of ILC and ALC Schemes During Speed Fluctuations

In this section, the control performance of ILC and ALC schemes during speed fluctuations will be compared. The rotational speed is firstly set to be 3000rpm. ILC controller is set to compensate unbalance force at this speed, i.e., the time of one learning cycle is set to be 0.02 second (or $t_f = 200$), i.e., one turn revolution. Because ALC controller can automatically adjust itself to different rotational speed, so it can directly work at this speed without any manual configuration. The forgetting factor is 0.005 for both controllers in the experiment. The experiment is carried out in three strategies: (1) PID control only, (2) PID + ILC, (3) PID + ALC. Rotor runout and top coil current of axis X_1 are recorded.

Both ILC and ALC schemes present satisfied performance when the speed is constant with little fluctuations. The steady-state rotor runouts in axis X_1 at 3000rpm with the three control strategies are shown in Fig. 5.39.

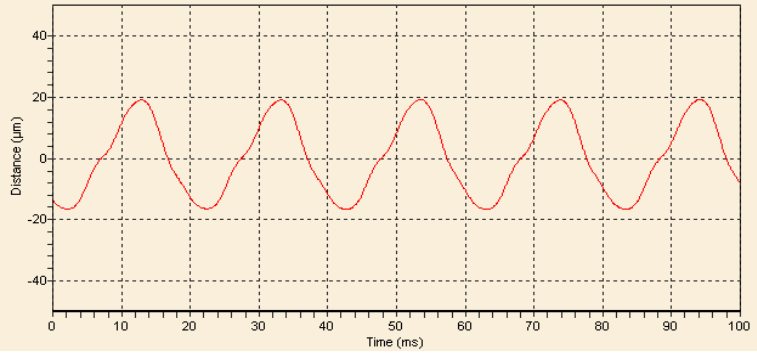

(a) With PID control only

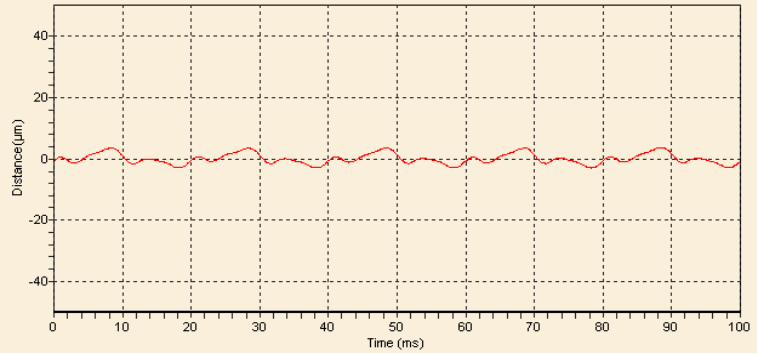

(b) With ILC scheme.

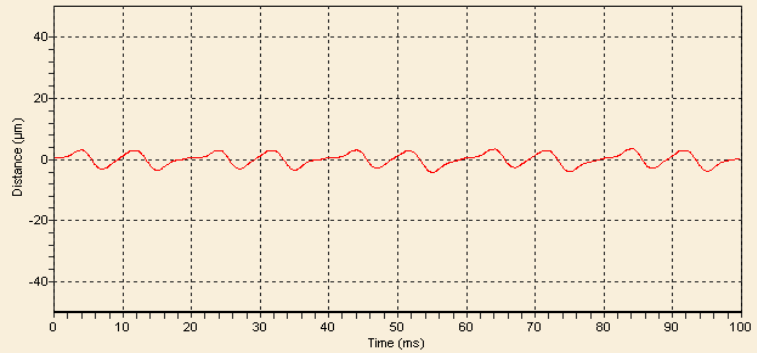

(c) With ALC scheme

Fig. 5.39. Rotor runout at 3000rpm.

During the experiment, there exists small rotational speed fluctuation and this fluctuation could negatively affect performance of the ILC controller. In order to see controller performances during speed fluctuation, we set the speed to be 3010rpm, which is within the range of fluctuation. The rotor runouts in axis X_1 at 3010rpm are shown in Fig. 5.40. ALC control still works well, but the ILC controller cannot obtain satisfactory performance when the rotational speed is not equal to 3000rpm. Because ALC controller can adjust its learning cycle and keep it equal to synchronous period according to the rotational speed, ALC controller can automatically work well during speed fluctuations.

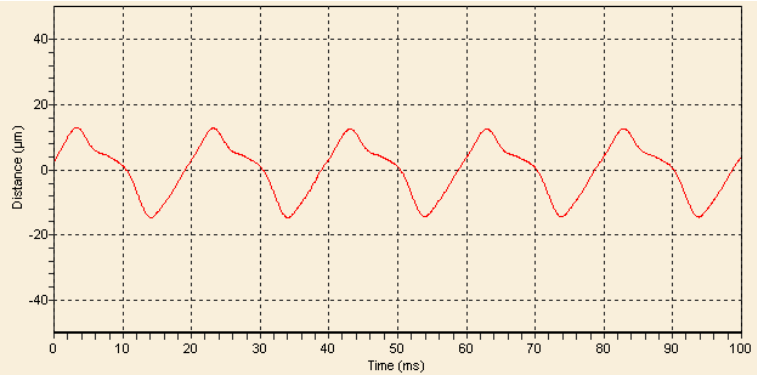

(a) With ILC scheme

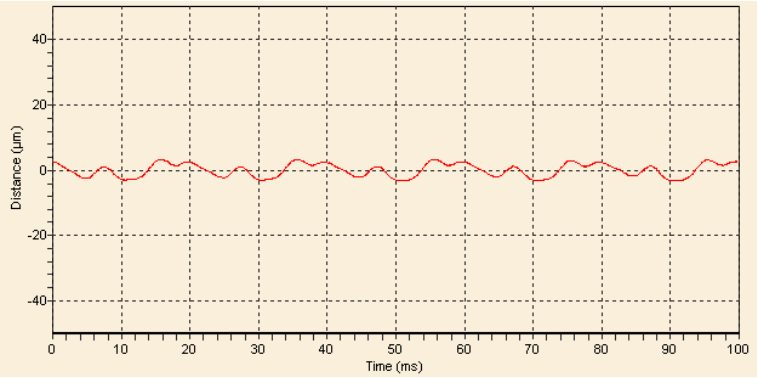

(b) With ALC scheme

Fig. 5.40. Rotor runout at 3010rpm.

Peak-to-peak rotor runouts at some rotational speeds around 3000rpm are recorded in Table 5.1. ALC scheme provides much better performance than ILC scheme when the rotational speed is not equal to 3000rpm.

Table 5.1. Comparison between ILC and ALC during speed fluctuations (1)

Speed (rpm)	PID (μm)	ALC (μm)	ILC (μm)
3000	35.7	7.23	6.93
3010	35.7	7.05	19.86
3020	35.7	7.33	20.78
3030	35.7	7.59	37.80
2990	35.7	7.05	15.11
2980	35.7	7.14	18.77
2970	35.7	7.31	21.80

When ILC scheme and ALC scheme are used to reduce coil current fluctuation, the speed disturbance also negatively affect compensation performance of ILC controller. Fig. 5.41 shows currents of the top electromagnet with three control strategies, (1) PID control only, (2) PID + ILC, (3) PID + ALC. Because the learning cycle of ILC controller is set to be 0.02 second, it works well at the speed of 3000rpm. ALC controller provides similar performance as ILC controller.

When the speed changes to 3010rpm, ALC controller still maintains good control performance. However, learning cycle of the ILC controller cannot change during operation, so it is not suitable for working at 3010rpm. Fig. 5.42 shows the coil current fluctuation when the rotational speed is 3010rpm. It can be observed that ALC presents better control performance than ILC controller.

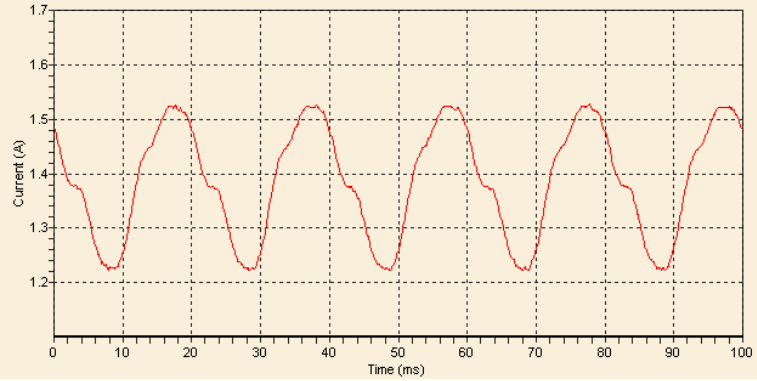

(a) With PID control only

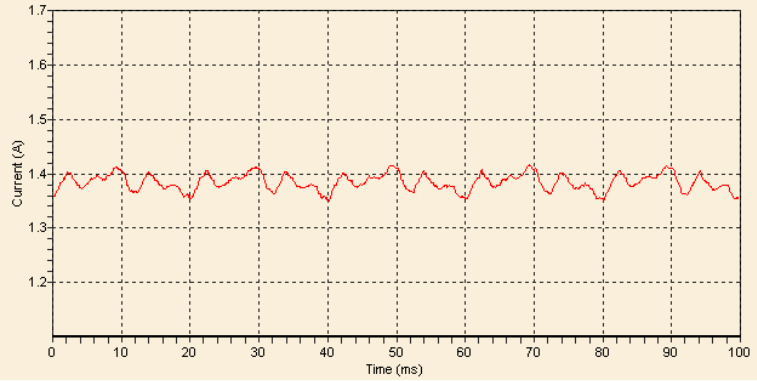

(b) With ILC scheme

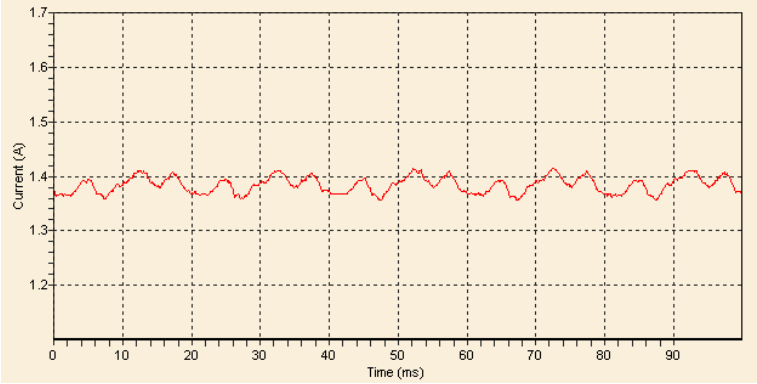

(c) With ALC scheme

Fig. 5.41. Fluctuation of coil current in axis X_1 at 3000rpm.

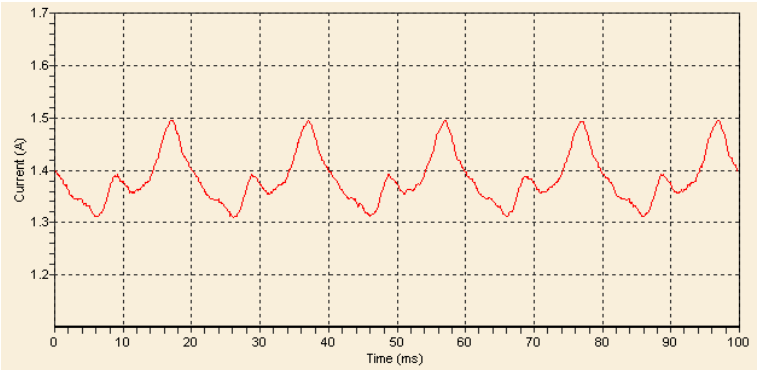

(a) With ILC scheme

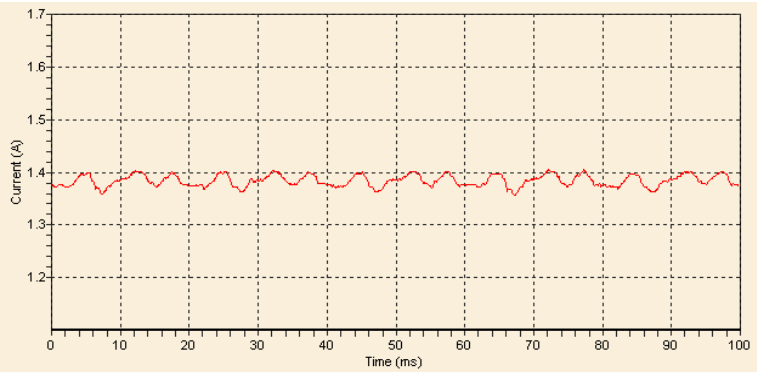

(b) With ALC scheme

Fig. 5.42. Fluctuation of coil current at 3010rpm.

Values of peak-to-peak coil current fluctuation at some rotational speed around 3000rpm are listed in Table 5.2.

Table 5.2. Comparison between ILC and ALC during speed fluctuations (2)

Speed (rpm)	PID (A)	ALC scheme (A)	ILC scheme (A)
3000	0.25	0.0571	0.06
3010	0.25	0.0498	0.186
3020	0.25	0.0601	0.312
3030	0.25	0.0454	0.318
2990	0.25	0.0572	0.117
2980	0.25	0.0483	0.163
2970	0.25	0.0439	0.179

5.7 Observations and Discussions

The experimental results prove the effectiveness of time-domain ILC scheme and ALC scheme in unbalance compensations with AMB. Both rotor runout and control current ripple can be substantially reduced through ALC within short time.

In constant speed test, time-domain ILC and ALC present almost identical compensation performances. The only difference is that the small speed disturbance could negatively influence the learning process of time-domain ILC, while ALC has much better performance against speed disturbance. ALC has another advantage that it could work at different rotational speeds, which make it suitable for more applications. The variable speed test proves its performance under the condition of rotational speed variation.

It can be observed that there still exist small amount of rotor runout and control current fluctuations although time-domain ILC or ALC is turned on. The reasons can be concluded as follows.

1. The existence of forgetting factor. According to the analysis before, forgetting factor in ILC can increase the robustness of the controller with the expense of nonzero steady-state tracking error. Therefore, forgetting factor should be kept as small as possible when the controller robustness is enough for the application requirement. If the robustness were not a problem in some cases, the forgetting factor could be set zero.
2. The existence of higher-order components. The unbalance analysis in previous chapters is based on the assumption that the rotor (shaft) is a rigid body. However,

this proximity doesn't consider the characteristics of a flexible body. In a flexible body, higher-order harmonics could be excited by the unbalance force and other external forces. The amplitude of the excited vibrations depends on characteristics of the flexible body, excitation frequency, and controllers. In the frequency plots of the experimental result, higher-order components of rotor runouts and AMB coil currents can be observed, but only synchronous components are managed to eliminate. The higher-order components of rotor runouts and control current fluctuations are left unprocessed. These residual higher-order components can be further processed to meet higher operation requirements. For example, if the higher-order components could be detached from the filter and input to the ALC controller, the controller could suppress the higher-order components as well as synchronous components in the iterative learning process.

3. Transient response during rotational speed fluctuations or unbalance conditions variations. Changes of unbalance conditions or rotational speed could result in the variation of control effects. During the process of speed changing, the transient rotor runout or coil current fluctuation could rise temporarily both in time-domain ILC and in ALC. Both the simulation and experimental results prove that time-domain ILC is sensitive to rotational speed fluctuation, so it takes time-domain ILC more time than ALC to reach the steady state. ALC can automatically adjust its parameters according to the rotational speed so that the influence of speed variation can be minimized.

6. Conclusions and Future Works

6.1 Conclusions

AMB, as a promising bearing candidate to be employed in high performance motors, is desired to present high rotational precision and vibration-free characteristics. Unbalance, commonly occurs in rotating machinery, results from the misalignment of rotor's geometric axis, inertial axis, and magnetic axis of AMB. It brings vibration and acoustic noise in rotational systems. In this thesis, time-domain ILC and ALC strategies are introduced, analyzed, and applied to solve the unbalance problem with AMB.

In the first chapter, the working principle of AMB is briefly introduced. The reasons to cause unbalance in motors are analyzed in detail. Mass unbalance results from the fact that rotor's geometric axis is not coincident with inertial axis. The magnetic unbalance is due to the misalignment of rotor's geometric axis and AMB's magnetic axis. The mass unbalance force and magnetic unbalance force are both synchronous with rotational speed. As a result, the resulting composite unbalance force has a synchronous speed and it leads to synchronous rotor runout and fluctuations of coil current in AMB. Since manufacture perfection is costly and impossible in practice, active control current strategies are necessary for better operation performance. The literature review of various unbalance control techniques for AMB is also presented

in Chapter 1. Generally these control techniques are classified into two categories, (a) to modify the complementary sensitivity function of the system, (b) to explicitly construct an "add-on" compensator. Although the existing unbalance control methods can yield good control result, they cannot be directly employed in AMB for HDD spindle motors. Most of the existing methods require precise knowledge of AMB parameters, which may be not unique for each AMB due to manufacture errors. Furthermore, most of the methods impose large amount of computational loads and memory space requirement on digital processors. It is not practical in many applications like HDD to afford those requirements for bearings in spindle motors. As a result, a simple but effective control strategy is needed to compensate unbalance effects for AMB spindle motors.

In Chapter 2, the method of time-domain ILC is discussed. An unbalance compensation scheme based on time-domain ILC is proposed. The unbalance compensation is carried out in two ways, rotation about geometric axis and rotation about system inertial axis. To realize rotation about geometric axis, the rotor runout in all 4 radial DOF should be minimized. To realize rotation about system inertial axis, the method is to reduce fluctuations of coil currents in AMB. The proposed ILC scheme is implemented in the decentralized mode to simplify its control algorithm greatly. ILC controller can works with a conventional feedback controller without changing system stability. The feedback controller, which can be already designed for optimum transient response, is responsible for stabilizing the AMB system, while ILC provides the desired current to compensate unbalance.

The proposed ILC scheme has a drawback that the parameters of the controller must be predetermined for one rotational speed and cannot automatically change during

operation. This character results in controller's sensitivity to rotational speed disturbances, degrading the controlling effect when the speed is fluctuating. To cope with this problem, The ALC control scheme with the capability of working at different rotational speeds is proposed in Chapter 3. ALC is based on time-domain ILC. It also incorporates gain-scheduled learning gains and memory with variable length for different rotational speeds. Fourier analysis theory is employed to process synchronous signals. With these improvements, ALC can automatically adjust its controller parameters according to the rotational speed.

Chapter 4 deals with computer simulations of the time-domain ILC scheme and ALC scheme. A 4-DOF AMB model considering gyroscopic effect is built for simulations. The simulation results of ILC without forgetting factor, ILC with forgetting factor, and ALC with forgetting factor are compared and analyzed. All controllers present good performance at constant speed. However, when the speed disturbance is added, ALC shows much better control effect than ILC controllers. The simulation results prove the previous analysis that ALC has better transient response during rotational speed fluctuations.

Experiments are carried out to further validate the effectiveness of proposed ILC and ALC schemes. The experimental setup and experimental results are reported in Chapter 5. The performances of ILC scheme and ALC scheme are compared with those of a conventional PID controller. It is proved that both ILC and ALC are effective in suppressing the unbalance effect when the rotational speed is constant. They produce similar steady-state compensation results in the constant-speed test. However, it can be observed from the experimental results that rotational speeds

fluctuation negatively affects the performance of ILC, while its influence to ALC can be hardly observed. The Variable-speed test of ALC scheme is also performed and figures of rotor runout and fluctuations of coil currents at a wide range of speeds are obtained.

In HDD, the spindle motor may run at two speeds for the purpose of power management. When the process of reading/writing happens, the spindle motor rotates at the nominal speed. At the rest of time, the spindle motor rotates at a lower speed for reducing power consuming. Therefore, the ALC can be arranged with two operation states: read/write state and non-read/write state. During the read/write state servo needs to accurately follow the track, so rotation precision is important to AMB. Rotation about geometric axis is desired in this case. During the non-read/write state rotation precision is not important because the magnetic head doesn't need to read/write information from/to the disk. Therefore, rotation about system inertial axis is preferred to reduce acoustic noise and consuming power. ALC controller can judge which state is on from motor speed information**.** Because the acceleration process and deceleration process are short, ALC doesn't work at that time. When a steady state is reached, ALC begins to work and chooses a working mode according to motor speed. With this working style, ALC needs to work at only two speeds, so two low-pass filters, one for high rotational speed and the other for low speed, can be used instead of synchronous signal processing unit in section 3.1.1 to eliminate noise. The ALC controller can select the right one from the outputs of these two filters according to the working state. Thus, the computation load is further reduced while the unbalance compensation capability remains same.

6.2 Future Works

To further improve the performance of ALC in unbalance compensation, some proposals are suggested in the following.

1. Robustness analysis of ALC controller. Robustness of the ALC controller can be analyzed to keep the controller stable with optimal forgetting factor. Therefore, the controller can have enough robustness with minimal expense of compensation performance.
2. Function analysis in an AMB spindle motor for HDD. The two-state working style proposed in section 6.1 can be validated to observe its performance in an AMB spindle motor. Both vibration test and consuming power test are also needed to compare the control effects of conventional PID controller and proposed ALC controller.
3. AMB is considered as a potential solution for next generation HDDs. However, as the limitations in the research facility and time, the proposed control schemes have not been used directly in the mini AMB designed for HDD spindle motor. When the AMB size is reduced to a certain level, some special phenomena may appear. Experiments and researches on the mini AMB are also good topics for future works.
4. As the PM-biased AMB has potential in realizing mini AMB for the applications like HDD spindle motors, it is expected to apply the ALC to this type of AMB, and develop more effective control modes for it.

Bibliography

[1] P.L. Tímár (Ed). Noise and Vibration of Electrical Machines. Elsevier Science Publishing Company, 1989.

[2] M. Aenis, E. Knopf and R. Nordmann. Active Magnetic Bearings for the Identification and Fault Diagnosis in Turbomachinery. Mechatronics, Vol.12, Issue 8, October 2002, pp.1011-1021.

[3] N. Grum, B. Green and P. Schroder. Active Magnetic Bearing Requirements for Turbomachinery. In IEE Colloquium on High Speed Bearings for Electrical Machines, April 25, 1997, pp.7/1-7/9

[4] D.A. Weize. Turbomachinery Advances Made Possible By Active Magnetic Bearings. In Proceedings of the 25th Intersociety Energy Conversion Engineering Conference, 1990, Vol.6, Aug. 12-17, 1990, pp.154-159.

[5] N. Koshizuka et al. Present status of R&D on superconducting magnetic bearing technologies for flywheel energy storage system, Physica C: Superconductivity, Vol.378-381, Part 1, 1 October 2002, pp.11-17.

[6] M. Komori and N. Akinaga. A Prototype of Flywheel Energy Storage System Suppressed by Hybrid Magnetic Bearings with H^{∞} Controller. IEEE Transactions on Applied Superconductivity, Vol.11, Issue 1, March 2001, pp.1733-1736.

[7] D. Howe. Magnetic actuators. Sensors and Actuators A: Physical, Vol.81, Issues 1-3, 1 April 2000, pp.268-274.

[8] J. X. Shen, K. J. Tseng, D. M. Vilathgamuwa and W. K. Chan. A Novel Compact PMSM with Magnetic Bearing for Artificial Heart Application. IEEE Transactions on Industry Applications, Vol.36, No.4, July/August 2000, pp.1061-1068.

[9] G. Schweitzer (Ed). Magnetic Bearings: Proceedings of the First International Symposium. Berlin; New York: Springer-Verlag, 1988.

[10] G. Schweitzer, H. Bleuler, and A. Traxler. Active magnetic bearings: basics, properties and applications of active magnetic bearings. Zurich: vdf Hochschulverlag, 1994.

[11] Y. Okada and K. Nonami. Research Trends on Magnetic Bearings (Overview of the 8th International Symposium on Magnetic Bearings (ISMB-8)). JSME International Journal, Series C, Vol.46, No.2, pp. 341-342, June 2003.

[12] R. Vuillemin et al. Low Cost Active Magnetic Bearings for Hard Disk Drive Spindle Motors. In Proceedings of the 6th International Symposium on Magnetic bearings, 1998, Cambridge, USA, pp.3-9.

[13] M. Kümmerle, B. Aeschlimann, J. Zoethout, and H. Bleuler. Acceleration Feedforward for Increase of Bearing Stiffness Application for Very Small AMBs. In Proc. the 7th International Symposium on Magnetic Bearings, August 2000, Zurich, Switzerland, pp.89-93.

[14] H. Kanebako and Y. Okada. New Design of Hybrid-Type Self-Bearing Motor for Small, High-Speed Spindle, IEEE/ASME Transactions on Mechatronics, vol.8, no.1, pp.111-119.March 2003.

[15] F Betschon. Design Principle of Integrated Magnetic Bearings," Ph.D Dissertation, ETH Zürich, 2000.

[16] C.K. Sortore, P.E.Allaire, E.H. Maslen, R.R. Humphris, and P.A. Studer. Permanent Magnet Biased Magnetic Bearings-Design, Construction and Testing. In Proceedings of the 2nd International Symposium on Magnetic Bearings, July 1990, Tokyo, Japan, pp. 175-182.

[17] N. Motee, M.S. de Queiroz, Y. Fang and D.M. Dawson. Active Magnetic Bearing Control with Zero Steady-State Power Loss. In Proceedings of the American Control Conference, Anchorage, USA, May 2002.

[18] P. Tsiotras and B.C. Wilson. Zero- and Low-Bias control Designs for Active Magnetic Bearings. IEEE Transactions on Control Systems Technology, Vol.11, No.6, Nov. 2003, pp. 889-904.

[19] C. Knospe and C. Yang. Gain-scheduled control of a magnetic bearing with low bias flux. In Proc. 36th Conference on Decision and Control, San Diego, USA, 1997, pp. 418–423.

[20] C. Bi, D.Z. Wu, Q. Jiang and Z.J. Liu. Optimize Control Current in Magnetic Bearings Using Automatic Learning Control. In Proceedings of 2004 IEEE International Conference on Mechatronics. Istanbul, Turkey, June, 2004.

[21] C.R. Knospe. Stability and Performance of Notch Filter Controllers for Unbalance Response. In Proceedings of the International Symposium on Magnetic Suspension Technology, Nasa Langley Research Center, Hampton, USA, Aug. 1991.

[22] R. Herzog, P. Bühler, C. Gähler and R. Larsonneur. Unbalance Compensation Using Generalized Notch Filters in the Multivariable Feedback of Magnetic Bearings. IEEE Transactions on Control Systems Technology, Vol.4, No.5, Sept. 1996, pp.580-586.

[23] L. Li, T. Shinshi, C. Iijima, X. Zhang and A. Shimokohbe. Compensation of Rotor Imbalance for Precision Rotation of A Planar Magnetic Bearing Rotor. Precision Engineering, Vol. 27, Issue 2, April 2003, pp.140-150.

[24] F. Matsumura, M. Fujita and K. Okawa. Modeling and Control of Magnetic Bearing Systems Achieving a Rotation Around the Axis of Inertia. In Proceedings of the 2nd International Symposium on Magnetic Bearings, July 12-14, 1990, Tokyo, Japan, pp.273-280.

[25] T. Mizuno and T. Higuchi. Design of Magnetic Bearing Controllers Based on Disturbance Estimation. In Proceedings of the 2nd International Symposium on Magnetic Bearings, July 12-14, 1990, Tokyo, Japan, pp.281-288.

[26] T. Higuchi, T. Mizuno and M. Tsukamoto. Digital Control System for Magnetic Bearings with Automatic Balancing. In Proceedings of the 2nd International Symposium on Magnetic Bearings, July 12-14, 1990, Tokyo, Japan, pp.27-32.

[27] B. Shafai, S. Beale, P. LaRocca, and E. Cusson. Magnetic Bearing Control Systems and Adaptive Forced Balancing. IEEE Control Systems Magzine, Vol.14, Issue 2, pp.4-13, April 1994.

[28] S. Beale, B. Shafai, P. LaRocca, and E. Cusson. Adaptive Forced Balancing for Magnetic Bearing Control Systems. In Proceedings on the 31st IEEE Conference on Decision and Control, Tucson, USA, Dec. 1992, pp.3535-3539.

[29] K. Nonomi, Qi-fu Fan and H. Ueyama. Unbalance Vibration Control of Magnetic Bearing systems Using Adaptive Algorithm with Disturbance Frequency Estimation. In Proceedings of the 6th International Symposium on Magnetic bearings, 1998, Cambridge, USA, pp.663-672.

[30] F. Betschon and R. Schob. On-Line-Adapted Vibration Control. In Proceedings of the 6th International Symposium on Magnetic bearings, 1998, Cambridge, USA, pp.362-371.

[31] J. Shi, R. Zmood and L. Qin. Synchronous Disturbance Attenuation in Magnetic Bearing Systems Using Adaptive Compensation Signals. Control Engineering Practice, Vol. 12, Issue 3, March, 2004, pp.283-290.

[32] N. Taguchi, T. Ishimatsu, S.J. Woo and C. Gaehler. Unbalance Compensation of Magnetic Bearings. In Proceedings of 20th International Conference on Industrial Electronics, Control and Instrumentation. Vol.3, 5-9 Sept.1994, pp.2051–2056.

[33] J.D Setiewan, R. Mukherjee, E.H. Maslen, Synchronous Sensor Runout and Unbalance Compensation in Active Magnetic Bearings Using Bias Current Excitation. Transactions of the ASME. Journal of Dynamic Systems, Measurement and Control, Volume 124, Issue 1, 2002, Pages 14-24.

[34] T. Higuchi, M. Otsuka, T. Mizuno and T. Ide. Application of Periodic Learning Control with Inverse Transfer Function Compensation in Totally Active Magnetic Bearings. In Proceedings of the 2nd International Symposium on Magnetic Bearings, July 12-14, 1990, Tokyo, Japan, pp.257-264.

[35] X. Zhang, T. Shinshi, L. Li and A. Shimokohbe. A Combined Repetitive Control for Precision Rotation of Magnetic Bearing. Precision Engineering, Vol. 27, Issue 3, July 2003, pp.273-282.

[36] C.R. Knopse, R.W. Hope, S.J. Fedigan and R.D. Williams. Adaptive On-Line Rotor Balancing Using Digital Control. In Proceedings of MAG'93 Magnetic Bearing, Magnetic Drives, and Dry Gas Seals Conference, July 1993, Lancaster, USA.

[37] C.R. Knopse, R.W. Hope, S.J. Fedigan and R.D. Williams. Experiments in the Control of Unbalance Response Using Magnetic Bearings. Mechatronics, Vol.5, No.4, pp. 385-400, 1995.

[38] C.R. Knopse, S.M. Tamer and S.J. Fedigan. Synthesis of Robust Gain Matrices for Adaptive Rotor Vibration Control. ASME Journal of Dynamic Systems, Measurement and Control, pp. 298-300, June 1997.

[39] C.R. Knopse, S.M. Tamer and R.Fittro. Rotor Synchronous Response Control: Approaches for Addressing Speed Dependence. Journal of Vibration and Control, Vol.3, pp.445-458, 1997.

[40] F. Betschon and C.R. Knopse. Reducing Magnetic Bearing Currents via Gain Scheduled Adaptive Control. IEEE/ASME Transactions on Mechatronics, Vol.6, No.4, Dec. 2001, pp.437-443.

[41] M. Paul, W. Hofmann and H.F. Steffani. Compensation for Unbalances with Aid of Neural Networks. In Proceedings of the 6th International Symposium on Magnetic bearings, 1998, Cambridge, USA, pp.693-701.

[42] A.M. Mohamed and I. Busch-Vishniac. Imbalance Compensation and Automation Balancing in Magnetic Bearing Systems Using the Q-Parameterization Theory. IEEE Transactions on control Systems Technology, Vol.3, No.2, June 1995, pp.202-211.

[43] A.M. Mohamed, I.M.M. Hassan and A.M.K. Hashem. Application of Discrete-Time Gain-Scheduled Q-Parameterization Controllers to Magnetic Bearing Systems with Imbalance. In Proceedings of the American Control Conference, June, 1999, San Diego, USA, pp.598-602.

[44] M.L. Long, J.J. Carroll and R. Mukundan. Adaptive Control of Active Magnetic Bearings Under Unknown Static Load Change and Unbalance. In Proceedings of the 1996 IEEE International Conference on Control Applications, Sept. 1996, Dearborn, USA, pp. 876-881.

[45] S. Arimoto, S. Kawamura and F. Miyazaki. Bettering Operation of Robots by Learning. Journal of Robotic Systems. Vol.1, No. 2, pp.123–140, 1984.

[46] J.X. Xu and Y. Tan. Linear and Nonlinear Iterative Learning Control. Springer Verlag, 2003.

[47] Z. Bien and J.X. Xu (Ed). Iterative Learning Control: Analysis, Design, Integration, and Applications, Norwell, MA: Kluwer Academic, 1998.

[48] K. Hamamoto and T. Sugie. Iterative Learning Control for Robot Manipulators Using the Finite Dimensional Input Subspace. IEEE Transactions on Robotics and Automation. Vol.18, Issue 4, Aug.2002, pp.632-635.

[49] C.-C. Cheah and D. Wang. Learning Impedance Control for robotic manipulators. IEEE Transactions on Robotics and Automation, Vol. 14, Issue 3, June 1998, pp.452-465.

[50] D.R. Yang, K.S. Lee, H.J. Ahn and J.H. Lee. Experimental Application of a Quadratic Optimal Iterative Learning Control Method for Control of Wafer Temperature Uniformity in Rapid Thermal Processing. IEEE Transactions on Semiconductor Manufacturing. Vol.16, Issue 1, Feb.2003, pp.36-44.

[51] M. Mezghani, G. Roux, M. Cabassud, M.V. Le Lann, B. Dahhou and G. Casamatta. Application of Iterative Learning Control to an Exothermic Semibatch Chemical Reactor. IEEE Transactions on Control Systems Technology, Vol.10, Issue 6, Nov. 2002, pp.822-834.

[52] N.C. Sahoo, J.X. Xu and S.K. Panda. Low Torque Ripple Control of Switched Reluctance Motors Using Iterative Learning. IEEE Transactions on Energy Conversion, Vol.16, No.4, Dec. 2001, pp.318-326.

[53] W. Qian, S.K. Panda and J.X. Xu. Torque Ripple Minimization in PM Synchronous Motors Using Iterative Learning Control. IEEE Transactions on Power Electronics, Vol. 19, Issue. 2, March 2004, pp.272-279.

[54] H. Elci, R.W. Longman, M.Q. Phan, J.-N. Juang and R. Ugoletti. Simple Learning Control Made Practical By Zero-Phase Filtering: Applications to Robotics. IEEE Transactions on Circuits and Systems—I: Fundamental Theory and Applications, Vol.49, No.6, June 2002, pp.753-767.

[55] P. Scholten, Iterative Learning Control: A Design for A Linear Motor Motion System. M.Sc. Thesis, University of Twente, 2000.

[56] R.W. Longman. Designing Iterative Learning and Repetitive Controllers. In Iterative Learning Control: Analysis, Design, Integration, and Applications, Ed by Z. Bien and J.-X. Xu, ch. 7, pp.107-146, Norwell, MA: Kluwer Academic, 1998.

[57] B.H. Lam, S.K. Panda, and J.X. Xu. Periodic Torque Ripples Minimisation in Permanent Magnet Synchronous Motor Drives Using Iterative Learning Control. In the 9th European Conference on Power Electronics and Applications. EPE 2001, Aug. 2001, Graz, Austria.

[58] S. Arimoto, T. Naniwa and H. Suzuki. Robustness of P-type Learning Control with a Forgetting Factor for Robotic Motions. In Proceedings of the 29th IEEE Conference on Decision and Control, Vol.5, Dec. 1990, pp.2640-2645.

[59] A. Wood. Introduction to Numerical Method. Reading, Mass.: Addison-Wesley, 1999.

List of Publications

1. "Optimize Control Current in Magnetic Bearings Using Automatic Learning Control," In *Proceedings of IEEE International Conference on Mechatronics 2004*, June 3-5, 2004, Istanbul, Singapore.
2. "Runout Compensation in Active Magnetic Bearings with Iterative Learning Control Scheme (an invited paper)," *In Proceedings of Asia-Pacific Magnetic Recording Conference '04*, Aug. 16-19, 2004, Seoul, Korea.
3. "Automatic Learning Control for Unbalance Compensation in Magnetic Bearings," submitted to *IEEE Transactions on Magnetics*.